RANDOM VIBRATION FATIGUE ANALYSIS OF BRACKETS INSTALLED ON TRACKED LAND VEHICLE

PALETLİ KARA ARACINA TAKILAN MONTAJ BRAKETLERİNİN RASTSAL TİTREŞİM YORULMA ANALİZLERİ

ONUR OKCU

PROF. DR. BORA YILDIRIM

Supervisor

Submitted to

Graduate School of Science and Engineering of Hacettepe University

as a Partial Fulfillment to the Requirements

for the Award of the Degree of Master of Science

in Mechanical Engineering

May 2022

To My Family with Gratitude…

ABSTRACT

RANDOM VIBRATION FATIGUE ANALYSIS OF MOUNTING BRACKETS INSTALLED ON TRACKED LAND VEHICLE

Onur OKCU

Master of Science Degree, Department of Mechanical Engineering

Supervisor: Prof. Dr. Bora YILDIRIM

May 2022, 111 Pages

Fulfilling the operational static requirements may not be enough for the materials used in engineering applications. Generally, failures occur due to dynamic loadings, especially in the military environments. If these dynamic loadings are cyclic, fatigue failure is more likely to occur even if stresses are under the yield strength. Vibration induced fatigue is one of the most important phenomena that is used in the structural analysis of components. Therefore, an accurate and reliable fatigue life investigations are necessary.

In this thesis, theoretical and experimental random vibration induced fatigue analysis of mounting brackets that are installed on tracked land vehicle is carried out. Fatigue life estimations are conducted considering both uniaxial and multiaxial loading cases and results are compared. Assuming the loading case as uniaxial may cause overestimation of service life. Therefore, multiaxial vibration fatigue analysis will give more accurate results since it contains cross effects of loadings to each other. However, simultaneous multiaxial shakers are not commonly available in the world, so testing of these types of loadings may be challenging. To overcome experimental difficulties, multiaxial loading is converted to the equivalent uniaxial loading that gives same damage to the critical location of the structure.

The loading data is collected in the time domain with the help of the accelerometers, then, it is transformed into frequency domain. Theoretical calculations are performed using frequency domain approach by developing a numerical code in MATLAB for fatigue life estimations of the structure. Also, using commercial fatigue life estimation software, nCode DesignLife, finite element (FE) analysis is performed, and FE model is verified using the modal testing results. In addition to the theoretical stuff, experiments are conducted to compare the results and verify fatigue life estimation of the structure.

Keywords: Random Vibration Induced Fatigue, Multiaxial Vibration Fatigue Analysis, Modal Testing, Frequency Domain Approach

ÖZET

PALETLİ KARA ARACINA TAKILAN MONTAJ BRAKETLERİNİN RASTSAL TİTREŞİM YORULMA ANALİZLERİ

Onur OKCU

Yüksek Lisans, Makine Mühendisliği Bölümü

Tez Danışmanı: Prof. Dr. Bora YILDIRIM

Mayıs 2022, 111 Sayfa

Mühendislik uygulamalarında kullanılan malzemelerin, sadece operasyonel statik gereksinimleri yerine getirmesi yeterli olmayabilir. Özellikle askeri ortamlarda, hasarlar dinamik yüklemeler kaynaklı oluşurlar. Eğer bunlar periyodik yüklemeler ise, gerilmeler akma dayanımının altında olsa bile yorulma hasarının gerçekleşmesi daha olasıdır. Titreşim yorulması, parçaların yapısal analizlerinde kullanılan en önemli fenomenlerden birisidir. Bu yüzden, isabetli ve güvenilir yorulma ömrü hesaplamaları zorunludur.

Bu tezde, paletli kara aracına entegre edilen montaj braketlerinin teorik ve deneysel rastsal titreşim kaynaklı yorulma analizleri ele alınmıştır. Yorulma ömürleri hem tek eksenli yükleme koşulu hem de çok eksenli yükleme koşulu için hesaplanmıştır ve sonuçlar karşılaştırılmıştır. Yükleme koşulunu tek eksenli olarak kabul etmek servis ömrünün olduğundan fazla hesaplanmasına yol açabilir. Dolayısıyla, çok eksenli titreşim yorulma analizleri tüm eksenlerin birbirine olan etkisini içerdiğinden, daha isabetli sonuçlar vermektedir. Fakat, tüm eksen yüklemelerini aynı anda uygulayabilen tahrik sistemleri dünya genelinde yaygın olmadığından, bu tip yüklemeleri deneysel ortamda uygulamak zor olmaktadır. Bu deneysel zorluğu aşmak için, çok eksenli yükleme, yapıya aynı hasarı verecek eşdeğer tek eksenli yüklemeye çevrilmiştir.

Yükleme verileri, zaman düzleminde ivmeölçerler yardımıyla toplanmıştır ve daha sonra bu veriler frekans düzlemine çevrilmiştir. Yapının yorulma ömrünü bulmak için yapılan teorik hesaplamalar, MATLAB kullanılarak yazılan numerik kod yardımıyla frekans düzleminde gerçekleştirilmiştir. Ayrıca, ticari bir yorulma ömrü hesaplama yazılımı olan nCode DesignLife kullanılarak sonlu elemanlar analizi gerçekleştirilmiştir ve bu model deneysel mod analizi sonuçları kullanılarak doğrulanmıştır. Teorik olarak gerçekleştirilen hesaplamalara ek olarak, sonuçları karşılaştırmak ve yapının bulunan yorulma ömürlerini doğrulamak amacıyla deneyler gerçekleştirilmiştir.

Anahtar Kelimeler: Rastsal Titreşim Kaynaklı Yorulma, Çok Eksenli Titreşim Yorulması, Modal Test, Frekans Düzlemi Yaklaşımı

ACKNOWLEDGEMENTS

I would like to express my appreciation to my supervisor, Prof. Dr. Bora Yıldırım for his leading guidance and contributions throughout this thesis.

I would like to express my sincere gratitude to my mentor, Dr. Güvenç Canbaloğlu for his technical support and recommendations for enhancing the work in this thesis. I would also like to thank him for helping and supporting me to improve my technical background since I started working with him.

I would like to express my special thanks to my colleague, Öner Murat Akbaba for making it easier for me to progress by the help of his leading works about my thesis topic.

I also would like to thank my colleagues, Ahmet Özdemir, Osman Kızıltaş and Emin Alp Uyanık for their moral support and help during experiments.

I would like to thank my managers and ASELSAN Inc. for giving me the opportunity to use computational and testing capabilities of company.

Finally, I would like to express my huge appreciation to my dear parents for their unwavering moral support and trust throughout this study as in every stage of my life.

TABLE OF CONTENTS

LIST OF FIGURES

LIST OF TABLES

LIST OF SYMBOLS AND ABBREVIATIONS

- **List of Symbols**

K	: Stress Intensity Factor
a	: Crack Length
S	: Applied Stress
$n(S)$	: Number of Cycles of Particular Stress Range
$N(S)$	: Maximum Number of Cycles without Failure
C	: Material Constant
b	: Basquin Exponent
S_a	: Alternating Stress
S_r	: Stress Range
S_m	: Mean Stress
S_{max}	: Maximum Stress
S_{min}	: Minimum Stress
R	: Stress Ratio
A	: Amplitude Ratio
K_t, K_{ts}	: Stress Concentration Factor
K_f	: Fatigue Strength Concentration Factor
q	: Notch Sensitivity
S_e	: Modified Endurance Limit
S_e'	: Endurance Limit
$k_a, k_b, k_c, k_d, k_e, k_f$	: Endurance Limit Modifying Factors
S_0	: Fatigue Strength
S_{UTS}	: Ultimate Tensile Strength
S_Y	: Yield Strength
$E[D]$	: Expected Cumulative Damage
a_e	: Biaxiality Ratio
φ_p	: Principal Stress Angle
$\sigma_1, \sigma_2, \sigma_3$	: Principal Stresses
σ_{AMP}	: Absolute Maximum Principal Stress
σ_{eq}	: Equivalent von-Mises Stress

$\sigma_x, \sigma_y, \sigma_z$: Local Normal Stresses

$\tau_{xy}, \tau_{xz}, \tau_{yz}$: Local Shear Stresses

σ_φ : Combined Stress on φ^{th} Angle Plane

φ : Plane Angle

$y(f_n)$: Frequency Domain Signal

$y(t_k)$: Time Domain Signal

T_p : Period of $y(t_k)$

FFT_{rsp} : FFT of Response

FFT_{inp} : FFT of Input

$H(f)$: Transfer Function

$G_{rsp}(f)$: Response PSD

$G_{inp}(f)$: Input PSD

$G_{xx}(f), G_{yy}(f), G_{zz}(f)$: Input PSD on x, y and z Directions

$G_{xy}(f), G_{xz}(f), G_{yz}(f)$: CPSDs

$H_x(f), H_y(f), H_z(f)$: Transfer Functions on x, y and z Directions

f : Frequency

δf : Frequency Interval

m_n : Spectral Moment

$E[0]$: Expected Number of Zero Crossings per Second

$E[P]$: Expected Number of Peaks per Second

γ : Irregularity Factor

x_m : Mean Frequency

$p(S)$: Probability Density Function

dS : Bin Width

S_t : Total Number of Cycles in History

T : Exposure Duration

ρ_{WL} : Wirsching's Empirical Correction Factor

$a(k), b(k)$: Wirsching's Best Fitting Parameters

ε : Spectral Width Parameter

α_i : Spectral Width

σ : RMS of Stress PSD

$D(f_n)$: Fatigue Damage Spectrum

f_n	: Resonant Frequency
Γ	: Gamma Function
ζ	: Damping Ratio
k	: Spring Stiffness
$DP(f_n)$	: Damage Potential
DP_{total}	: Total Damage Potential
G_{test}	: Accelerated Test PSD
T_{test}	: Aimed Test Duration of Exposure
m	: Constant Used for Accelerating the PSD
G_{org}	: Original PSD
T_{org}	: Original Duration of Exposure
$G_{inp_{(eq)}}$	: Equivalent Input PSD
$G_{rsp_{(ma)}}$	: Output Stress PSD of Multiaxial Analysis

- **List of Abbreviations**

FE	: Finite Element
FFT	: Fast Fourier Transform
$IFFT$	: Inverse Fast Fourier Transform
PSD	: Power Spectral Density
$CPSD$	: Cross Power Spectral Density
RMS	: Root Mean Square
$gRMS$	: Root Mean Square of Acceleration
FDS	: Fatigue Damage Spectrum
DP	: Damage Potential
$SDOF$	: Single Degree of Freedom

1. INTRODUCTION

Designing components for military usage requires high durability and low costs. Therefore, fatigue failure becomes very important phenomenon to consider carefully. Increasing the life of the materials during their operational usage helps lowering the costs. This situation makes fatigue calculations essential for design stage while satisfying the needs of the industry.

1.1. Overview of Fatigue

Generally, loading environments involve different type of loadings including static and dynamic loadings. In most of the applications in engineering, materials are subjected to both loading types at the same time. However, behavior of materials under dynamic loadings is harder to predict. Therefore, designing these components considering only static requirements may cause unexpected failures. If the loading is cyclic or repetitive, fatigue damage becomes dominant to consider. Even the stresses are under the yield strength of the material, due to repetitive characteristics, failure may occur and it is known as the fatigue failure. It can be described roughly as tiredness of metallic materials.

Mechanical fatigue failure is a physical process that starts with formation of cracks due to the fluctuating loads encountered by materials. Due to these fluctuating loads, alternating stresses arise in material surfaces which lead cracks to be formed. Although it seems like brittle fracture due to appearance of cracked surfaces that arise without necking, the fatigue failure mechanism is quite different than failure of brittle materials as fatigue failure involves stages as shown in Figure 1.1.

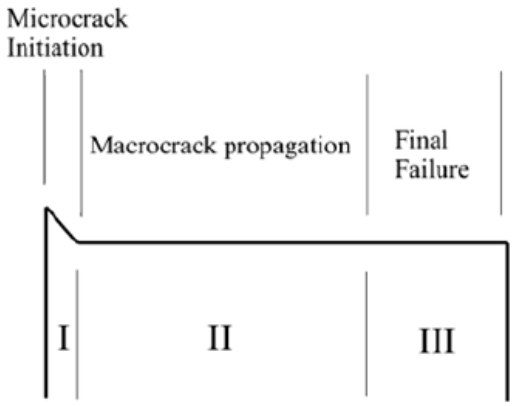

Figure 1.1 Stages of Fatigue Failure [1]

Fatigue damage is very insidious that crack initiation appears suddenly and starts to propagate. In addition, most of the failures in engineering applications tend to occur because of fatigue. Therefore, having a proper investigations of fatigue behavior of materials is essential.

1.2. History of Fatigue Research

The reason for failure of components under cyclic loadings are investigated over the centuries since failures start to occur unexpectedly. For this reason, the beginning of the fatigue research goes back to the 19th century. Instant failure of metal railway axles was believed to be caused by metal fatigue due to the appearance of fractured surface, but this has been disclaimed [2]. The timeline of fatigue research history can be given chronologically as follows.

The very first known study is conducted by Wilhelm Albert in 1837. He published the first article on fatigue about prediction of life of conveyor chains that are used in Clausthal mines. He invented a test machine for predicting the life of them [3].

Jean-Victor Poncelet first used the word ‘tired’ for metallic materials in 1839 in his lectures at military school at Metz [2].

In 1842, William John Macquorn Rankine pointed out for significance of stress concentrations during his studies on failures of railroad axles [4].

In 1843, fatigue on locomotive tender axle is reported by Joseph Glynn. Then, one of the first tire failures that stems from a rivet hole is reported in 1848 [2].

A term ‘fatigue’ is first introduced by F. Braithwaite in 1854 [5].

In 1860, fatigue testing is started to be realized by Sir William Fairbairn and August Wöhler [2]. Then, A. Wöhler resolved that stress range is more critical than peak stress based on his study about railroad axles in 1870. In addition, he first introduced the term ‘endurance limit’ [3].

In 1903, Sir James Alfred Ewing showed how surface fatigue cracks propagate as material is exposed to cyclic loads [2].

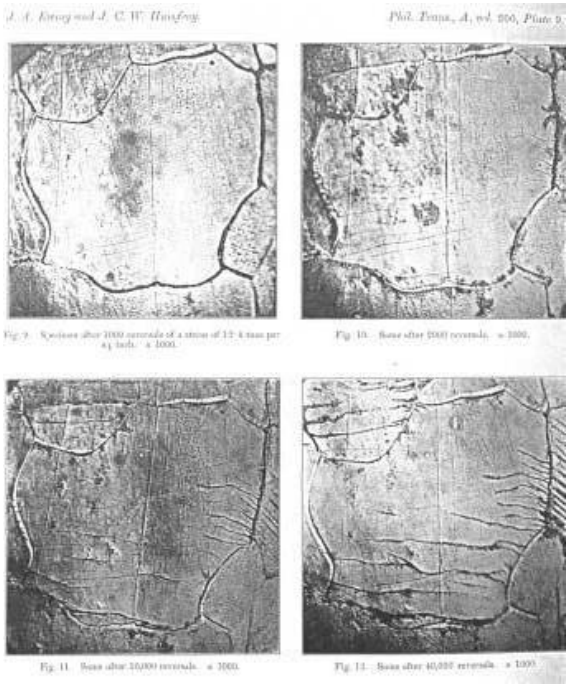

Figure 1.2 Microscopic View Showing Crack Growth [2]

In 1910, O. H. Basquin defined the empirical law for S-N curves in logarithmic scale based on Wöhler's test data [6]. He concluded that the stress versus the number of cycles have linear relationship, $\Delta\sigma N_f^b = C$. Basquin's law is still used today.

In 1924, Palmgren had the study about linear damage accumulation for fatigue life estimations [7]. Then, in 1945, A. M. Miner worked on Palmgren's study and he described the well-known Palmgren-Miner cumulative damage theory which is expressed as $\sum {n_i}/{N_i} = Cons.$ [8]. The constant is experimentally found between 0.7 and 2.2 but, $Cons. = 1$ is utilized for design purposes [9].

In 1954, L. F. Coffin and S. S. Manson expressed fatigue growth as means of plastic strains in the tip of the cracks [2].

Irwin first introduced the stress intensity factor, $K = S\sqrt{\pi a}$ in 1958 that represents the relationship between crack growth and stress at crack tip [10].

In 1962, P. C. Paris introduced a method for predicting the crack growth rate of the individual cracks in materials exposed to variable loadings. His works are known as Paris-Erdogan Law which is described by the equation $\frac{da}{dn} = C\Delta K^n$ [11].

In 1968, T. Endo and M. Matsuishi invented the rainflow cycle counting algorithm which allows the trustworthy application of Miner's cumulative damage theory. Their algorithm helps converting random loadings into simpler stress reversals [12].

In 1970, W. Elber enlightened the mechanism and significance of crack closure for slowing down the fatigue crack growth [13].

In 1973, M. W. Brown and K. J. Miller investigated that fatigue life of materials under multiaxial loading conditions strictly depends on the plane having the most damage which is called the critical plane. They defined the critical plane as the one experiencing the maximum shear stress strain amplitude [14].

In 1988, A. Fatemi and D. F. Socie had an assumption that the plane with maximum shear strain amplitude when the crack initiation is governed by Mode II, can be classified as the critical plane [15].

In 1993, M. W. Brown proposed a modified version of his study with C. H. Wang by characterizing the critical plane as the plane not only experiencing the maximum shear stress strain amplitude, but also having maximum value of normal strain excursion [16].

After many experimental and theoretical studies performed until recent years, L. Susmel proposed an algorithm in 2010, known as the shear stress maximum variance method, which defines the critical plane as the plane that experiences the maximum variance of resolved shear stress [17].

1.3. Historical Disasters Caused by Fatigue Failure

The first known accident which is caused by fatigue failure happened on 1842 in France. As the train is heading back to Paris from Versailles, the leading locomotive axle had broken and it caused the train to derail. This leads pileup of many locomotives and scattering of engine fire boxes had caused to catch fire which is reason for many deaths. It is estimated that around 55 passengers are dead due to the accident and subsequent fire [18] [19]. When this accident happened, the behavior and reasons of metal fatigue were not understood well enough and this created a confusion among all population. However, at the same time, it has motivated scientist to research more about the nature of fatigue [19].

In 1919, a huge tank filled with about 7.5 million liters of molasses fractured in service catastrophically in Boston and all molasses poured into streets [20]. When investigated in detail, it is understood that basic leak and pressure tests are ignored before putting the tank in service [19].

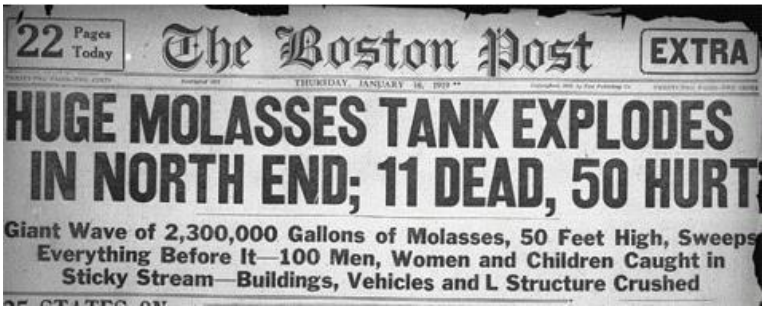
22 Pages Today
The Boston Post
EXTRA
HUGE MOLASSES TANK EXPLODES IN NORTH END; 11 DEAD, 50 HURT
Giant Wave of 2,300,000 Gallons of Molasses, 50 Feet High, Sweeps Everything Before It—100 Men, Women and Children Caught in Sticky Stream—Buildings, Vehicles and L Structure Crushed

Figure 1.3 The Boston Post Headlines on January 16, 1919 [21]

The De Havilland 'Comet' was the first commercial aircraft with turbojet engines produced in Great Britain in 1948. On these days, it was treated as aerodynamically clean and comfortable design. However, just a few years after its introduction, in 1954, it experienced its first disaster by tearing apart in mid-flight in which all 35 passengers and crew were reported as dead. After this accident, all Comets were immediately grounded and it was believed that engine turbine explosion had caused the accident. Then, with turbine modifications, all Comets were allowed to fly. A few weeks later after being allowed for flight again, another Comet aircraft experienced similar disaster in mid-flight again in which all 21 passengers and crew were died. This made investigators to interrogate their findings about turbines as a reason for crash. After extensive research for both aircrafts, including full-scale fatigue tests, it was understood that the crack is initiated from square window edges of automatic direction finder. Moreover, supports around windows were riveted instead of gluing and these riveted holes helped fatigue crack to initiate [19] [20].

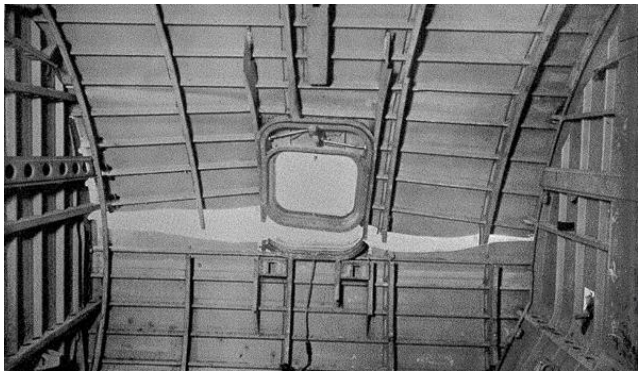

Figure 1.4 Fuselage Failure Initiated from Square Window [21]

In 1977, a Dan-Air B707-321C aircraft experienced separation of entire right-hand horizontal stabilizer as it is about to land. All six passengers were reported as dead. The aircraft had been designed by considering fail-safe philosophy which means failure of any structural element would not cause a catastrophic failure. For this reason, an extra chord was added at the center of the web on horizontal tail. By this addition, it was aimed that if any of the upper or lower chords were failed, remaining two was able to carry loads. The accident occurred after 16,723 flight hours were completed, which is lower than design life of 20,000 flights. Although upper chord had failed about 75-100 flights before the accident, additional fail-safe chord together with lower chord could not withstand the flight loads for remaining flight hours. Moreover, it has examined that the crack in upper chord would have been perceptible for approximately 3000 flights before the accident. Since it was not required for fail-safe design philosophy, there was no regular inspection on the location where failure has occurred. This showed that a fail-safe design philosophy is not sufficient to guarantee the safety of structures, additional inspections are needed [22].

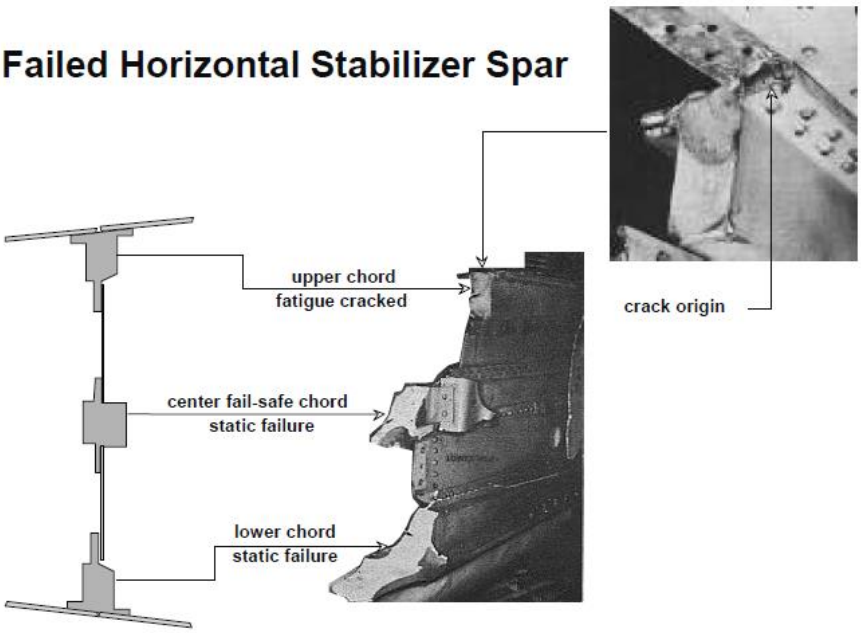

Figure 1.5 Failed Horizontal Stabilizer of Aircraft [22]

In 1988, a Boeing 737 aircraft which belongs to Aloha Airlines, had failed at a 24,000 ft altitude by tearing of upper portion of fuselage. Luckily, it was managed to land safely, only one cabin attendant was swept out of airplane out of 95 passengers. Although the aircraft had been designed for 75,000 flights, the accident has occurred after approximately 89,680 flight hours [22].

Figure 1.6 Boeing 737 Aircraft After Emergency Landing [22]

In 1998, one of the biggest train crashes in the history had occurred in Eschede, Germany. A high-speed train travelling from Munich to Hamburg was derailed because of the fatigue failure of wheel rim on the first passenger coach causing a very large pileup. It was reported that 101 people were dead along with nearly 100 injuries [19].

Figure 1.7 Eschede Train Accident [23]

1.4. Scope of the Thesis

Predicting the life of the components under random vibration environments is an essential concern in engineering applications. Vibration loads have dominance over other static loads especially in military environments. The subjects studied in this thesis cover the implementation of multiaxial loading environments which reflects the real-life exposure conditions. Analyzing components considering only uniaxial loading conditions may cause under or over-prediction of life of structures which is also covered in one of the case studies performed in later chapters. Since cross effects of each direction to another are neglected in uniaxial approaches, the resulting life may be deceptive. Therefore, having more realistic results that represent the conditions arise in real applications, multiaxial fatigue analysis is performed.

In addition to the numerical and FE analyses performed, experimental verification of results is necessary to check whether modelling and approximations are correct. However, multiaxial shakers that can excite the system simultaneously in all three axes are not commonly available worldwide. Hence, for experimental purposes, multiaxial load is converted to an equivalent uniaxial load that gives exactly same damage to structure. This is done relying completely on mathematical background of the fatigue theory, performing backward mathematics using input-output relationship. By using this converted input, fatigue tests are performed uniaxially in the most critical direction of the structure.

Throughout this study, all analyses, containing numerical and FE analyses, are performed on frequency domain since it generally gives reasonable results too, compared to time domain analyses. Time domain analysis requires repetitive processes to reach response of the structure when the model is updated. Solving the complex system using transient analysis at every turn makes it more challenging and time-consuming. However, frequency domain approach offers simpler way to reach response of the structure by multiplying input and the transfer function. Therefore, having benefit of simplicity and time-efficient approximations of frequency domain approach, it is selected as calculation method.

1.5. Outline of the Thesis

This thesis contains eight chapters totally, which are Introduction, Literature Survey, Theory of Fatigue, Construction of FE Model, Verification of FE Model, Fatigue Life Analysis of Brackets, Case Studies and Discussions & Conclusion, respectively.

The first chapter contains brief information about how fatigue failure mechanism works and importance of fatigue on engineering applications. In addition, historical evaluation of fatigue research and major disasters in history caused by metal fatigue is presented.

The second chapter involves the literature survey about random vibration induced fatigue. Studies of important scientists that are milestones for the development of fatigue research on vibration-based fatigue phenomenon are presented in this chapter chronologically.

The third chapter includes more detailed information about the theory of vibration-based fatigue. Fatigue life prediction methods and their formulations are explained in this chapter. Strain-life and crack propagation approaches are given briefly while stress-life approach is explained more in detail. Similarly, time domain cycle counting method is shortly explained while frequency domain approaches are given elaborately. In the last part of this chapter, accelerated life testing methodology used in experiments are mentioned.

The fourth chapter is devoted to construction of FE model of structure. Detailed information about how FE model is constructed is given by explaining the contact and screw modelling in FE model. Moreover, meshing of structures presented in assembly is explained in detail. In the last part of this chapter, mesh convergence analysis is presented by mentioning on singularity points arise in FE model.

The fifth chapter contains the verification process of FE model. The modal tests performed are presented in detail with results obtained. All results, including natural frequencies and damping ratios, are given in tabulated form. Moreover, non-linearity of the system is checked by using the results acquired by exciting the system with increasing amplitude loadings. Then, iterations made to verify the FE model with modal test results are presented. Also, analysis types that are used for verification and how they are implemented are shown in this chapter.

The sixth chapter involves the fatigue life analysis of brackets using FE model that is previously verified. Field data acquisition process and converting time domain data to frequency domain is explained in this chapter. In addition, accelerating the loading for experimental purposes is briefly presented. All input matrix that is used in fatigue analysis is represented graphically for both original and accelerated loadings. In addition, developed numerical code is verified with simpler model than bracket assembly by comparing the results with nCode DesignLife. Then, using verified numerical code and commercial software, fatigue life analysis of brackets under previously defined input loading is realized using different cycle counting methods. Moreover, accelerated life testing of brackets is investigated in this chapter. For having reasonable fatigue life testing durations, loading input is rearranged and all procedures are explained in detail. Effect of damping ratio on fatigue life results are examined and results are presented for different damping ratios. Converting multiaxial input to an equivalent uniaxial input is explained and finally, accelerated life testing is realized and results are presented.

The seventh chapter contains case studies performed for understanding the effect of different parameters to resultant fatigue life. There are totally three case studies presented in this chapter. The very first one includes the effect of using different stress combination methods. The second case study includes the effect of variety of approaches to fatigue analysis other than multiaxial analysis. These are enveloping the PSDs obtained for separate directions and using this enveloped PSD for uniaxial analysis and having a sequential fatigue analysis for all x, y and z directions, separately. Results obtained for all three analyses are compared. The last case study represents the effect of tightening torque of mounting screws to damping ratio of the structure and so, fatigue life. Torques of mounting screws are increased in controlled manner in experiments and transmissibility curves are obtained separately for each step. Damping ratios are calculated for each torque and results are presented with corresponding fatigue life.

The eighth and the last chapter involves discussions and conclusion of results obtained for studies conducted during the thesis.

2. LITERATURE SURVEY

S. O. Rice [24] proposed a relationship in order to find number of upward zero crossings per second and number of peaks per second by the help of spectral moments of random signal. This relationship is widely used in vibration-based fatigue techniques and it is one of the first attempts to estimate a fatigue damage from random stress history.

Bendat [25] presented a Narrow-Band solution by using the relationship proposed by Rice. He derived a formulation to find expected damage using first four spectral moments of the stress history. As indicated in its name, a proposed method is eligible for only narrowband signals. It gives conservative results for signals showing wideband characteristics.

After Bendat's method, many trials have been made to develop a method that gives reasonable results for wideband signals. For improving Bendat's solution, Wirsching et al. [26], Chaudhury and Dover [27], Tunna [28] proposed different methods by empirically correcting the conservatism of Narrow-Band method.

Steinberg [29] presented a simple fatigue life estimation method for electronic components under random vibration excitation using three band technique. His method involves probability of stress ranges according to the Gaussian distribution.

Dirlik [30] proposed one of the best cycle counting methods in frequency domain in his PhD thesis. He derived an empirical solution by using extensive computer simulations and Monte Carlo technique. Dirlik's empirical solution is robust and it gives reasonable results for both narrowband and broadband signals. It is accepted as one of the best-fitted method to real-life results.

Bishop et al. [31] treated the fatigue life calculations based on FE models in very extensive perspective in their book. Different design philosophies and approaches as stress-life, strain-life and crack-propagation are investigated in detail. Although time domain approaches are presented, main effort is about vibration fatigue analysis which is also known as frequency domain approach. This approach and its applications explained in detail step by step. Bishop concluded that frequency domain approaches are more effective that time domain approaches since time domain analysis requires transient processes which are computationally ineffective.

Woodward and Bishop [32] revealed a paper about the fatigue analysis of missile shaker table mounting brackets. They used frequency domain approach in their study. They used both experimental and FE modelling approaches as investigating the fatigue life. Test results come out to be lower than the FE analysis results. The boundary conditions are examined carefully and tolerance mismatch between flanges of bracket and actuator face is reported. For this reason, it is concluded that there was possibility of arising mean stress effects which cause the difference between experimental and FE analysis results.

Halfpenny [33] presented a paper at International Conference on Damage Assessment of Structures in Dublin about a frequency domain approach for fatigue life estimation from FE analysis. Comparison about time domain and frequency domain analysis are presented and it is shown that Dirlik approach has only 4% discrepancy from results obtained from time domain. In addition, Dirlik approach is defined as remarkably robust.

Tovo [34] proposed a new cycle counting method in frequency domain which can be used for both narrowband and broadband signals. Then, based on Tovo's approach, Benasciutti [35] proposed another method which is known as Tovo-Benasciutti cycle counting technique to improve accuracy of previous method.

Lalanne [36] used Rice's original formula that is based on weighed sum of Rayleigh and Gaussian distributions to demonstrate probability density function of rainflow ranges and offered a new cycle counting technique. His method is seen as equally robust as Dirlik's method and can be used for both narrowband and wideband signals.

Karpanan [37] presented a conference paper about critical plane search method for biaxial and multiaxial fatigue analysis. He introduced critical plane search method in detail both in 2D and 3D stress states. Fatigue analysis for proportional and non-proportional loading cases has been discussed.

Guangzong He et al. [38] investigated the fatigue behavior of structures under multiaxial random loading. Theoretical analysis is performed by implementing the equivalent von-mises stress combination method in multiaxial loading case. Three different vibration fatigue tests are performed as full tri-axial, uniaxial and sequential uniaxial vibration tests. It is concluded that fatigue life obtained from uniaxial test is far longer than that obtained from full tri-axial test.

Mrsnik et al. [39] examined different cycle counting methods on frequency domain and their application to real data. It is founded that Tovo-Benasciutti is the best method, followed by Dirlik method. Moreover, it is concluded that the Dirlik, Zhao-Baker and Tovo-Benasciutti frequency domain methods are all very consistent with the materials that have lower (k~3) S-N curve slope. Relative error increased with steeper S-N curve slope.

Aykan [40] analyzed fatigue life of chaff flare dispenser bracket using vibration fatigue approach. Multiaxial analysis is performed using commercial fatigue software. However, in fatigue life tests, excitations are applied in three axes sequentially. This lead to have longer fatigue life results than that obtained from multiaxial analysis, since cross correlations of input Power Spectral Densities (PSD) are not considered in sequential three axes fatigue life testing.

Kocer [41] proposed a new method to create a modified input loading with zero mean to get approximately equivalent fatigue damage to that obtained from input with non-zero mean. Case study is performed to analyze the utility of the proposed method.

Eldogan [42] analyzed a bracket that is installed on air platform and notched cantilever beam as a case study. He developed a numerical code that calculates the fatigue life of any structure both in time and frequency domains. Results are compared and it is concluded that Dirlik method gives the best-fitted results to time domain.

Akbaba [43] worked about fatigue life analysis of brackets installed on unmanned aerial platform. He discussed the effect of damping ratio on fatigue life in detail, concluding that it has major effect on fatigue life of structures. In addition, he performed several case studies to show that fatigue life is very sensitive to different parameters. In one of his case studies, he founded that there is about 30% difference on fatigue life results of points which are only 0.42 millimeters apart from each other. It is understood that small stress differences may cause major fatigue life discrepancies.

3. THEORY OF FATIGUE

As indicated several times, fatigue failure is most likely to occur in the environments in which cyclic loadings are dominant. Different than static failure types, fatigue failure may occur even the arising stresses are under the yield strength of materials. This makes fatigue very essential phenomenon to investigate.

Fatigue comes out in stages as illustrated in Figure 1.1, which mainly consists of crack initiation and crack propagation phases before final failure occurs. The length of each phase varies with geometry and material properties. For example, ductility of materials directly affects the length of propagation phase, higher ductility means longer crack propagation phase. After crack propagation is started, it becomes evident that material can fail suddenly.

To sum up, fatigue life can be specified as the sum of crack initiation and crack propagation phases and each phase should be examined carefully to have better understanding of fatigue failure mechanisms.

3.1. Fatigue Life Prediction Methods

There are mainly three different fatigue life prediction methods which are stress-life, strain-life and crack propagation approaches. Each method has different characteristics about treating the life of the materials. The main difference between these methods is that stress-life and strain-life approaches estimate the fatigue life until crack initiates while crack propagation approach estimates fatigue life after crack initiates.

Since stress-life approach is implemented in this study and initiation of crack is taken as reference, it will be covered in all its details while strain-life and crack propagation approaches will be explained very briefly.

3.1.1. Stress-Life (S-N) Approach

Stress-life approach is mainly suitable for loading cases in which stresses arise on structure are under the yield strength, i.e., stresses always stay below the elastic limit. It is the oldest method of all three methods mentioned and used if the number of cycles to failure is relatively large [31]. Generally, number of cycles to failures is greater than 10^4-10^5 cycles in the scope of stress-life approach. For this reason, this approach is also known as high cycle fatigue method.

Figure 3.1 shows the common example of stress cycles reversing between tension and compression with two different loading conditions. Figure 3.1 a) has zero mean stress since it has same amplitude of maximum and minimum stresses with different signs that reflects tension and compression and it is called as fully reversed stress cycle. This is an idealized loading condition which may be reflecting the motion of rotating shafts operating in constant speed. Figure 3.1 b) has non-zero mean as clearly understood from the plot since it has different maximum and minimum stress amplitudes which both are in tension. This illustrates more general situation than one in Figure 3.1 a).

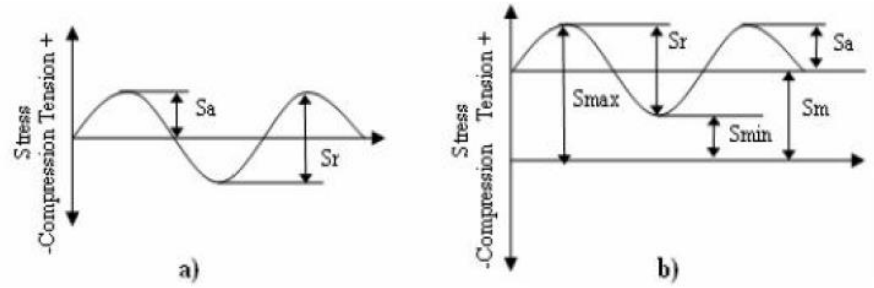

Figure 3.1 Example of Stress Cycles, a) Fully Reversed, b) Offset [31]

There are some useful parameters to be defined from the plots shown in Figure 3.1 for characterizing the stress cycles better. S_a, S_r and S_m represents the alternating stress, the stress range and the mean stress, respectively while S_{max} and S_{min} represents the maximum and the minimum stresses in the stress cycle. Moreover, there are some other parameters as stress ratio, R and amplitude ratio, A that can be defined using previously defined parameters. All relations are given in Equation (3.1).

$$\begin{aligned} S_a &= \frac{S_{max} - S_{min}}{2} \\ S_m &= \frac{S_{max} + S_{min}}{2} \\ S_r &= S_{max} - S_{min} \\ R &= \frac{S_{min}}{S_{max}} \\ A &= \frac{S_a}{S_m} = \frac{1 - R}{1 + R} \end{aligned} \tag{3.1}$$

3.1.1.1. The S-N Curve

Measuring the fundamental fatigue properties of materials requires ideal geometries that are free of any stress concentrations as fillets, grooves, holes etc. In the past, it is ensured with a cylinder that has very little changes of cross section and a polished surface in the region where crack is expected to initialize. This cylinder was loaded in bending and procedure was known as Wöhler test. However, it has some limitations. Therefore, a similar cylinder with very small changes in cross section and polished surface at expected crack location is used in axial tension testing instead of bending. Several tests are performed with number of identical specimens by recording the total number of cycles, N to separation. Load is kept constant during experiments and the nominal stress, S is calculated using simple elastic formulae [31]. Both number of cycles and stresses are recorded and results are plotted to construct S-N curve which is a fundamental material property to indicate fatigue life. A typical S-N curve is represented in Figure 3.2.

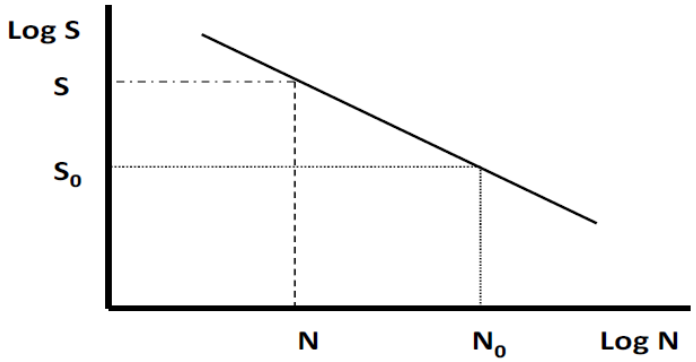

Figure 3.2 A Typical S-N Curve [42]

As clearly understand from Figure 3.2, the number of cycles to failure, N is plotted on the x-axis of the graph while corresponding stress value, S is presented on y-axis. Generally, logarithmic scale is used in both axes of S-N diagrams. Stress values can be represented using either alternating stresses or stress ranges. The common relation that represents the S-N curve is given in Equation (3.2).

$$N = C.S^{-b} \tag{3.2}$$

In the equation above, b represents the inverse of slope which is also called as Basquin exponent and C is related to the intercept on the y-axis.

S-N curves of ferrous and non-ferrous materials show different characteristics. S-N curve of ferrous materials simply consists of two lines, including horizontal straight line. This horizontal line arises after certain number of cycles and it indicates that material has fatigue limit which is also known as endurance limit. If stresses are under the endurance limit, there is no corresponding number of cycles to failure in S-N curve and the material is said to have infinite life. Steel is one of the most common ferrous alloys and can have an infinite life depending on loading conditions. In contrast to ferrous materials, non-ferrous materials do not have any horizontal straight line in their S-N curves. Therefore, they cannot experience infinite life in any case. Instead of endurance limit, fatigue strength is defined for non-ferrous material at about 10^8 or $5x10^8$ cycles [44]. Aluminum, magnesium and copper alloys are the most common examples of non-ferrous materials.

Different S-N curve characteristics of ferrous and non-ferrous metals can be seen below in Figure 3.3. In addition, endurance limit and fatigue strength parameters can be understood clearly from the figure below.

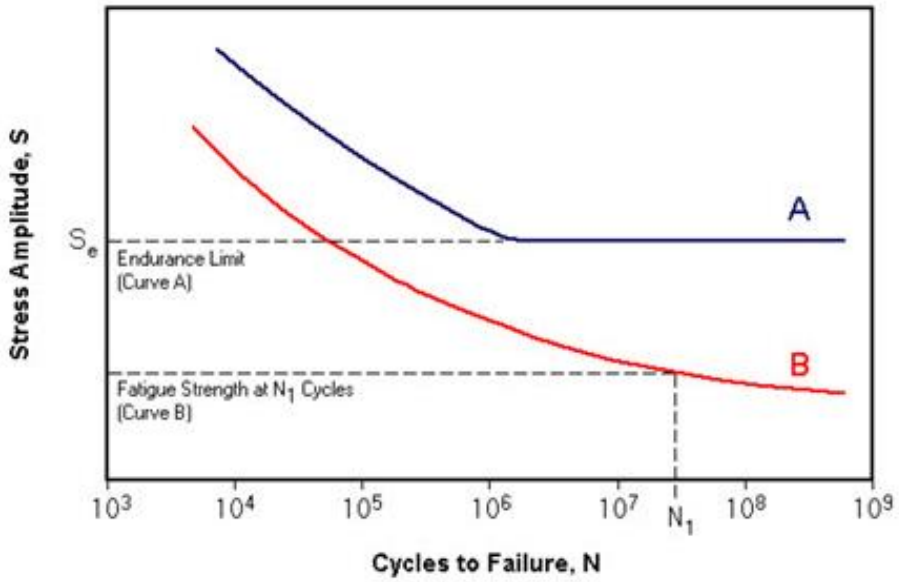

Figure 3.3 S-N Curves for Ferrous (A) and Non-ferrous (B) Materials [44]

3.1.1.2. Stress Concentration and Notch Sensitivity

As mentioned in previous chapter, S-N curve of materials are obtained experimentally using the specimens free from sudden geometrical changes that may cause stress concentrations and discontinuities. However, it is not possible to have these kinds of ideal materials in real-life designs. Generally, grooves, notches, holes, or discontinuous cross sections appear in engineering designs which lead to have locally concentrated stresses at specific regions. Therefore, effect of these stress concentrators cannot be neglected. For handling this situation, the stress concentration factor, K_t and K_{ts} are defined for normal stresses and shear stresses, respectively [45].

$$K_t = \frac{Maximum\ stress\ in\ the\ region\ of\ the\ notch}{Nominal\ stress\ remote\ from\ the\ notch} \tag{3.3}$$

In some of the experiments, it is noticed that the effect of notches on fatigue life is lower than predicting with the factor of K_t. Hence, another factor for reducing the effect of K_t is defined as fatigue strength concentration factor, K_f in Equation (3.4) [45].

$$K_f = \frac{Maximum\ stress\ in\ notched\ specimen}{Stress\ in\ notch-free\ specimen} \tag{3.4}$$

Using previously defined K_t and K_f, notch sensitivity, q can be defined as follows [45].

$$q = \frac{K_f - 1}{K_t - 1} \quad or \quad q_s = \frac{K_{fs} - 1}{K_{ts} - 1} \tag{3.5}$$

Notch sensitivity, q usually takes values between zero and unity. It can be concluded by analyzing Equation (3.5) that $q = 0$ means $K_f = 1$ and the material has no sensitivity to notches. On the other hand, $q = 1$ means $K_f = K_t$ and the material has full sensitivity to notches. Notch sensitivities for materials are generally acquired experimentally. In design process, K_t should be found from geometry, then specifying the material, q is found. Then, Equation (3.5) can be used to reach K_f [45].

3.1.1.3. Endurance Limit Modifying Factors

Endurance limit of ferrous metals is obtained in controlled laboratory tests using very carefully prepared test specimens. It is not possible to reflect real-life environments with these laboratory conditions. In real-life conditions, environment, manufacturing, or design have major effect on endurance limit of materials. Therefore, similar to modifying stresses with stress concentration factors, endurance limit should be considered after some modifying factors are applied [45]. Modified endurance limit is given in Equation (3.6).

$$S_e = k_a k_b k_c k_d k_e k_f S_e' \tag{3.6}$$

k_a = surface condition modification factor

k_b = size modification factor

k_c = load modification factor

k_d = temperature modification factor

k_e = reliability factor

k_f = miscellaneous effects modification factor

S_e' = rotary-beam test specimen endurance limit

S_e = endurance limit at the critical location of a machine part in the geometry and condition of use

3.1.1.4. Mean Stress Effect

Fatigue life of any structure strongly depends on the resultant stresses arise in the critical location under repetitive excitations. However, if these stresses have a mean value, a correction is needed to precisely predict the fatigue life.

S-N curves are traditionally acquired using fully reversed cycles in which mean stress is zero. However, these ideal fully reversed cycles are hard to experience in real-life environments which generally propose a stress cycle with non-zero mean. Basically, presence of a tensile mean stress (See Figure 3.1 b)) has negative effect on allowable amplitude of applied fatigue stresses. To overcome this situation, different models are proposed by Goodman, Soderberg and Gerber as indicated in equations below. All these methods are used to modify alternating stresses due to presence of mean stress.

$$\text{Goodman's Model:} \quad S_a = S_0\left(1 - \frac{S_m}{S_{UTS}}\right) \tag{3.7}$$

$$\text{Soderberg's Model:} \quad S_a = S_0\left(1 - \frac{S_m}{S_Y}\right) \tag{3.8}$$

$$\text{Gerber's Model:} \quad S_a = S_0\left[1 - \left(\frac{S_m}{S_{UTS}}\right)^2\right] \tag{3.9}$$

where S_a, S_m, S_0, S_Y, S_{UTS} represent the alternating stress, mean stress, fatigue strength, yield strength and ultimate tensile strength, respectively.

One of the main differences between these methods is that Goodman and Soderberg assumes linear reduction in alternating stress while Gerber's curve assumes parabolic reduction. The corresponding curves of all three methods are given in Figure 3.4.

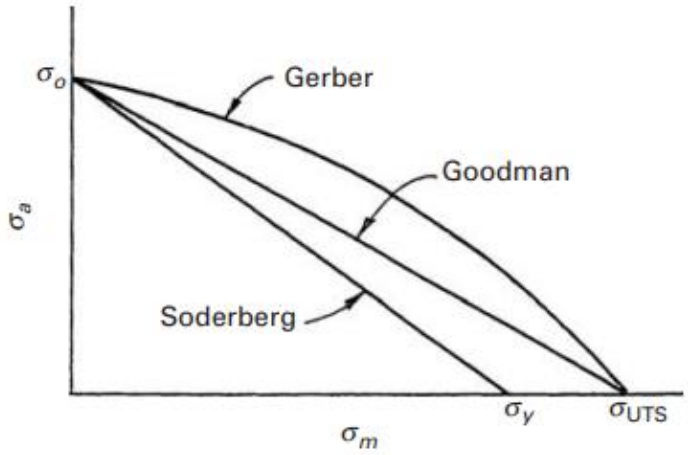

Figure 3.4 Representation of Goodman, Soderberg and Gerber Models [46]

Since right side of the lines means failure, Soderberg's model can be named as the most conservative approach among all three approaches. However, experiments show that the majority of data lies between the Goodman and Gerber's lines. Hence, Goodman's model is the most used one as it is more conservative than Gerber's model [46].

3.1.1.5. Cumulative Damage

In real-life environments, it is hard to encounter with the constant amplitude responses. Generally, it is more common to have variable amplitude loading cases. Then, investigation of fatigue life under this type of loadings requires the study of cumulative damage. Time history may involve loadings with different constant amplitudes in sequence. A typical illustration of block loading sequence is given in Figure 3.5.

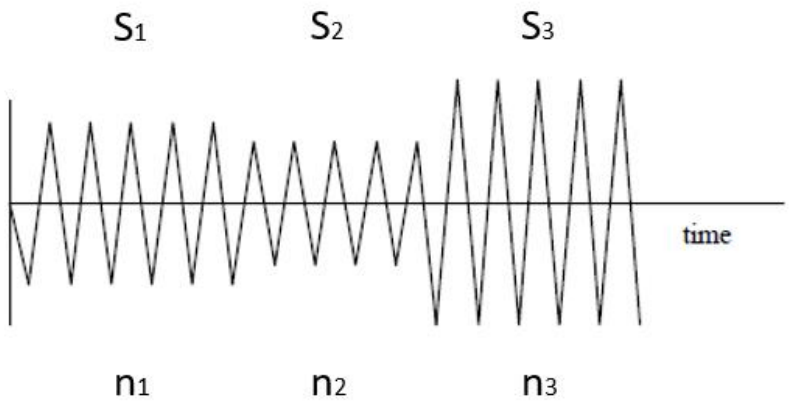

Figure 3.5 Block Loading Sequence [31]

The stress history consists of n_1 cycles of amplitude S_1, n_2 cycles of amplitude S_2 and so on. The aim is to understand the damage of each individual loading blocks. For this reason, Palmgren and Miner [8] suggests a method to find the cumulative damage by summing the contributions of each individual damages. According to Palmgren-Miner rule, damage accumulation is assumed to be linear and it is given in Equation (3.10).

$$E[D] = \sum_{i=1}^{k} \frac{n_i}{N_i} \tag{3.10}$$

$E[D]$ stands for the cumulative damage while n_i represents the individual cycles that corresponding stress amplitude is experienced. In addition, N_i represents the allowable number of cycles until failure according to S-N curve of the material. When $E[D]$ is equal to 1, the entire life is assumed to be consumed and failure occurs.

Although it has a very simple representation, Miner's rule has some limitations as well. As mentioned before and clearly understood from Equation (3.10), it assumes linear damage accumulation and the order of loading is not important. In other words, sequence effects are not considered. Despite all of its limitations, wide use of this hypothesis has shown that it gives reasonable result is most of the cases [31].

3.1.1.6. Cycle Counting

So far, mentioned loadings are either single amplitude as sine waves or variable amplitude with block sequence as shown in Figure 3.5. However, random loadings have more complex characteristics by nature. Therefore, it is not possible to implement Miner's theorem for such loadings since stress cycles are not clearly recognized in random environments. Stress cycles of individual ranges should be distinguished carefully to obtain ordered stress history of random data. For this purpose, cycle counting techniques are used. Rainflow cycle counting, peak counting, level crossing counting are the examples of cycle counting techniques.

Among all of these cycle counting methods, one of the most well accepted and commonly used technique is rainflow cycle counting which is proposed by Endo and Matsuishi in 1968 [12]. The name 'rainflow' comes from the flow of rain falling down from roof of the Pagoda building [47].

The rainflow cycle counting method consists of some steps for reaching closed loading reversals and these steps can be summarized as follows [47];

1. Rotate the stress-time loading history 90 degrees clockwise such that the time axis becomes vertically downward and the load axis becomes horizontal resembling the Pagoda roof. (See Figure 3.6)
2. Realize a flow of a rain stating at each successive extremum point.
3. Define a loading reversal by allowing each flow to continue to drip down until;
    a. It falls opposite a larger maximum (or smaller minimum) point.
    b. It meets a previous flow falling from above.
    c. It completely falls below the roof.
4. Identify each cycle by pairing up the same counted reversals.

An example of above-mentioned procedure is given below for representing the rainflow cycle counting algorithm better.

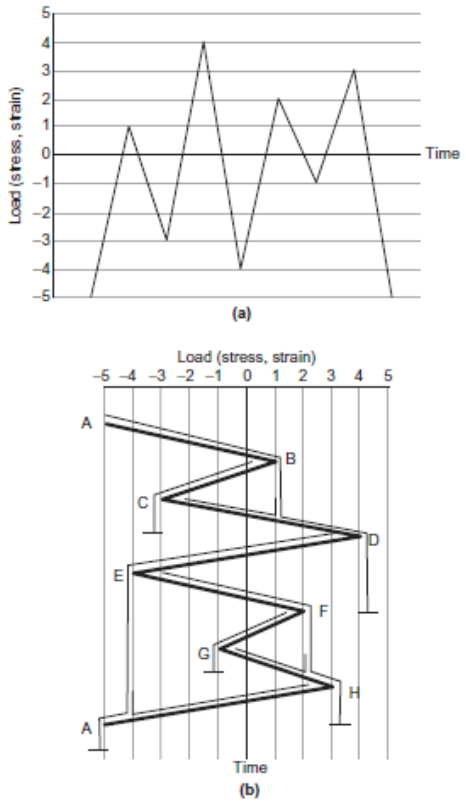

Figure 3.6 (a) Service Load-Time History, (b) Rotated Load-Time History [47]

As shown in Figure 3.6 (b), it is realized that flow starts from each extremum points which are named as A, B, C and so on. Results based on rainflow counting method are given below.

Table 3.1 Reversal Counts Based on Rainflow Counting Technique [47]

No. of Reversals	From	To	From	To	Range	Mean
1	A	D	-5	4	9	-0.5
1	B	A	4	-5	9	-0.5
1	B	C	1	-3	4	-1
1	C	B	-3	1	4	-1
1	E	H	-4	3	7	-0.5
1	H	E	3	-4	7	-0.5
1	F	G	4	-1	3	0.5
1	G	F	-1	2	3	0.5

Table 3.2 Cycle Counts Based on Rainflow Counting Technique [47]

No. of Cycles	From	To	From	To	Range	Mean
1	A	D	-5	4	9	-0.5
1	B	C	1	-3	4	-1
1	E	H	-4	3	7	-0.5
1	F	G	2	-1	3	0.5

After getting range and mean information of individual stress cycles in complex loadings, Miner's theorem can be easily implemented to find cumulative fatigue damage. Results obtained using rainflow cycles counting method can be represented using a three-dimensional histogram which consists of number of cycles, range and mean information at individual axes. An example of such range-mean histogram is shown in Figure 3.7.

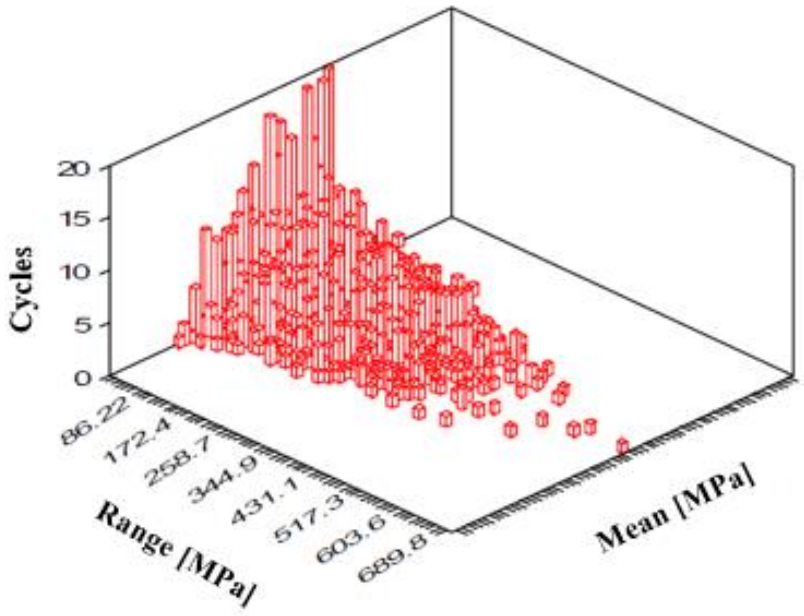

Figure 3.7 An Example of Range-Mean Histogram [33]

3.1.1.7. Stress Combination

In stress-life method, obtaining true stress history of the location of interest is very essential. Since this method focuses on an equivalent stress arise on the critical location, stress combination is needed to reach that equivalent value. In other words, stress combination is used to reduce the stress tensor to an equivalent scalar value. Stress combination can be realized using different equivalent stress theories. However, choosing the best method for particular stress state and loading case is very important to reach reliable fatigue life results.

Normally, any stress state includes nine components in three-by-three matrix including normal and shear stresses for each x, y and z directions. However, in most of the cases, fatigue cracks initiate at free surfaces in which no direct or shear stress is applied [48]. Hence, all terms including surface normal direction disappear and only three non-zero terms are left in the stress tensor. Since stresses in the normal direction of free surface is taken as zero, there are only two non-zero principal stresses are left to consider for this approximation.

As mentioned previously, loading case is one of the parameters for deciding the proper stress combination method. If the loading is multiaxial, proportionality of loading should be checked carefully to determine best fitted stress combination method. Biaxiality ratio, a_e and principal stress angle of maximum principal, φ_p are the two measures of proportionality.

$$a_e = \frac{\sigma_2}{\sigma_1} \tag{3.11}$$

In Equation (3.11), σ_1 is the maximum principal stress and σ_2 is the middle principal stress. σ_3 is taken as zero due to free surface conditions mentioned above.

If biaxiality ratio and principal stress angle do not vary much with varying loading, loading case can be named as proportional. On the contrary, if these parameters change much with varying loadings, it can be classified as non-proportional loading case. Behavior of biaxiality ratio and principal stress angle of near proportional and non-proportional multiaxial loading cases are shown in Figure 3.8 and Figure 3.9, respectively.

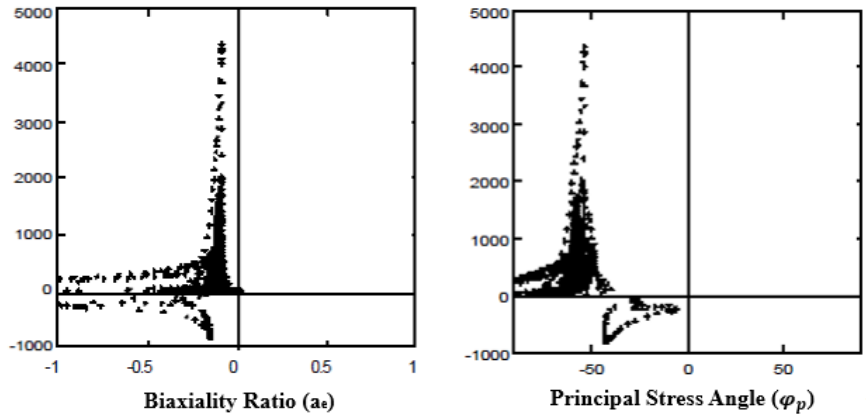

Figure 3.8 Near Proportional Response [31]

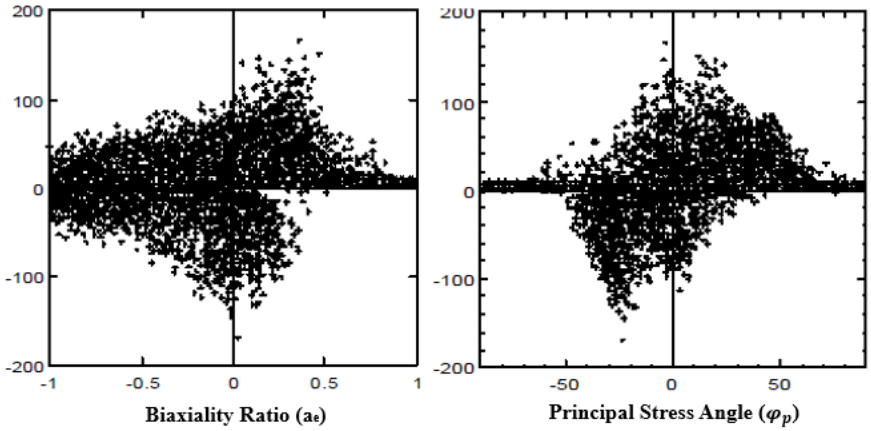

Figure 3.9 Non-proportional Response [31]

After determining the proportionality of stress state, Table 3.3 can be used for determining the proper stress combination method.

Table 3.3 Determination of Proper Stress Combination Method [31]

Stress State	**Principal Stress Angle, φ_p**	**Biaxiality Ratio, a_e**	**Combination Method**
Uniaxial	Constant	0	Uniaxial Theories
Multiaxial Proportional	Constant	$-1 < a_e < 1$ (Constant)	Equivalent Stress Theories
Multiaxial Non-proportional	May Vary	$-1 < a_e < 1$ (May Vary)	Critical Plane

3.1.1.7.1. Absolute Maximum Principal Theory

The absolute maximum principal stress can be defined as the largest principal stress in magnitude. This approach basically takes the maximum of three of the principal stresses for each time or frequency step depending on the analysis domain for combination of principal stresses.

$$\sigma_{AMP} = max(|\sigma_1|, |\sigma_2|, |\sigma_3|) \tag{3.12}$$

3.1.1.7.2. Equivalent von-Mises Theory

This method focuses on equivalent von-Mises stress for finding combined stress state. It uses all six local stress components as shown in Equation (3.13) to find an equivalent von-Mises stress.

$$\sigma_{eq}{}^2 = \sigma_x{}^2 + \sigma_y{}^2 + \sigma_z{}^2 - \sigma_x\sigma_y - \sigma_x\sigma_z - \sigma_y\sigma_z + 3\tau_{xy}{}^2 + 3\tau_{xz}{}^2 + 3\tau_{yz}{}^2 \tag{3.13}$$

Introducing a constant A matrix, the equivalent von-Mises stress can be expressed as follows in matrix form [38].

$$\sigma_{eq}{}^2 = Tr[A\sigma\sigma^T] \tag{3.14}$$

where,

$$A = \begin{pmatrix} 1 & -0.5 & -0.5 & 0 & 0 & 0 \\ -0.5 & 1 & -0.5 & 0 & 0 & 0 \\ -0.5 & -0.5 & 1 & 0 & 0 & 0 \\ 0 & 0 & 0 & 3 & 0 & 0 \\ 0 & 0 & 0 & 0 & 3 & 0 \\ 0 & 0 & 0 & 0 & 0 & 3 \end{pmatrix}$$

In Equation (3.14), σ and σ^T represent stress vector that includes six local stresses and its transpose, respectively. In addition, Tr stands for trace of the corresponding resulting matrix.

Using the above-mentioned equation and constant A matrix, equivalent stress can be found easily. This theory can be suitable for near proportional multiaxial cases as it is used to find an equivalent uniaxial stress state of the multiaxial stress states.

3.1.1.7.3. Critical Plane Theory

The critical plane approach is the best suitable option for multiaxial non-proportional loading cases. Basically, it searches for the most critical plane of corresponding critical location on the structure by increasing the plane angle. Since most of the fatigue damages occur in the free surfaces as mentioned before, it becomes applicable on 2-D.

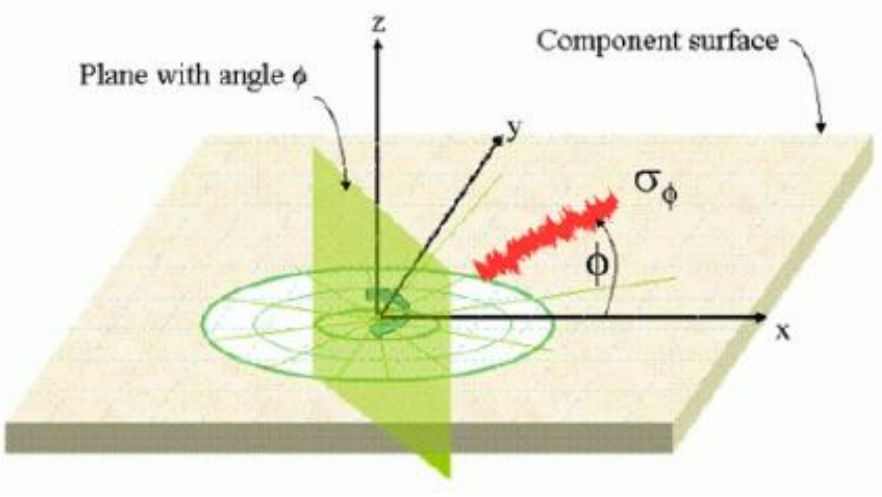

Figure 3.10 Representation of Critical Plane Search Method [48]

The combined stress on each searched plane can be calculated using Equation (3.15).

$$\sigma_{\varphi} = \frac{\sigma_x + \sigma_y}{2} + \frac{\sigma_x - \sigma_y}{2} cos2\varphi + \sigma_{xy} sin2\varphi \tag{3.15}$$

φ takes values between 0° and 170°. Generally, 10-degree intervals are used for not having a computationally heavy analysis.

The critical plane is defined as the plane with the most predicted fatigue damage. Since it searches all selected planes one by one, critical plane search method is computationally expensive and does not give fast results. However, it gives reliable results for both proportional and non-proportional multiaxial stress states.

3.1.2. Strain-Life (E-N) Approach

If loading conditions are hard enough to generate stresses higher than the yield strength of the materials, stress-life approach becomes inapplicable. Since yield strength is exceeded, significant amount of plastic deformation may occur. Fatigue life becomes shorter as loads are relatively large. Generally, failures under 10^3 cycles can be considered as in this category and it is known as the low-cycle fatigue.

3.1.3. Crack Propagation Approach

Different than the stress-life and strain-life approaches, crack propagation approach examines the life after an initial crack appears. The shape and the size of the crack should be known very well for implementing this approach. The growth of a crack can be predicted by using theories of Linear Elastic Fracture Mechanics.

3.2. Random Vibration Induced Fatigue

As mentioned before, main source of failures for materials used in military environments is dynamic loadings resulting from platforms' characteristics. Generally, these dynamic excitations exist as randomly fluctuating vibrations for engineering applications. Hence, random vibration induced fatigue becomes an essential topic to be covered carefully.

Random vibrations can be classified as non-deterministic excitations as they may change at every sample of taking data. In other words, in every turn that sample is taken, result is different for any time value. This means that random vibrations can only be represented truly using statistical methods. Although each individual data point has different vibration amplitude for different measurements, their statistical parameters such as mean, number of zero crossings and number of peaks are quite similar if data is taken for sufficient durations to represent the dynamic characteristics correctly.

The fatigue behavior of structures under random vibration excitation can be predicted using either time or frequency domain approaches. The procedure used for both analysis types is given in next chapters. Since frequency domain approach is implemented in the scope of this study, it is given more in detail, while time domain approach is explained briefly.

3.2.1. Time Domain Approach

Fatigue analysis in time domain is realized using transient analysis of FE model. Response of the system is acquired by applying random vibration excitation in time domain. In addition to FE analysis, stress response history can be obtained experimentally by using strain-gages at a particular critical location. Firstly, strain history is obtained directly from strain-gages and it is transformed into a stress history using Hooke's Law. After obtaining a time-stress history, proper cycle counting method is applied and stress-range histogram is obtained including mean stress information. Then, using Miner's rule, expected cumulative damage can be found. Generally, rainflow cycle counting method is used for cycle counting in time domain. The summary of the procedure is given below in Figure 3.11.

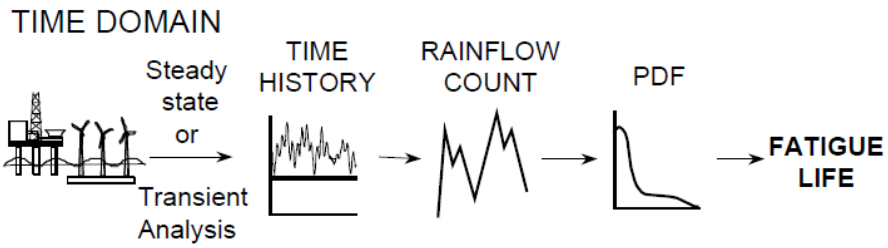

Figure 3.11 Time Domain Approach [32]

Time domain analysis can include all non-linearities in the structure since it uses transient analysis for solving the system. Although it gives quite good fatigue life results, solving each time step separately including non-linearities cause a time-consuming process. If the input changes for some reason, the system should be analyzed again from the starting point since analyses is completely time dependent. Therefore, time domain approach can be seen as computationally expensive method.

In addition to the computational burden, experimental procedure is also hard to implement. Since strain-gages are used to get stress response of the structure, they should be located exactly on the critical location which is very challenging. Since fatigue is very sensitive to the stress history, small differences that stem from placing the strain-gage can cause unexpected results.

To sum up, although it gives reliable fatigue life results, using time domain approach requires extensive effort and time. Any change in the geometry or input causes a start over which is very time-consuming.

3.2.2. Frequency Domain Approach

Frequency domain approach requires converting time data to frequency domain. Different from time domain approach, transfer function of the system is used for correlating input and stress history of the structures in frequency domain analysis. Using this transfer function obtained from FE analysis, stress response PSD of the critical location of the system is obtained. Then, using a proper cycle counting method such as Narrow-Band, Dirlik, Lalanne, Tovo-Benasciutti etc., Probability Density Function (PDF) is acquired. PDF is the way of representing occurrences of stress ranges in the history. Finally, expected cumulative damage and fatigue life is found using Miner's cumulative damage theory. The summary of the frequency domain approach procedure is given below in Figure 3.12.

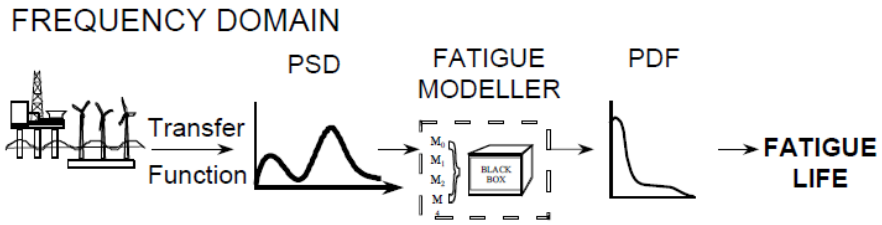

Figure 3.12 Frequency Domain Approach [32]

As mentioned above, frequency domain approach uses transfer function of the system which is acquired from FE analysis. This transfer function is obtained using harmonic analyses which is based on mode superposition method. Since modal analysis provides a basis for this harmonic analysis, obtained transfer function is linear. Hence, frequency domain approach does not include structural non-linearities. Since linear structural model is calculated, the structure must behave linearly, which is the case in most of the engineering applications [32].

Since frequency domain approach uses linear transfer function for calculating the response of the structure, it is much more time-efficient than time domain analysis. Linear transfer function is calculated only once and different load cases are related to that transfer function. Therefore, it does not require solving the system again for different load cases which makes it computationally efficient.

Signals in time domain can be transformed into frequency domain using Fourier Transform. Reverse can be implemented using Inverse Fourier Transform. If data is not continuous but in discrete form which is the case in most of the applications, process is called Fast Fourier Transform (FFT) and Inverse Fast Fourier Transform (IFFT). A simple representation of process is given below in Figure 3.13.

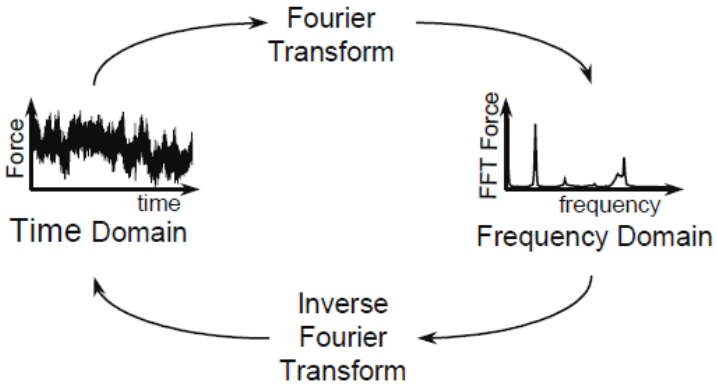

Figure 3.13 Representation of Fourier Transform [32]

The formulations for FFT and IFFT are given in Equation (3.16) and Equation (3.17), respectively.

$$y(f_n) = \frac{T_p}{N}\sum_{k} y(t_k)e^{i\left(\frac{2\pi n}{N}\right)k} \tag{3.16}$$

$$y(t_k) = \frac{1}{T_p}\sum_{n} y(f_n)e^{i\left(\frac{2\pi k}{N}\right)n} \tag{3.17}$$

In above-mentioned equations, T_p represents the period of $y(t_k)$ while N represents the number of data points.

Fourier transform basically decomposes any complex signal in time domain into the sine waves of different amplitudes and phases. This allows representing the complex signals in much simpler way in frequency domain. Figure 3.14 shows a clear representation of a complex signal which is decomposed to three sine waves in time and frequency domains. As can be seen from the figure, frequency domain plot includes only three vertical lines which shows the frequency content of the time signal.

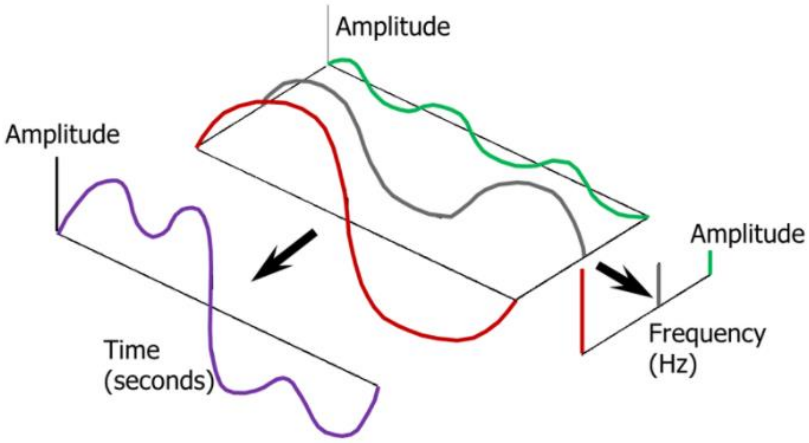

Figure 3.14 Time and Frequency Domain Representations of Complex Signal [49]

Generally, PSD is used for representing the random vibration data in frequency domain. The PSD represents the frequency content of any random time signals preserving their vibration amplitudes, without any phase information. In addition to PSD, Cross Power Spectral Density (CPSD) is used to correlate two PSDs to each other. PSD and CPSD are similar in behavior in general. However, CPSD includes phase differences in addition to the vibration amplitudes. PSD content of any time domain data can be obtained by taking the modulus squared of FFT and dividing by two times of the signal period as shown in Equation (3.18).

$$PSD = \frac{1}{2T_p}|FFT|^2 \tag{3.18}$$

One of the very useful statistical parameters that can help for characterizing the random signal is root mean square (RMS) value which is defined as square root of the area under the PSD curve. Figure 3.15 shows the schematic representation of a simple PSD. The area under each spike represents the mean square of the sine wave at corresponding frequency.

Figure 3.15 Schematic Representation of PSD [41]

Figure 3.16 shows different types of time histories and corresponding PSDs. As clearly understood from figure, a sine wave is represented with a single spike which is centered at its frequency and it has infinitely narrow width. In addition, broadband process involves different peaks covering wide range of frequencies while narrowband process involves these peaks in more spare frequency range. White noise is a special type of PSD that encounters same amount of energy at every frequency interval, then it appears as a single horizontal line.

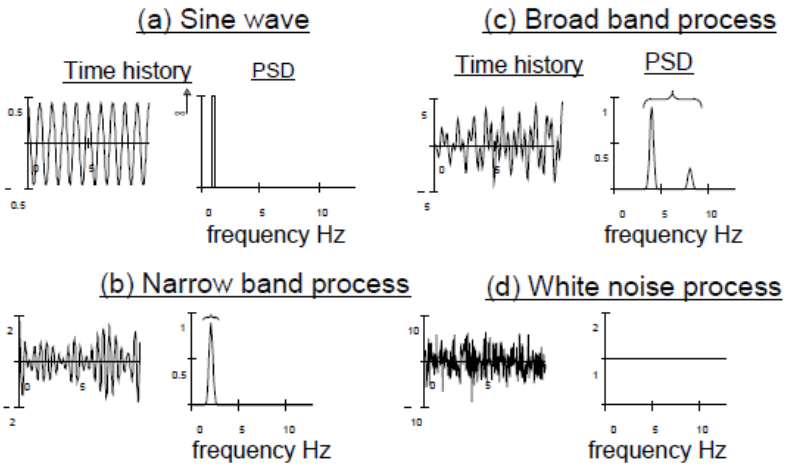

Figure 3.16 Time Histories and Corresponding PSDs [32]

As mentioned previously, a linear transfer function is used in the frequency domain approach for calculating the response of the system. This simple relation is shown below in Equation (3.19).

$$FFT_{rsp} = H(f).FFT_{inp} \tag{3.19}$$

where FFT_{rsp} and FFT_{inp} stand for the FFT of the response and FFT of the input, respectively. In addition, $H(f)$ represents the linear transfer function of the system in frequency domain.

Combining Equation (3.18) and Equation (3.19), PSD of the response can be written as given in Equation (3.22).

$$G_{rsp}(f) = \left(\frac{1}{2T_p}\right)\left(H(f).FFT_{inp}(f).H^*(f).FFT^*_{inp}(f)\right) \tag{3.20}$$

$$G_{rsp}(f) = H(f).H^*(f).G_{inp}(f) \tag{3.21}$$

$$G_{rsp}(f) = |H(f)|^2.G_{inp}(f) \tag{3.22}$$

In Equation (3.22), $G_{rsp}(f)$ and $G_{inp}(f)$ represent the PSD of response and PSD of input, respectively. $H^*(f)$ and FFT^*_{inp} stand for the complex conjugates of transfer function and FFT of input.

Since stress history is needed for fatigue life calculations, $G_{rsp}(f)$ should be in the form of stress while $G_{inp}(f)$ is in the form of acceleration. Therefore, transfer function should be determined carefully in correct units. Proper units for reaching stress response are given in Equation (3.23).

$$\frac{MPa^2}{Hz} = \left[\frac{MPa}{g}\right]^2 . \frac{g^2}{Hz} \tag{3.23}$$

Equation (3.22) is useful for uniaxial loading cases. If there exists a simultaneous multiaxial loading case, input is in the form of a 3x3 symmetrical matrix including PSDs in diagonal terms and CPSDs in off diagonal terms. Representation of input loading matrix is given below in Equation (3.24).

$$G_{inp}(f) = \begin{pmatrix} G_{xx}(f) & G_{xy}(f) & G_{xz}(f) \\ G_{yx}(f) & G_{yy}(f) & G_{yz}(f) \\ G_{zx}(f) & G_{zy}(f) & G_{zz}(f) \end{pmatrix} \tag{3.24}$$

It can be noted that the PSDs in the diagonal of input loading matrix are real, whereas CPSDs in the off diagonals are complex because of the phase differences between direct PSDs.

$H(f)$ can also be represented in matrix form containing transfer functions obtained from applying unity acceleration for x, y and z directions, separately.

$$H(f) = [H_x(f) \quad H_y(f) \quad H_z(f)] \tag{3.25}$$

Using matrices given for input and transfer functions, the response stress PSD can be calculated in matrix form using Equation (3.26).

$$G_{rsp}(f) = H^*(f).G_{inp}(f).H^T(f) \tag{3.26}$$

where $H^T(f)$ represents the transpose of the transfer function matrix, $H(f)$.

In addition to the matrix form given in Equation (3.26), the response stress PSD can also be introduced as given below in Equation (3.27) in more robust form.

$$G_{rsp}(f) = \sum_{i=x}^{z} \sum_{j=x}^{z} H_i(f).H_j^*(f).G_{ij}(f) \tag{3.27}$$

where $G_{ij}(f)$ represents the components of input matrix, $G_{inp}(f)$.

Obtaining the stress response PSD of the structure is one of the most important steps of frequency domain fatigue calculations. Stress PSD includes all important statistical parameters to characterize the random signal. For acquiring these statistical parameters, spectral moments of stress PSD are used. In theory, all spectral moments are needed to fully characterize the signal. However, generally, only first four spectral moments (m_0, m_1, m_2, m_4) are sufficient to compute required information used in subsequent fatigue analysis [32]. Spectral moments of response PSD can be found using Equation (3.28).

$$m_n = \int_0^{\infty} f^n.G_{rsp}(f)\,.df = \sum_{k=1}^{N} f_k^n.G_{rsp_k}(f).\delta f \tag{3.28}$$

where f, N and δf stand for frequency, number of data points and selected frequency interval, respectively.

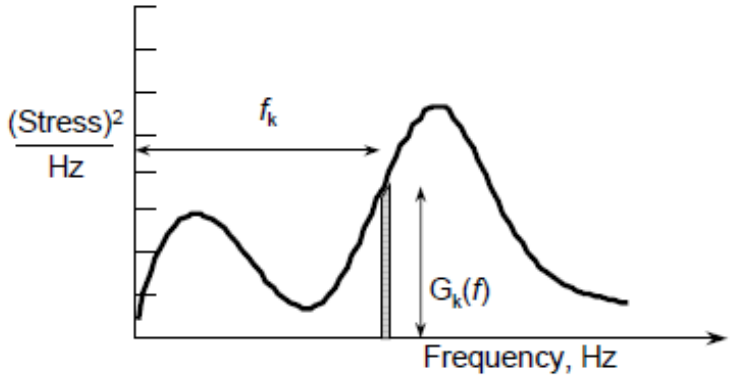

Figure 3.17 Representation of Spectral Moments Calculation [32]

Two of the most major statistical parameters that are used for classification of any random signals are expected number of upward zero crossings per second, $E[0]$ and expected number of peaks per second, $E[P]$. In 1954, S. O. Rice [24] proposed a relationship between spectral moments and these parameters which are given in Equation (3.29) and Equation (3.30).

$$E[0] = \sqrt{\frac{m_2}{m_0}} \tag{3.29}$$

$$E[P] = \sqrt{\frac{m_4}{m_2}} \tag{3.30}$$

Using $E[0]$ and $E[P]$, another useful parameter, irregularity factor, γ can be defined as in Equation (3.31). Irregularity factor is used for understanding whether the signal is narrowband or wideband. If the value is close to 1, the signal can be considered as narrowband. Otherwise, if it is close to 0, the signal is considered as wideband.

$$\gamma = \frac{E[0]}{E[P]} = \sqrt{\frac{m_2^2}{m_0 m_4}} \tag{3.31}$$

An example for demonstrating the concrete meaning of $E[0]$, $E[P]$ and γ is given in Figure 3.18. It can be noted that all these parameters are defined for one second time range as it is seen from the figure below.

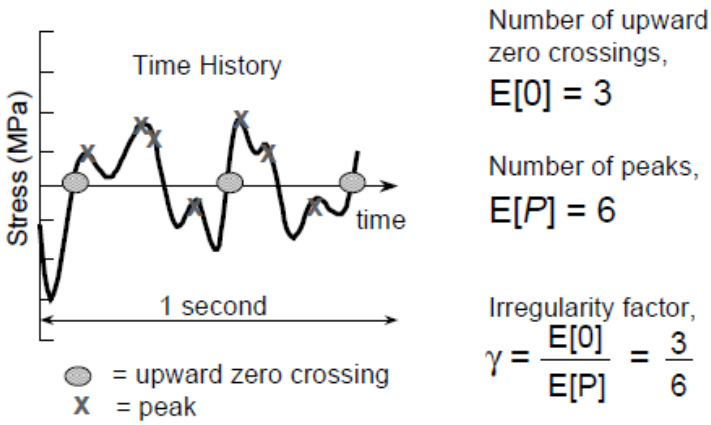

Figure 3.18 Upward Zero Crossings and Peaks [32]

In addition to the above-mentioned parameters, RMS and mean frequency, x_m are the other two statistical parameters.

$$RMS = \sqrt{m_0} \tag{3.32}$$

$$x_m = \frac{m_1}{m_0}\sqrt{\frac{m_2}{m_4}} \tag{3.33}$$

As demonstrated in Figure 3.12, the only step left for reaching the fatigue damage is calculating the PDF. It holds the information about occurrences of stress ranges in the stress history. PDF is another suitable way of representing the stress-range information and it is obtained from the stress-range histogram. The representation of a simple PDF is given below in Figure 3.19.

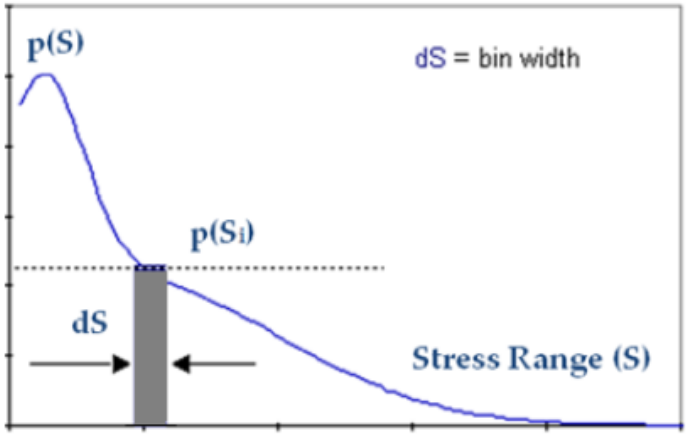

Figure 3.19 Representation of a Simple PDF [41]

The probability of stress ranges is occurring between $S_i - \frac{dS}{2}$ and $S_i + \frac{dS}{2}$ and it is described as $p(S)dS$ where dS represents the bin width.

There are lots of different methods for calculating the PDF, $p(S)$ which are proposed by Bendat as Narrow Band Method, Wirsching, Dirlik, Tovo-Benasciutti, Lalanne etc. These methods provide empirical solutions to reach a PDF basically from spectral moments and other statistical parameters of stress response PSD. Formulations of above-mentioned methods are given later in this chapter.

After obtaining the PDF using any of the cycle counting methods, the number of cycles at a particular stress level, $n(S)$ can be calculated using following equation.

$$n(S) = p(S).dS.S_t \tag{3.34}$$

where S_t stands for the total number of cycles in the history. S_t can also be represented as shown in Equation (3.35).

$$S_t = E[P].T \tag{3.35}$$

where $E[P]$ and T represent the number of peaks per second and exposure duration, respectively.

After acquiring the $n(S)$, Miner's Cumulative Damage Theory can be used for calculating the damages of individual stress ranges dividing the number of cycles at a particular stress level, $n(S)$ by the maximum number of cycles that material can withstand, $N(S)$. This parameter can be obtained from S-N curve as mentioned in previous chapters. Then, total expected damage, $E[D]$ can be found by summing all individual damages.

Equation (3.10) can be rewritten by inserting Equation (3.2), Equation (3.34) and Equation (3.35).

$$E[D] = \sum \frac{n(S)}{N(S)} = \int_0^\infty \frac{E[P].T.p(S).dS}{C.S^{-b}} = \frac{E[P].T}{C} \int_0^\infty S^b.p(S).dS \tag{3.36}$$

Equation (3.36) represents the final form of calculating the total expected damage. It should be noted that stresses can be defined either using alternating stresses or stress ranges. Both $n(S)$ and $N(S)$ must be in the same notation to calculate the expected damage properly. Generally, alternating stresses are used in S-N curves while PDF holds the information of stresses as ranges. Therefore, one must be converted to another before applying Miner's Theorem. Moreover, as shown above, integral is shown to have infinite limit which is not suitable for having numerical calculations. For this reason, proper integral limit should be determined. It is set to 3 RMS for alternating stresses and 6 RMS for stress ranges in general [31].

Setting the $E[D]$ equal to 1 in Equation (3.36) means that fatigue failure occurs and T becomes the fatigue life of the material in that case.

In order to use Equation (3.36), $p(S)$ should be calculated using any of the proper cycle counting approaches. Bendat [25] proposes Narrow Band Approach which gives conservative results for wideband signals. The reason for this is that Bendat assumes all peaks and valleys on wideband signal are matched with corresponding negative peaks of similar magnitude. This is illustrated clearly in Figure 3.20. This increases number of positive and negative peaks extensively and damage becomes exaggerated.

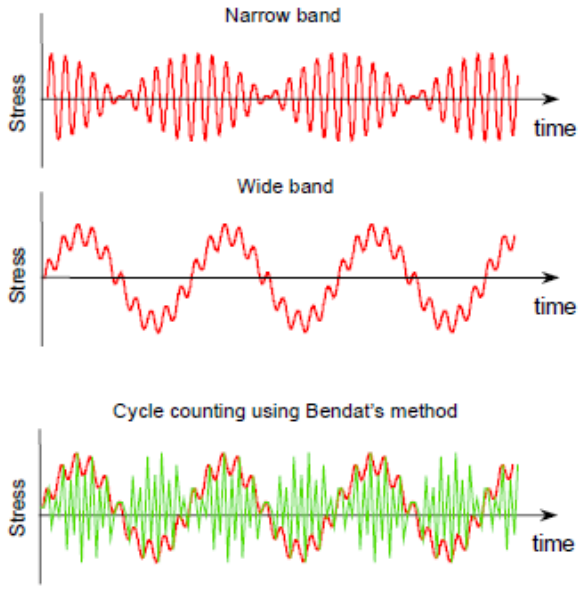

Figure 3.20 Representation of Bendat's Conservatism [33]

PDF obtained using Narrow Band Approach is given in Equation (3.37).

$$p(S) = \frac{S}{4m_0} e^{\left(\frac{-S^2}{8m_0}\right)} \tag{3.37}$$

Since Narrow Band Method gives conservative fatigue life results for wideband signals, many studies are conducted to correct this conservatism. One of these studies is conducted by Wirsching [26] who is used an empirical correction factor, ρ_{WL} to correct the conservatism of Bendat's approach.

$$E[D]_{WL} = \rho_{WL}.E[D]_{NB} \tag{3.38}$$

where $E[D]_{WL}$ and $E[D]_{NB}$ represent the cumulative damage for Wirsching and Narrow Band approaches, respectively.

$$\rho_{WL} = a(k) + [1 - a(k)](1 - \varepsilon)^{b(k)} \tag{3.39}$$

where k represents the slope of S-N curve while $a(k)$ and $b(k)$ are named as the best fitting parameters that are defined as function of k. In addition, ε is defined as the spectral width parameter.

$$\begin{aligned} a(k) &= 0.926 - 0.033k \\ b(k) &= 1.587k - 2.323 \\ \varepsilon &= \sqrt{1 - \alpha_2^2} \end{aligned} \tag{3.40}$$

where α_i is defined as the spectral width and it is defined as given in Equation (3.41).

$$\alpha_i = \frac{m_i}{\sqrt{m_0 m_{2i}}} \tag{3.41}$$

Another simple correction method that is based on Bendat's Narrow Band solution is proposed by Benasciutti and Tovo [50] and it is known as $\alpha_{0.75}$ Method.

$$E[D]_{AL} = \alpha_{0.75}^2 . E[D]_{NB} \tag{3.42}$$

where $E[D]_{AL}$ stands for cumulative damage acquired by having $\alpha_{0.75}$ Method. The constant, $\alpha_{0.75}$ can be found using the relation given in Equation (3.41).

Tovo and Benasciutti [34] [35] proposed another correction method by again building their work around Bendat's solution. This cycle counting method is known as Tovo-Benasciutti Method.

$$E[D]_{TB} = [b + (1 - b)\alpha_2^{k-1}]\alpha_2 . E[D]_{NB} \tag{3.43}$$

where $E[D]_{TB}$ represents the cumulative damage acquired by Tovo-Benasciutti Method. b is an unknown constant which is approximated by numerical simulations. It can be found using the equation below.

$$b = \frac{(\alpha_1 - \alpha_2)\left[1.112\left(1 + \alpha_1\alpha_2 - (\alpha_1 + \alpha_2)\right)e^{2.11\alpha_2} + (\alpha_1 - \alpha_2)\right]}{(\alpha_2 - 1)^2} \tag{3.44}$$

The next empirical approach for obtaining PDF is proposed by Dirlik [30] without using Bendat's Narrow Band solution. Dirlik's approach is accepted as one of the most robust methods which is suitable for both narrowband and wideband signals [33].

$$p(S) = \frac{1}{2\sqrt{m_0}}\left[\frac{D_1}{Q}e^{\frac{-Z}{Q}} + \frac{D_2 Z}{R^2}e^{\frac{-Z^2}{2R^2}} + D_3 Z e^{\frac{-Z^2}{2}}\right] \tag{3.45}$$

where D_1, D_2, D_3, Q and R are the constants that are functions of spectral moments while Z is function of spectral moments and given stress level together.

$$\begin{aligned} D_1 &= \frac{2(x_m - \gamma^2)}{1+\gamma^2} \qquad D_2 = \frac{1-\gamma-D_1+D_1^2}{1-R} \qquad D_3 = 1 - D_1 - D_2 \\ Q &= \frac{1.25(\gamma - D_3 - D_2 R)}{D_1} \qquad R = \frac{\gamma - x_m - D_1^2}{1-\gamma-D_1+D_1^2} \qquad Z = \frac{S}{2\sqrt{m_0}} \end{aligned} \tag{3.46}$$

Lalanne [36] proposed an empirical method that is useful and efficient for both narrowband and wideband signals. It is also accepted as a robust method as Dirlik's solution.

$$p(S) = \frac{1}{2\sigma}\left\{\frac{\sqrt{1-\gamma^2}}{\sqrt{2\pi}}e^{\frac{-S^2}{8\sigma^2(1-\gamma^2)}} + \frac{S\gamma}{4\sigma}e^{\frac{-S^2}{8\sigma^2}}\left[1 + \text{erf}\left(\frac{S\gamma}{2\sigma\sqrt{2(1-\gamma^2)}}\right)\right]\right\} \tag{3.47}$$

where $\text{erf}(x) = \frac{2}{\sqrt{\pi}}\int_0^x e^{-t^2}dt$ and σ represents the RMS of the stress response PSD.

3.3. Accelerated Life Testing

Life testing is one of the most reliable ways of validating the safety of the structure for operational usage. It is essential to guarantee that the material withstands the vibration loadings that emerge due to harsh environmental conditions throughout its service life. This can be ensured by simulating the vibration loads in laboratory conditions by shakers. However, it is not possible to realize these kinds of tests for long service life. Instead, accelerated life testing phenomenon is used for simulating real life conditions by scaling the loadings that can be applied for shorter and logical durations. Accelerated life testing enables to realize real life conditions by having the same damage capability on system. This is achieved by increasing the amplitudes of loadings.

For having an accelerated life testing, accelerated input should be found. For this reason, Fatigue Damage Spectrum (FDS) is used for the synthesis of the vibration loadings. FDS shows the cumulative damage that is caused by random responses of a series of Single Degree of Freedom (SDOF) systems with different natural frequencies [51].

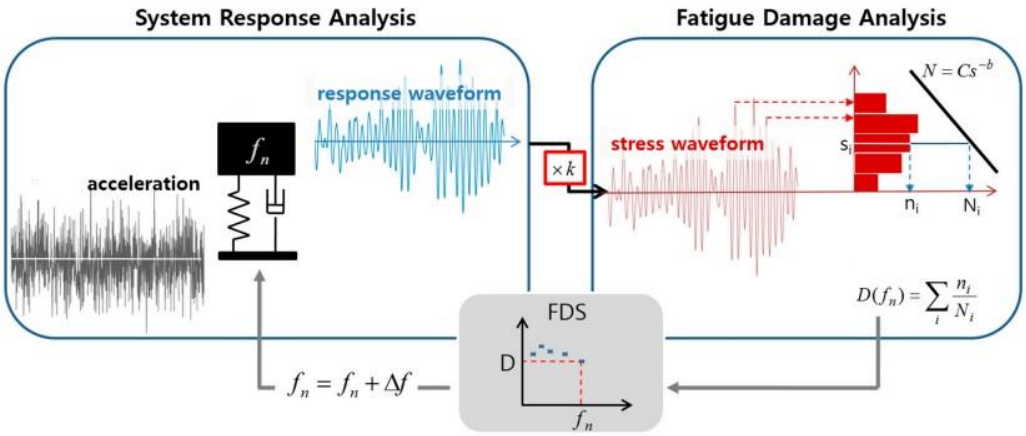

Figure 3.21 Flowchart of FDS [51]

Figure 3.21 shows that fatigue damage analysis procedure which is mentioned in detail in Chapter 3.2.2, is repeated for varying resonant frequencies and FDS is obtained. Hence, FDS is a function of natural frequency. The formulation for FDS is given below in Equation (3.48).

$$D(f_n) = \frac{f_n T}{C}\left[\frac{G(f_n)k^2}{8\pi f_n \zeta}\right]^{b/2} \Gamma[1 + b/2] \tag{3.48}$$

where Γ is the gamma function that is given as $\Gamma(x) = \int_0^\infty e^{-t}t^{x-1}dt$. f_n, k, ζ and T represent the resonant frequency, spring stiffness, damping ratio and duration, respectively. Moreover, C and b stand for the S-N curve parameters. If all constants in the Equation (3.48) are gathered together, remaining term, other than constant value, is called Damage Potential (DP) [52] and it is given as in Equation (3.49).

$$DP(f_n) = f_n T\left[\frac{G(f_n)}{f_n \zeta}\right]^{b/2} \tag{3.49}$$

DP can be used for synthesis of vibration loadings. Since fatigue damage is based on the cumulative effect of individual damages, total DP can be obtained by simply summing up individual damage potentials [51].

$$DP_{total}(f_n) = DP_1 + DP_2 + \cdots + DP_N = \sum_{i=1}^{N} DP_i(f_n) \tag{3.50}$$

Then, test PSD can be obtained by writing the Equation (3.49) in inverse form.

$$G_{test}(f_n) = f_n \zeta \left[\frac{DP_{total}(f_n)}{f_n T_{test}}\right]^{2/b} \tag{3.51}$$

Equation (3.51) means that the test PSD of G_{test} must be used to apply a total damage of DP_{total} in T_{test} seconds. Combining Equation (3.49), Equation (3.50) and Equation (3.51) gives the test PSD in simplified form.

$$G_{test}(f_n) = f_n \zeta \left[\sum_{i=1}^{N} \frac{T_i}{T_{test}} \left(\frac{G_i(f_n)}{f_n \zeta}\right)^{b/2}\right]^{2/b} = \left(\sum_{i=1}^{N} \frac{T_i (G_i(f_n))^{b/2}}{T_{test}}\right)^{2/b} \tag{3.52}$$

Equation (3.52) can be rewritten in much clear form as follows,

$$G_{test} = \left(\frac{T_1 G_1^{b/2} + T_2 G_2^{b/2} + \cdots + T_N G_N^{b/2}}{T_{test}}\right)^{2/b} \tag{3.53}$$

Equation (3.53) can be used for finding accelerated test PSD profile combining different PSDs together.

Since it is influenced by different parameters as the mean stress, the surface finish, the treatment etc., b is not directly equal to the slope of S-N curve. Hence, it is replaced with another constant m in MIL-STD-810G. It suggests that $m = 7.5$ is commonly used for random environments [53]. As mentioned before, accelerated the input increases the vibration amplitudes which means a raise in resultant stress levels. It should be noted that accelerating the input such that stress levels exceed the yield strength of material may cause an unexpected fatigue behavior. Exceeding the yield strength means plastic strains emerge and it is the topic of strain life approach. Therefore, resultant stress levels should be checked carefully before using the accelerated input for testing.

4. CONSTRUCTION OF FE MODEL

Construction of correct FE model of the structure is one of the most critical stages of the study. Accurate FE modeling is necessary since all fatigue calculations are conducted relying on the previously created FE model. The electronic unit to be analyzed during this thesis consists of electronic cards, electronic box and mounting brackets. Since using real electronic cards during tests is not feasible, dummies are designed and manufactured. In design stage of dummy electronic cards, mass, center of gravity and moments of inertia values of real cards are carefully examined and they are tried to be preserved as much as possible in the dummies. This has a major role for having an accurate fatigue analysis, since it directly affects dynamic behavior of the assembly. The 3D model of the assembly is created using PTC Creo and it can be seen in figure given below.

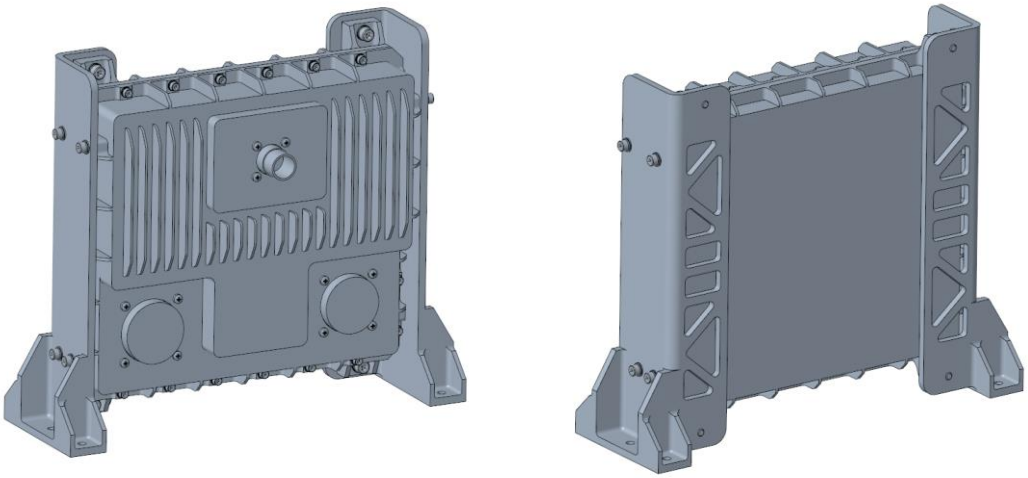

Figure 4.1 3D Model of the Assembly

After 3D model is created with dummies, model is transferred into ANSYS 2020 R2 which has a compatible nCode DesignLife version. In ANSYS Workbench module, all parts including dummy electronic cards are assigned aluminum 6061-T6. The material properties of aluminum 6061-T6 are given in Table 4.1.

Table 4.1 Material Properties of Aluminum 6061-T6

Density	2849 kg/m^3
Young's Modulus	68.9 GPa
Poisson's Ratio	0.33
Ultimate Tensile Strength	310 MPa
Yield Strength	276 MPa

In addition to the electronic unit, the base structure that the unit is mounted is created in SpaceClaim for proper modeling of the mounting screws. Detailed information about screw modeling will be given in next chapters. Since the main target is dealing with the mounting brackets but not the electronic unit itself, unnecessary screw holes and gasket groove on the unit is removed using SpaceClaim for having better mesh quality. The analysis model and coordinate system can be seen in Figure 4.2.

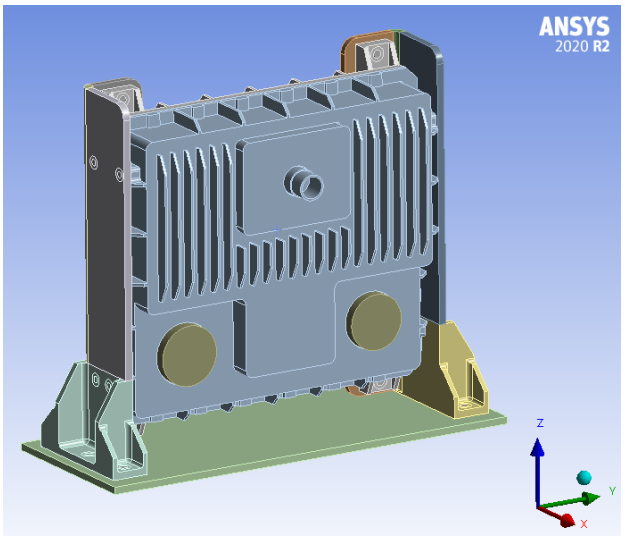

Figure 4.2 FE Model and Coordinate System

The coordinate system used in FE model matches with the coordinates used in the experiments. All axis notations used in experiments and analysis are coherent with coordinate system shown in Figure 4.2.

4.1. Modeling of Screws and Material Contacts

For having simpler FE model, 3D models of the screws are not included in model used in ANSYS. Instead, beam elements are used to model true behavior of the mounting parts. Since the local dynamic responses inside of the electronic unit are not the point of interest, screws inside the unit are not modeled. Bonded contact is defined inside electronic unit for mounting the electronic cards. Screws that are used for connecting brackets to electronic unit are modeled with deformable steel beam elements while screws that are used for connecting brackets to base structure are modeled with rigid steel beam elements. Beam element requires reference and mobile scopes for connecting two parts. For this reason, effective washer surface area and inner surface area of the corresponding hole is used for defining the beam elements as shown in Figure 4.3.

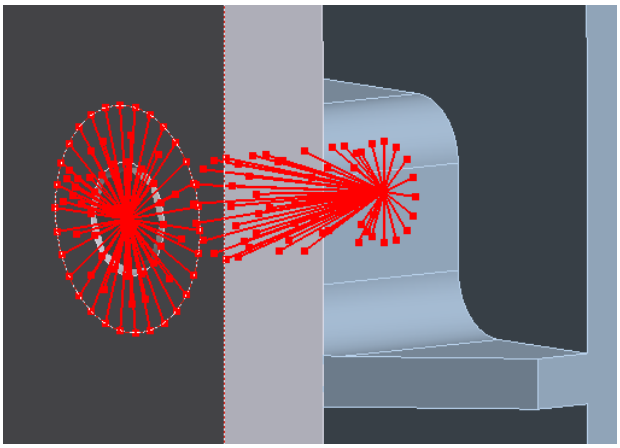

Figure 4.3 Beam Element Modeling

The other critical parameter for constructing the FE model is defining the contacts between parts in assembly. Although there are many types of contacts available in ANSYS, only linear contact types (bonded and no separation) can be used in modal analysis. Contact type and contact area have direct effect on natural frequencies of the structure as it affects dynamic behavior. Therefore, correct modeling of contact types and contact areas is very essential. Detailed information about iterations made for verification of the model will be given in next chapters. Having a lot of trials, optimized combination of contacts that represents the real behavior of the structure is figured out. Contacts between back faces of brackets and unit are modeled as bonded, while contacts between lateral faces of brackets and units are modeled as no separation. In addition, contacts between brackets and base are modeled as bonded. All contacts between brackets-electronic unit and between brackets-base are shown in Figure 4.4, Figure 4.5 and Figure 4.6, respectively.

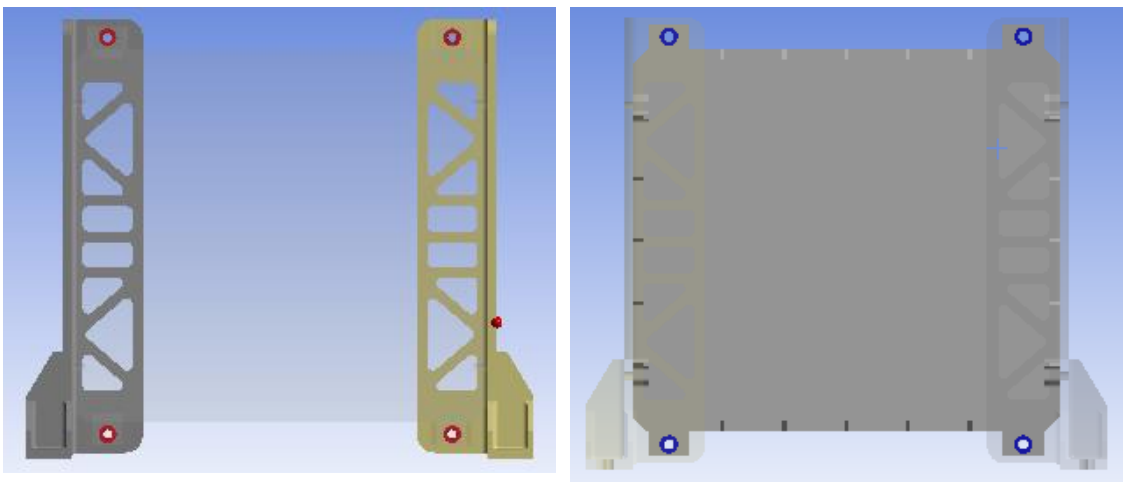

Figure 4.4 Contact Between Back Side of Brackets and Electronic Unit

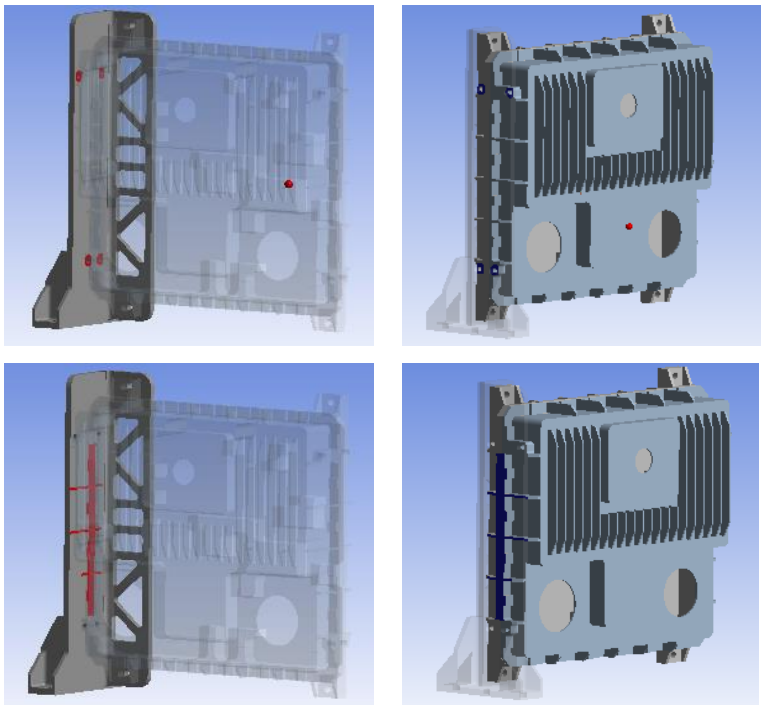

Figure 4.5 Contact Between Lateral Side of Brackets and Electronic Unit

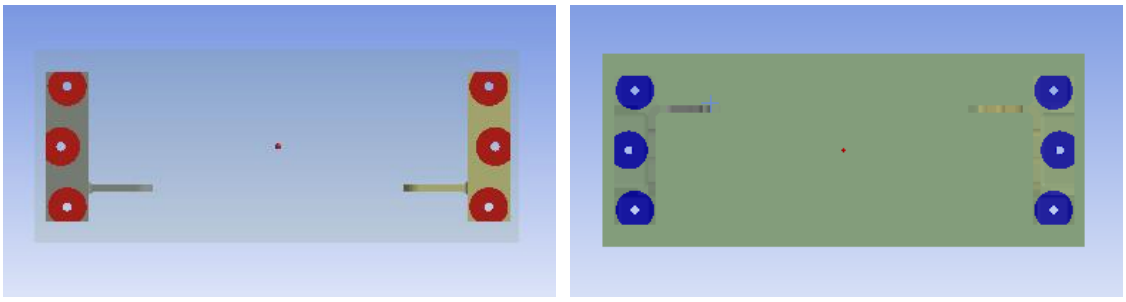

Figure 4.6 Contact Between Brackets and Base

4.2. Meshing of Structure

Proper meshing has a major role on getting accurate results. Especially on complex geometries as assemblies, this becomes more challenging issue. Generally, using default meshing of ANSYS in complex geometries without any adjustment results in meshing with tetrahedral elements. However, these types of elements may be ineffective in terms of solution times. In addition, with their sharp edges, tetrahedrons may act like stress concentration elements and can cause higher stresses than reality.

Electronic unit and cards are meshed with tetrahedrons and higher element sizes since they are not point of interest. Also, they do have a negligible effect on fundamental natural frequencies of the structure. On the other hand, brackets are paid more attention while meshing to have better mesh quality.

Brackets have complicated geometry to be meshed with sweep or hexahedral element types. In order to generate these types of meshes in critical local areas, brackets are split into different parts using SpaceClaim. This allows for meshing different bodies separately with desired mesh type. Splitting brackets into many components and combining them again by using shared topology do not change the dynamic behavior at all. Using shared topology, nodes on different components are connected to each other and this allows structure to act as a single geometry.

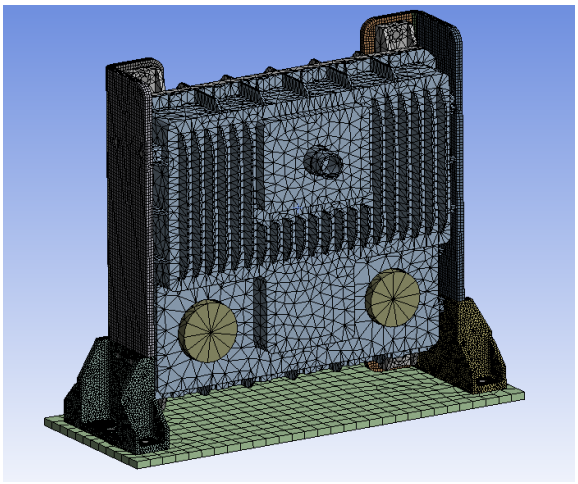

Figure 4.7 Meshing of Whole Structure

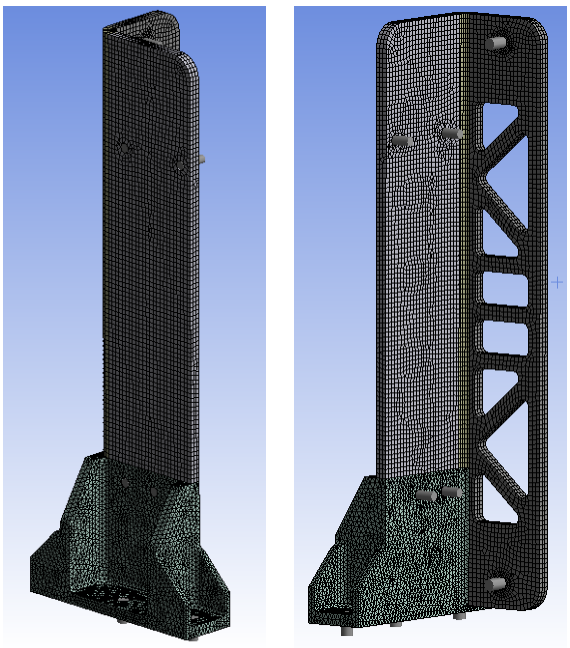

Figure 4.8 Meshing of Brackets

As mentioned previously, using sweep and hexahedral mesh type where it is possible results in lowering analysis times and increasing mesh quality. Therefore, in potential critical areas, smaller mesh sizes are used as shown in Figure 4.9.

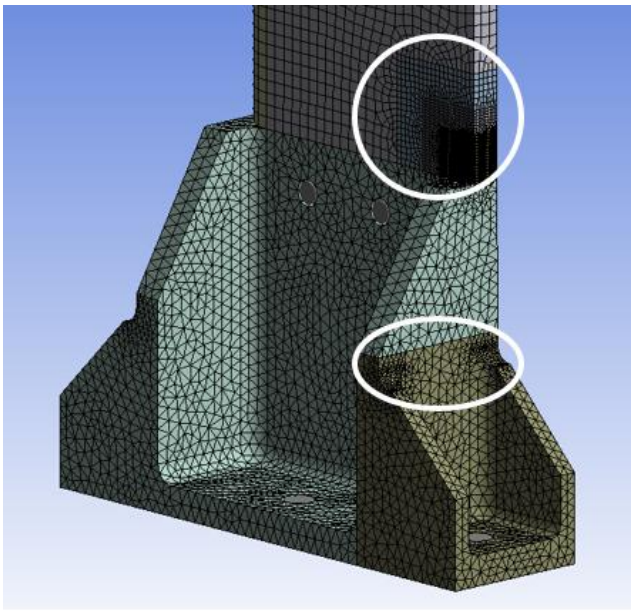

Figure 4.9 Local Areas with Smaller Mesh

Since electronic units and cards are meshed roughly for not being a burden to FE analysis, brackets have higher mesh quality than the whole structure. Mesh statistics of the whole structure and brackets can be seen below in Table 4.2.

Table 4.2 Mesh Statistics

Meshed Portion	Element Quality	Number of Elements	Number of Nodes
Brackets	83.54 %	223784	604138
Whole Structure	78.05 %	258084	674384

4.2.1. Mesh Convergence Analysis

One of the biggest issues in FE analysis of the structures is dealing with singularities. In most of the analyses with complicated installation scenarios, singularity arises. The possible locations for that phenomenon are split faces, sharp edges or hole edges. This condition should be carefully handled for not having unexpected results. Normally, stresses in the specific locations should converge to a true value while mesh size is getting smaller and results should be free from mesh size. However, this will not be the case when singularity appears.

In all of the analyses, getting the correct stresses are essential. However, fatigue is even more sensitive to stresses since it directly uses the nodal stress results. Therefore, stress history of the corresponding critical node should be acquired attentively.

Mesh convergence analysis will be performed on high-stress locations on structure and these locations are found running random vibration analysis in all three directions. Amplitude of 0.005 g^2/Hz white noise base excitation is applied in 10-2000 Hz frequency range as an input. When the result is examined, it is obviously seen that the x-direction is the most critical one among all three axes. High-stress locations on the structure when the system is excited in x-direction can be seen below in Figure 4.10.

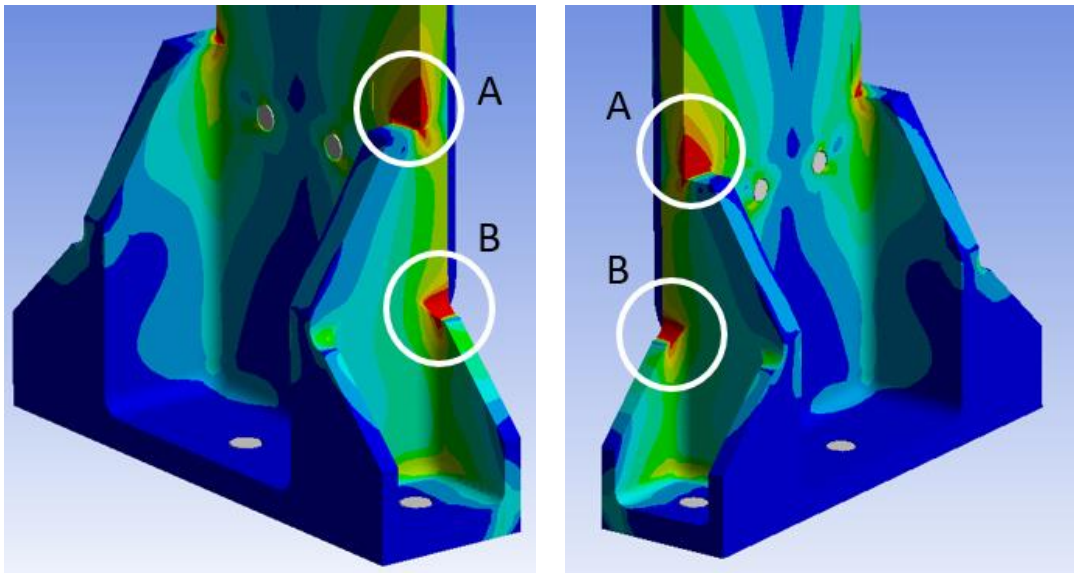

Left Bracket Right Bracket

Figure 4.10 High Stress Locations on Brackets (X-axis Excitation)

The above shown locations are the most critical ones in the structure. The left bracket has slightly higher stresses than the right bracket. Then, the stresses in left bracket are analyzed according to the mesh convergence. 'Location A' includes sharp edge and it is a potential singularity point. Mesh sizes are refined in these locations locally, starting from 2 mm to 0.25 mm. The path is drawn starting from 6 mm above from the sharp edge in corresponding sizes.

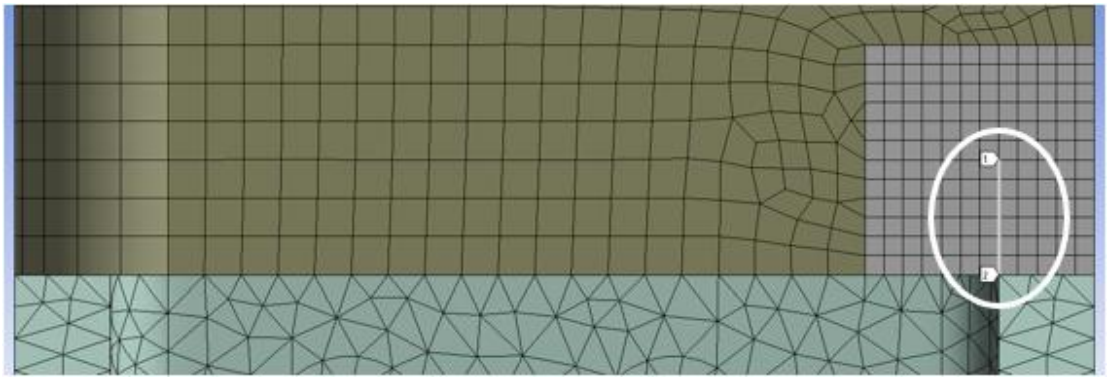

Figure 4.11 Path in 1 mm Mesh Size

When graphically represented as in Figure 4.12, it is clearly seen that the stresses on sharp edge do not converge to a specific value. Then, stresses at that point are not trustable.

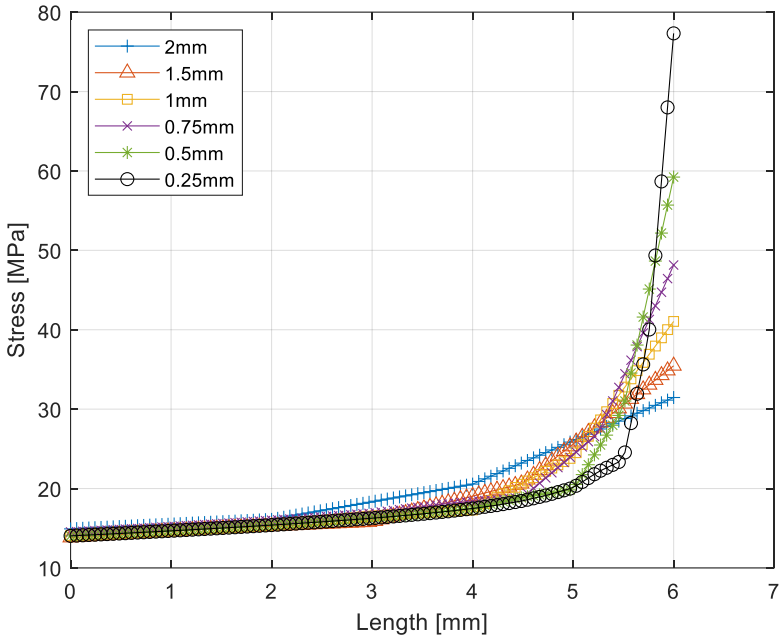

Figure 4.12 Stress Results for Different Mesh Sizes in 'Location A'

The other potential critical area that can be seen from Figure 4.10 is 'Location B'. Stresses in that location are examined in the same way by refining a mesh size locally. Since there is a fillet, it is not expected to have singularity here. Stress values in different mesh sizes clearly converge after 1 mm mesh size and it reflects the true value. Results are tabulated below.

Table 4.3 Stress Results for Different Mesh Sizes in 'Location B'

Mesh Size [mm]	**Maximum Stress at 'Location B' [MPa]**	**Difference Between Previous [%]**
2	22.68	-
1.5	23.31	2.8
1	24.95	7
0.75	25.22	1.1
0.5	25.60	1.5
0.25	25.81	0.8

Although there exists a singularity at sharp edge of 'Location A', there can still be higher stresses than maximum converged stress at 'Location B'. This should also be checked out very carefully not to be mistaken.

Figure 4.12 shows that the slope of the convergence graph changes at specific locations for different mesh sizes. The slope of the 0.25 mm mesh size graph changes dramatically at about 5.5 mm and this slope leads the divergence. Then, the stress just before this slope change can be taken into consideration. If stress at that location is compared with the one in 'Location B', it can be noticed that higher stresses without singularity appear in 'Location A', 0.5 mm above the sharp edge even stresses are very close to each other. Therefore, critical node of the brackets which is node 530142 in the left bracket is selected in 'Location A' as shown in Figure 4.13.

Table 4.4 Comparison of Maximum Stresses without Singularity

Mesh Size [mm]	Maximum Stress at 'Location A' [MPa]	Maximum Stress at 'Location B' [MPa]
2	25.54	22.68
1.5	28.03	23.31
1	30.21	24.95
0.75	30.02	25.22
0.5	29.80	25.60
0.25	26.10	25.81

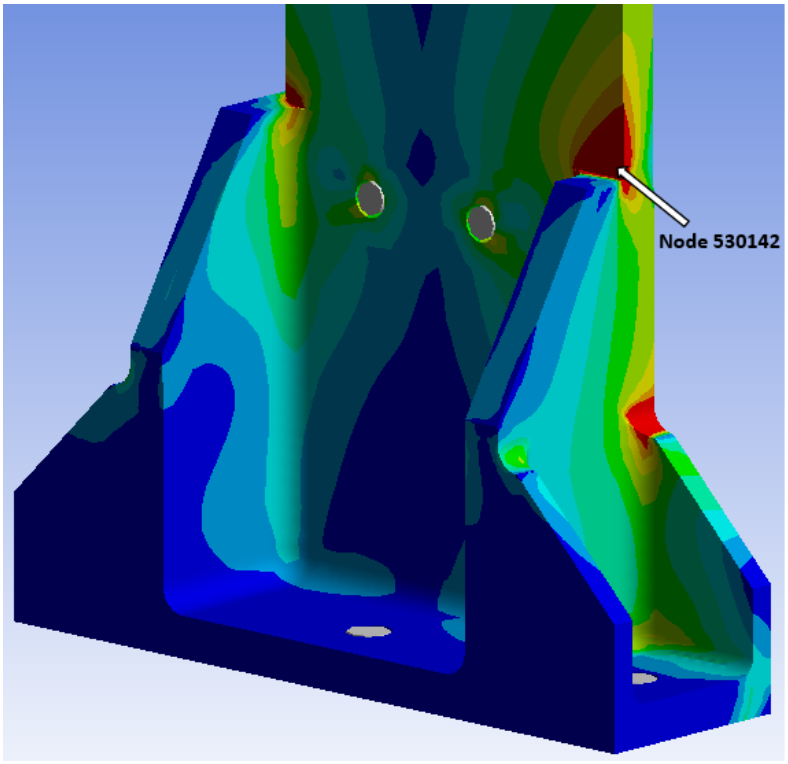

Figure 4.13 Location of Critical Node on Left Bracket (ID: 530142)

5. VERIFICATION OF FE MODEL

Since created FE model will be used in all steps of the theoretical analyses, it is crucial to verify the model with experimental analysis. Dynamic behavior of the structure should be represented decently in the FE model to get similar responses under the same loadings. As it is stated in previous chapters, fatigue calculations are very sensitive to the stress responses and damping ratios of the corresponding critical modes. Therefore, these parameters should be clarified using the experimental results.

Verification of FE model can be experienced by comparing the natural frequencies taken from experiments and ANSYS Modal Analysis. However, relying only on the coincidence of the natural frequencies may be deceptive. Modal damping values have a major role on the response of the structure. Then, in addition to the natural frequencies, peaks of the transmissibility curves should be close enough to get correct dynamic response. For this reason, acceleration transmissibility curves obtained from experiments are compared with transmissibility curves found by using ANSYS Harmonic Response Analysis.

In order to obtain a correct FE model, some geometric parameters need to be updated. The changeable parameters are contact types, contact areas and beam behaviors used in the analysis model. These alterations are realized in a controlled manner to be able to understand the sensitivity of modes to each specific change. Natural frequencies and transmissibility curves are compared for each iteration. At the end of the updating, optimum parameter set that gives the closest results with experimental modal testing is chosen. Detailed information about updated parameters will be given in Chapter 5.2.

5.1. Modal Testing

As mentioned before, the main idea of modal testing is to define dynamic behavior of the system by getting acceleration responses and transmissibility curves. Acceleration responses are taken in terms of PSDs.

For testing purposes, all previously designed parts as brackets, dummy electronic unit and cards are manufactured. All parts are assembled together properly and got ready for experimental analysis.

Totally, four accelerometers are placed on structure. Two of them are placed on sides of the brackets where maximum deflections are expected to be occurred. This results in reading the responses more clearly. The other two is placed on electronic unit where individual modes of chassis or internal components do not disturb the modes of brackets. In addition to the accelerometers on the structure, one more accelerometer is placed on vibration table for checking the shaker's input. Preliminary modal analysis is performed on ANSYS to place accelerometers correctly, avoiding from nodal points. Accelerometer locations are shown in Figure 5.1.

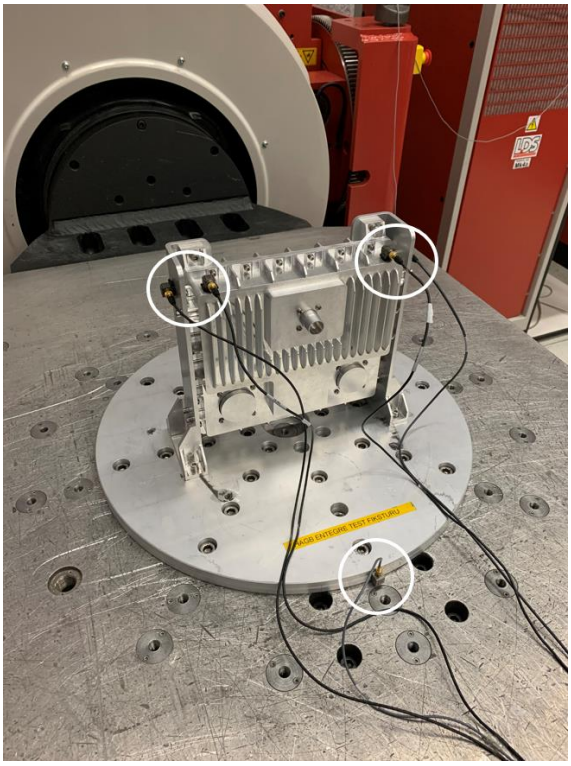

Figure 5.1 Accelerometer Locations

Software and equipment that are used in the experiments are listed below with their models and types in Table 5.1.

Table 5.1 Software and Equipment Used in Experiment

Software	Pulse Labshop 16.1
Electrodynamic Shaker	LDS V8-440
Data Acquisition Unit	Brüel & Kjaer 3560C
Accelerometers	Brüel & Kjaer Type 4507B and Type 4524B

Tests are performed in two directions using white noise inputs with variety of amplitudes. The white noise with an amplitude of 0.002 g^2/Hz applied in 10-2000 Hz frequency range is used for verification of FE model. Tests with other inputs are performed for checking the linearity of the system and detailed information will be given in later chapters. Test configurations are shown in Figure 5.2. As mentioned before, test directions are configured to be compatible with directions in FE model.

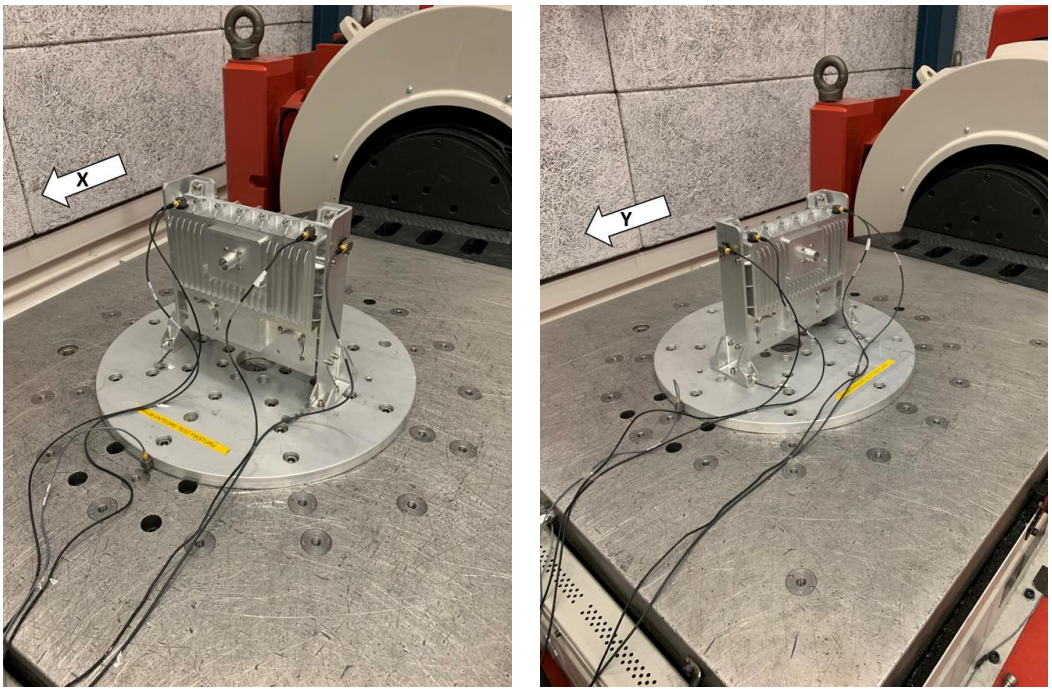

Figure 5.2 Test Directions

Attained acceleration responses as means of PSDs and transmissibility curves for an amplitude of 0.002 g^2/Hz white noise input in two directions are given in Figure 5.3, Figure 5.4, Figure 5.5 and Figure 5.6, respectively. It can easily be seen from the plots that there exists a breakdown on data from accelerometer mounted on right side of the chassis when the system is excided in y direction. This data does not seem proper and will not be used in further analysis.

Since there is one mode dominant on x direction, horizontal axis of plots belong to x-axis excitation is limited up to 500 Hz. Similarly, there are two modes dominant on y direction, horizontal axis of plots belong to y-axis excitation is limited up to 1000 Hz.

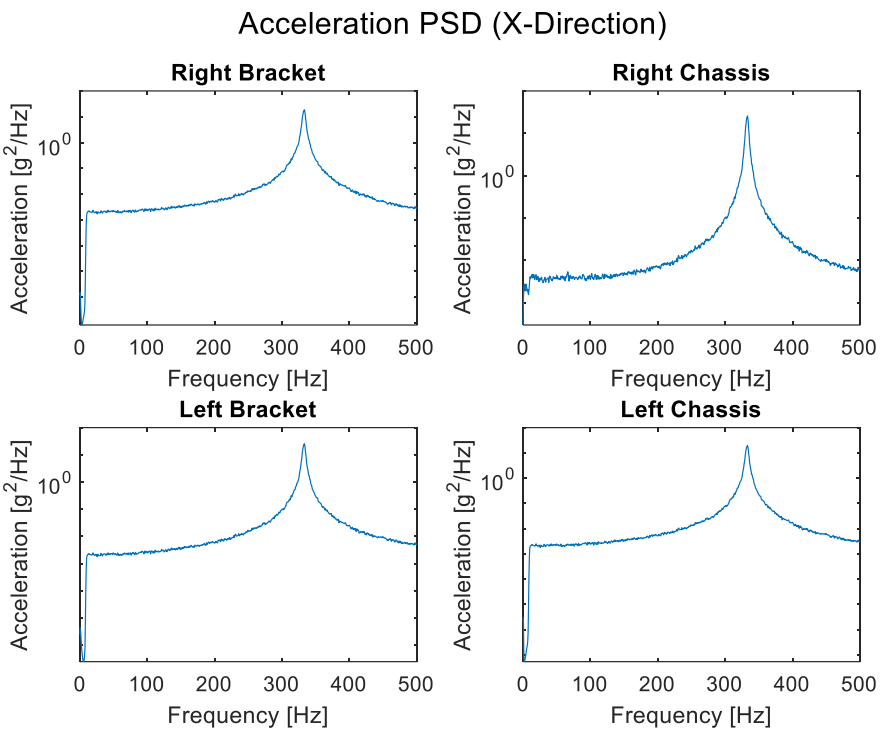

Figure 5.3 Acceleration PSDs (X-Direction)

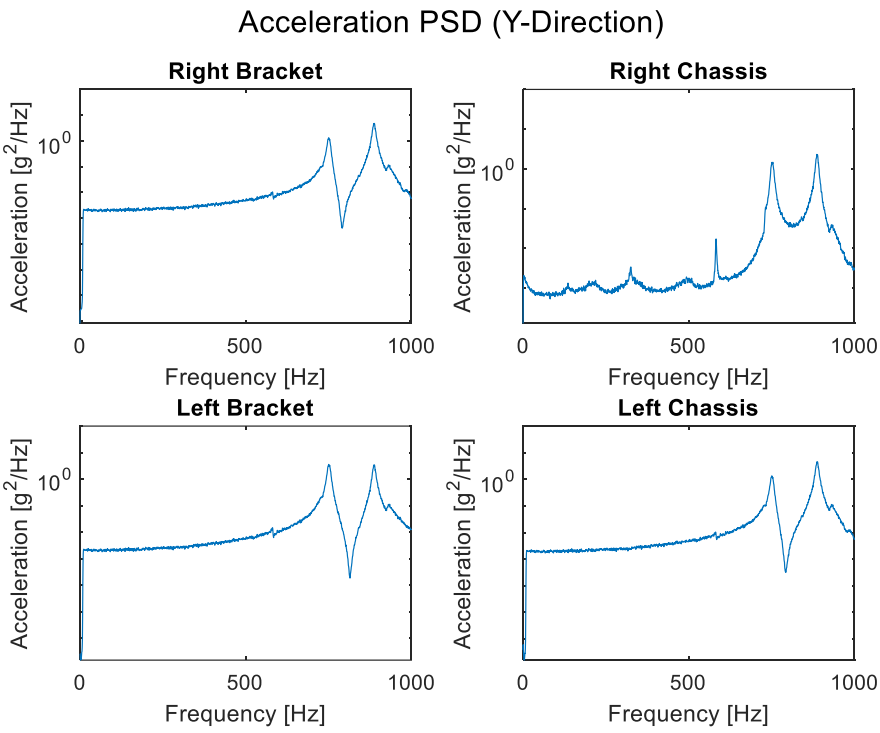

Figure 5.4 Acceleration PSDs (Y-Direction)

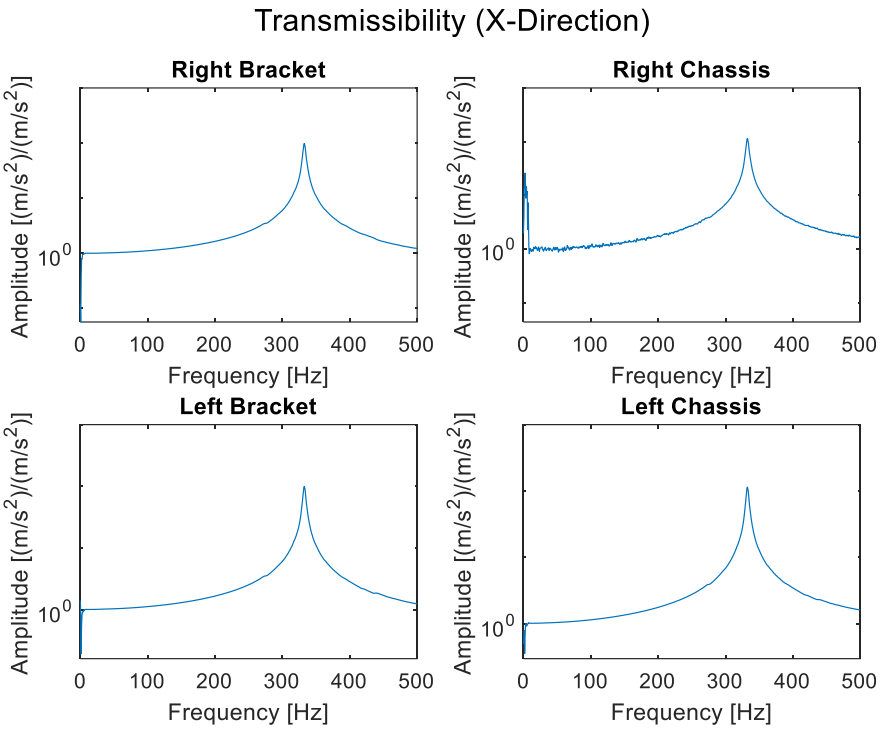

Figure 5.5 Transmissibility (X-Direction)

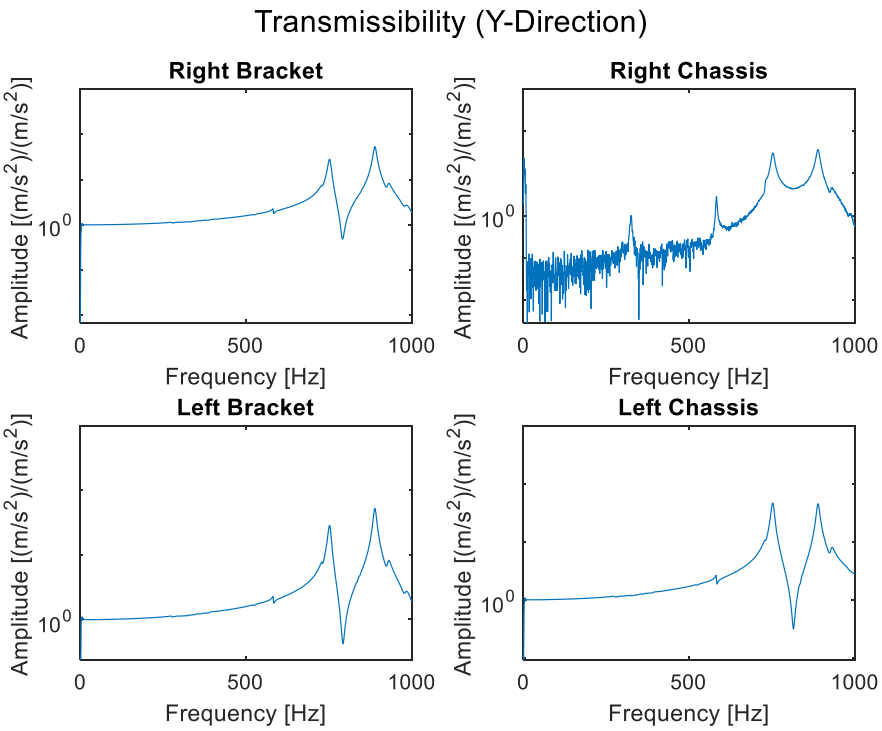

Figure 5.6 Transmissibility (Y-Direction)

Using transmissibility plots for both x and y axes excitations, first three natural frequencies of the brackets and corresponding damping ratios are acquired as given in Table 5.2. Half-power bandwidth method is used for calculating the damping ratios.

Table 5.2 Fundamental Natural Frequencies and Damping Ratios of Brackets

Mode	Natural Frequency [Hz]	Damping Ratio, ζ
1	332.5	0.0060
2	751.9	0.0064
3	888.8	0.0053

5.1.1. Checking Non-linearity of the Structure

As mentioned in previous chapter, modal test is repeated with white noise inputs with different amplitudes to see if system shows non-linear behavior. The structure will encounter much severe loads during fatigue life testing and this may cause shifting in natural frequencies or altering in damping ratios due to non-linearity. This directly affects the dynamic response of the structure and can lead unexpected results. Then, amplitude of white noise input is increased properly for x-axis starting from 0.002 g^2/Hz to 0.01 g^2/Hz with 0.002 g^2/Hz increments. This search is done for x axis excitation only, since the final fatigue life test will be performed in that direction. Transmissibility plots for different input levels are given in Figure 5.7.

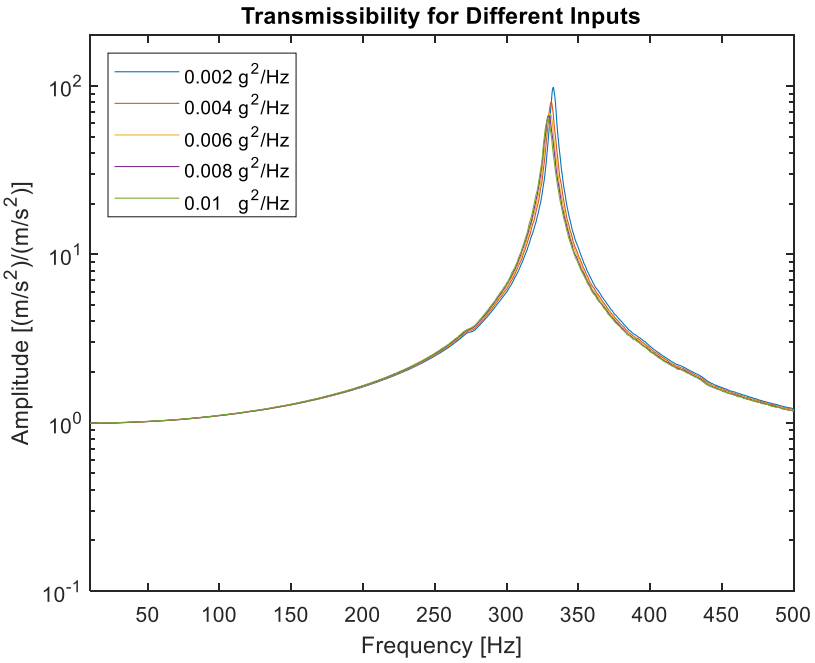

Figure 5.7 Transmissibility Plots for Different Inputs

When Figure 5.7 is carefully examined, it can be concluded that the damping ratios of the system is increasing while the first fundamental natural frequency of the structure is shifting down with increasing amplitude of the white noise input. Results that show the alteration of natural frequency and damping ratio is shown in Table 5.3.

Table 5.3 Change in First Natural Frequency and Damping Ratio

Amplitude of the Input [g^2/Hz]	**gRMS of the Input**	**Natural Frequency [Hz]**	**Damping Ratio, ζ**
0.002	2	332.5	0.0060
0.004	2.83	331.3	0.0071
0.006	3.46	330.0	0.0089
0.008	4	329.4	0.0091
0.01	4.47	328.8	0.0094

This is the indication of non-linearity in the system which is not a desirable condition since fatigue is highly susceptible phenomenon to damping of the system. This situation will be handled in detail in further chapters.

5.2. Verification Analysis

5.2.1. Modal Analysis

After building FE model and meshing has been done, modal analysis which is a prerequisite for further harmonic and fatigue life analysis is necessary. For acquiring the natural frequencies obtained from experiments, modal analysis is performed. Mainly, first three natural frequencies of the system are directly related to brackets. Therefore, only these frequencies are considered while iterations are realized.

As mentioned previously, there are some parameters that affect the behavior of the structure like contact types or contact areas. These should be determined by updating the model for getting closer results to modal test results. Many iterations are completed to reach true set of contacts by changing the contact type, contact area or behavior of beams. Figure 5.8 shows the convergence of first three natural frequencies with increasing number of iterations.

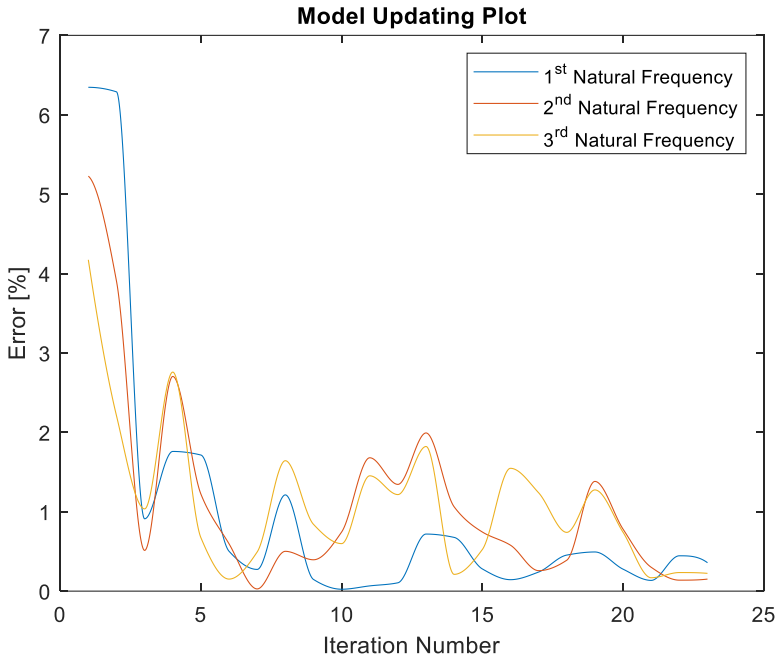

Figure 5.8 Convergence of First Three Natural Frequencies

Percentage of errors for corresponding natural frequencies drops below 0.5% which is satisfying enough for verification of FE model. Natural frequencies calculated from the last iteration and the comparison of them with ones obtained from experiment are given below in Table 5.4.

Table 5.4 Comparison of Natural Frequencies

Mode	Natural Frequency [Hz] (Experiment)	Natural Frequency [Hz] (Analysis)	Error [%]
1	332.5	331.4	-0.33
2	751.9	753.4	0.20
3	888.8	887.3	-0.17

After constructing an updated model, it is important to consider number of modes to be included for further analysis. Although all modes do not have significant effect on life of the structure, they affect the portion of effective mass contributed to analysis. Therefore, dynamic behavior of the system will be affected. At this point, participation factor needs to be checked.

Generally, it is better to have participation factors of around 90% in all directions [54]. This may be accomplished by increasing the number of modes included in the model. If it does not seem possible to reach that percentage by increasing the number of modes, it is advised to have modes up to 1.5 times the frequency of interest which corresponds to 3000 Hz [43]. Hence, 30 modes are found up to 3200 Hz. Participation factors of the analysis model and natural frequencies of 30 modes are given in Table 5.5 and Table 5.6, respectively.

Table 5.5 Participation Factors

X Direction	89%	**RotX Direction**	76%
Y Direction	92%	**RotY Direction**	77%
Z Direction	85%	**RotZ Direction**	76%

Table 5.6 Natural Frequencies of 30 Modes Included in Analysis

Mode	Frequency [Hz]	Mode	Frequency [Hz]
1	331.4	**16**	2053.2
2	753.4	**17**	2125.4
3	887.3	**18**	2289.9
4	907.1	**19**	2448.2
5	1273.2	**20**	2464.2
6	1291.3	**21**	2508.8
7	1406.2	**22**	2544.2
8	1629.6	**23**	2700.3
9	1652.3	**24**	2784.1
10	1671.6	**25**	2802
11	1749.8	**26**	2945.9
12	1809.9	**27**	2979.9
13	1835.6	**28**	3025.6
14	1904.4	**29**	3118.4
15	1954.6	**30**	3184.8

First three mode shapes that have significant effect on further analyses of the structure are given in Figure 5.9. Undeformed and deformed shapes are shown to clearly represent movement of brackets.

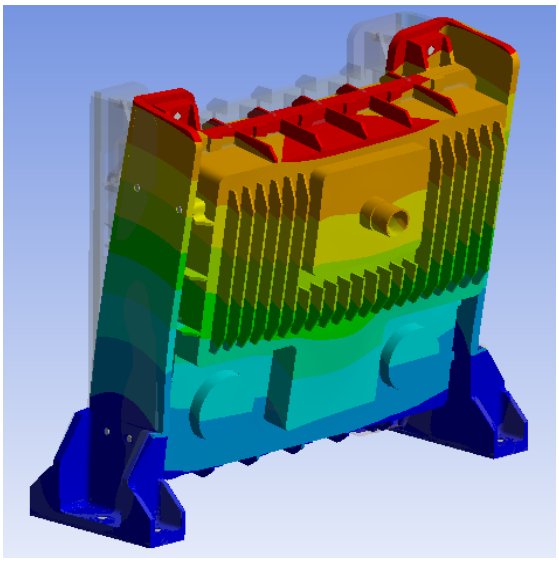

First Mode Shape

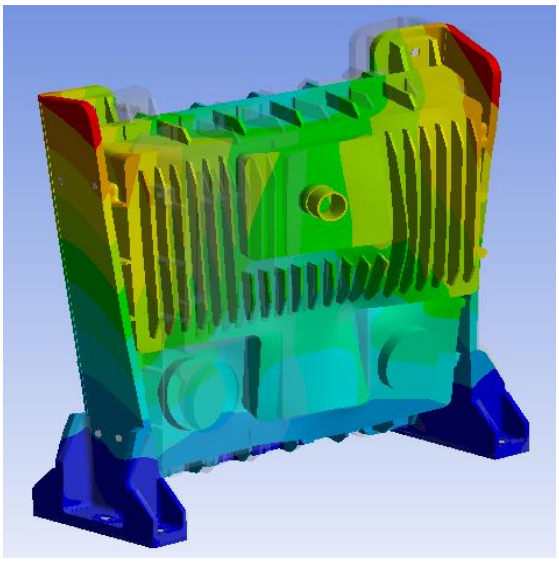

Second Mode Shape

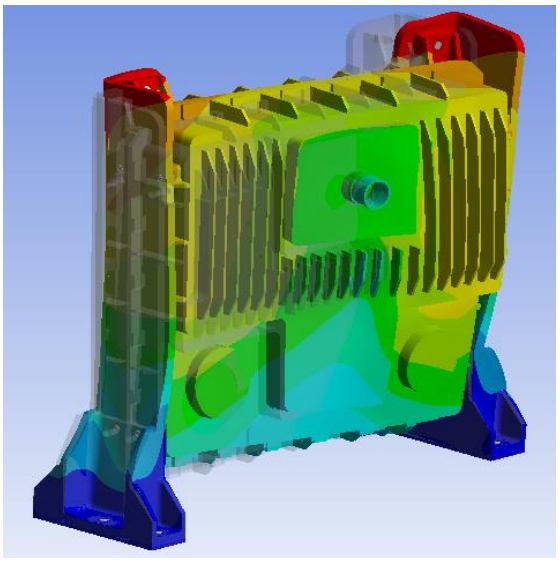

Third Mode Shape

Figure 5.9 First Three Mode Shapes

5.2.2. Harmonic Response Analysis

As specified earlier, comparing only natural frequencies of experimental and analysis results is not enough for the verification of the model. Therefore, transmissibility curves need to be obtained from FE analysis. To do this, harmonic response analysis is used. Acceleration transmissibility curves are acquired from the locations where accelerometers are attached by applying a unit g base excitation to system.

This analysis is performed in both x and y directions to verify the results obtained for both directions. Since mode superposition method is used in harmonic response analysis, it is connected to the solution of modal analysis in ANSYS Workbench. (See Figure 5.10)

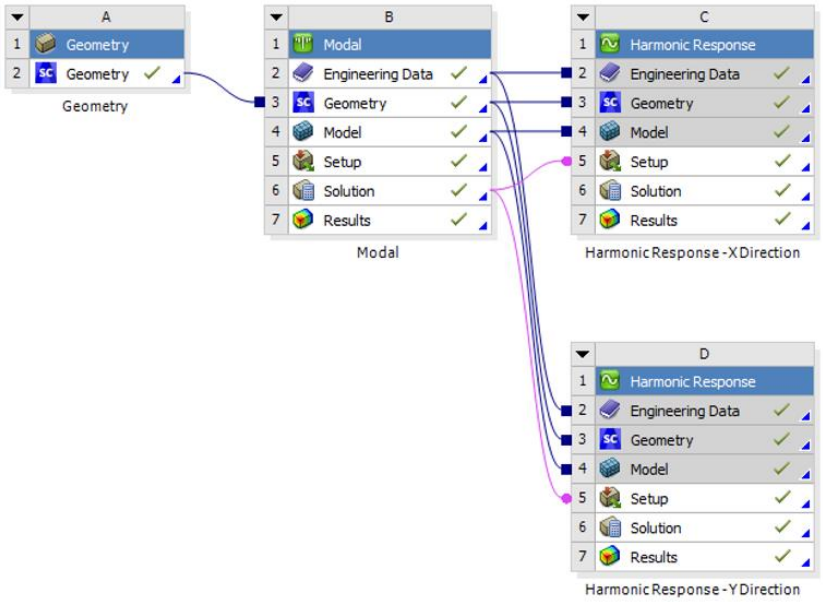

Figure 5.10 Relation of Harmonic Response Analysis with Modal Analysis

There are several possible options in analysis settings of harmonic response analysis for defining the frequency points in where solution will take place. The possible available options are dividing frequency interval into equally spaced points, using cluster method or solving with user defined frequency points. Using equally spaced frequency points is not sensible for long frequency ranges. Since it will be difficult to capture peaks with low frequency resolution, high resolution must be selected and this will make analysis times longer. On the contrary, cluster method becomes more logical since it uses higher resolutions only on natural frequency locations. This allows capturing peaks easily.

Up to 2000 Hz which harmonic response analysis is performed, there are totally 15 modes. Since only first three modes are in interest, capturing remaining natural frequency peaks sensitively is not necessary. Therefore, user defined frequencies are used which corresponds to approximately 15-20 cluster number in first three natural frequency locations and lower frequency resolutions on other peaks. This allows for having lower file sizes and analysis durations.

After analysis settings are adjusted, damping ratios of individual modes are defined. To be able to identify damping ratios of each natural frequency one by one, MDAMP command is used in ANSYS Mechanical interface. Damping values found from experiment in Table 5.2 are designated to first three natural frequencies, while damping ratios for other natural frequencies are assumed to be 0.005.

Since ANSYS adds up the damping value that is entered in MDAMP command to general damping value defined in analysis settings, difference between damping ratios of first three natural frequencies and 0.005 is indicated in command.

```
1  !   Commands inserted into this file will be executed just prior to the ANSYS SOLVE command.
2  !   These commands may supersede command settings set by Workbench.
3
4  !   Active UNIT system in Workbench when this object was created:  Metric (mm, kg, N, s, mV, mA)
5  !   NOTE:  Any data that requires units (such as mass) is assumed to be in the consistent solver unit system.
6  !                See Solving Units in the help system for more information.
7
8
9  MDAMP,1,0.001,0.0014,0.0003,,
10
```

Figure 5.11 Defining Damping Ratios with MDAMP Command

Transmissibility curves obtained from analyses are given in Figure 5.12 and Figure 5.13. As mentioned before, reference accelerometer location is chosen to be attached on right bracket. Therefore, transmissibility curves taken from ANSYS belong to that location.

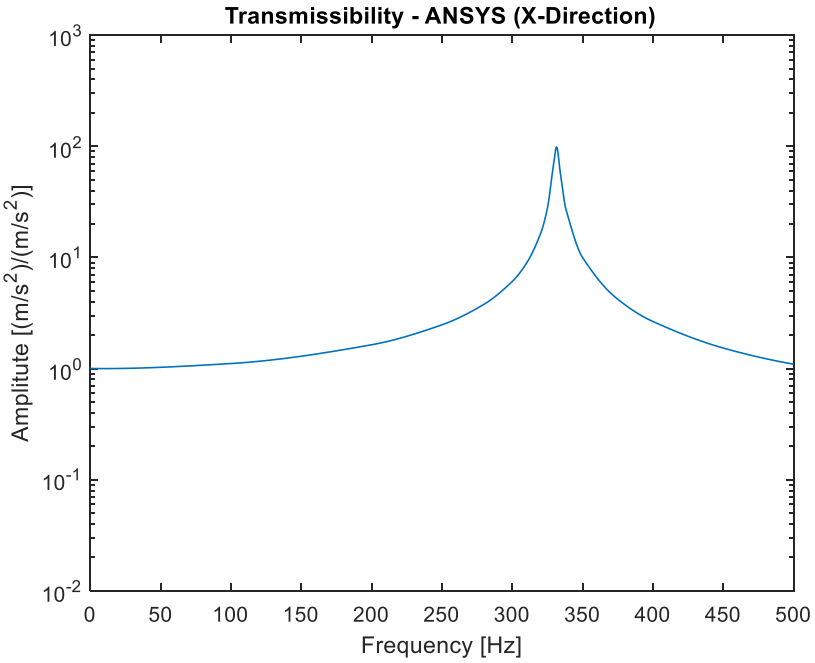

Figure 5.12 Transmissibility-ANSYS (X-Direction)

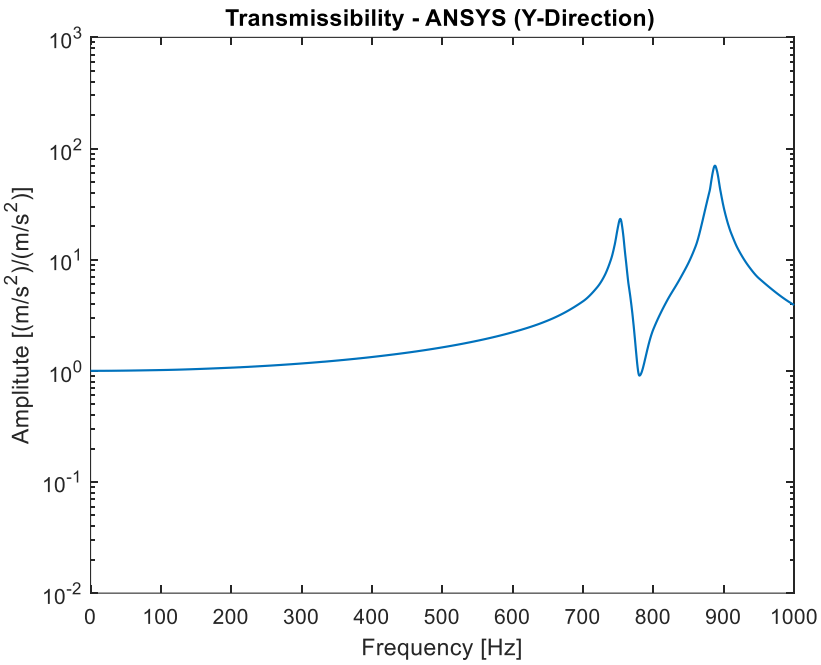

Figure 5.13 Transmissibility-ANSYS (Y-Direction)

5.2.3. Random Vibration Analysis

Random vibration analysis is realized for obtaining the acceleration responses of the structure. Since white noise with an amplitude of 0.002 g^2/Hz is used as input for 10-2000 Hz frequency range in experiment, random vibration analysis is set up considering these parameters. Acceleration PSDs taken from right bracket accelerometer are given below.

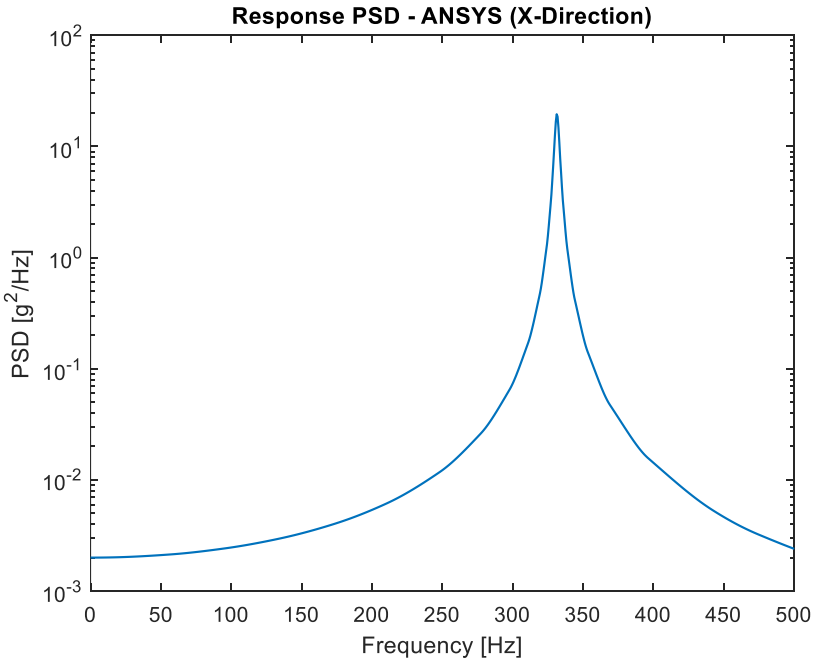

Figure 5.14 Response PSD – ANSYS (X-Direction)

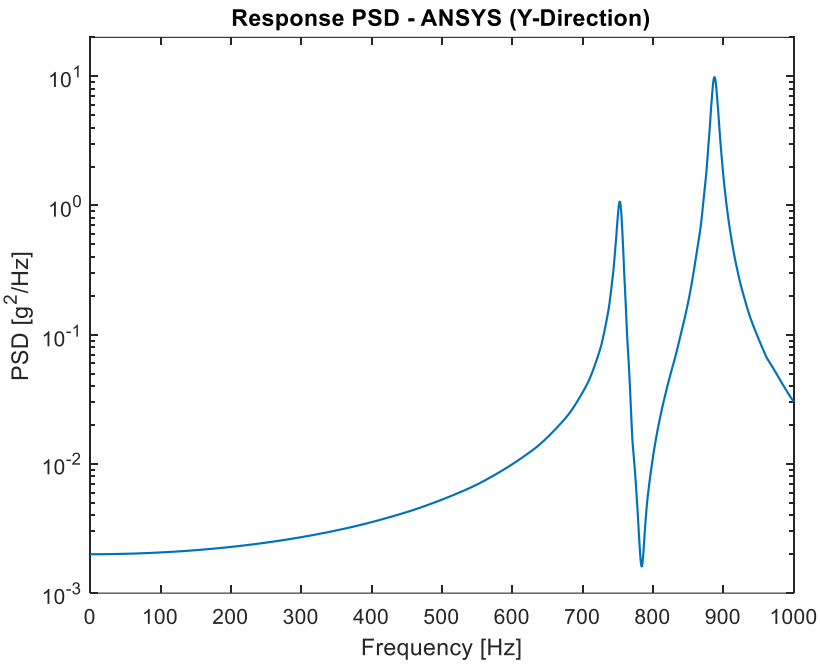

Figure 5.15 Response PSD – ANSYS (Y-Direction)

5.3. Comparison of Experimental and Analysis Results

First three natural frequencies taken from modal test and FE analysis are already compared in Table 5.4 with error values. Percent errors for each of them are in acceptable values and it can be concluded that natural frequencies are close enough to move on to further analysis. Since comparing natural frequencies is not adequate, transmissibility curves and acceleration response PSDs are compared to be sure that peak values are similar with same damping ratios. Comparison plots are given later in this chapter in Figure 5.16 and Figure 5.17.

When all plots examined in detail, the first thing to notice is that behavior of first mode which is obvious in x-direction, is captured very accurately. Natural frequency which corresponds to this mode does not appear on y-direction plots since it has a pure movement on x-axis. As a result, FE model represents the behavior of first mode close enough to real behavior. There are two modes of brackets dominant on y-direction, that's why two peaks appeared on y-axis plots. The second mode is captured very accurately similar to the first mode. However, there is a slight difference on peak values of the third mode. Analysis results seem to have higher peak which is the result of having lower damping ratio. Damping calculated from experiment data may be slightly different from the actual one. Since the experiment data is discrete, exact half-power points are hard to obtain. This may be the reason for calculation errors.

Although there is a small error on peak of third natural frequency, it is not predicted to have a significant effect on fatigue life results since life testing will take place on x-direction. Among all of these, it can be concluded that FE model closely represents the dynamic behavior of the structure and it can be used for the further analysis.

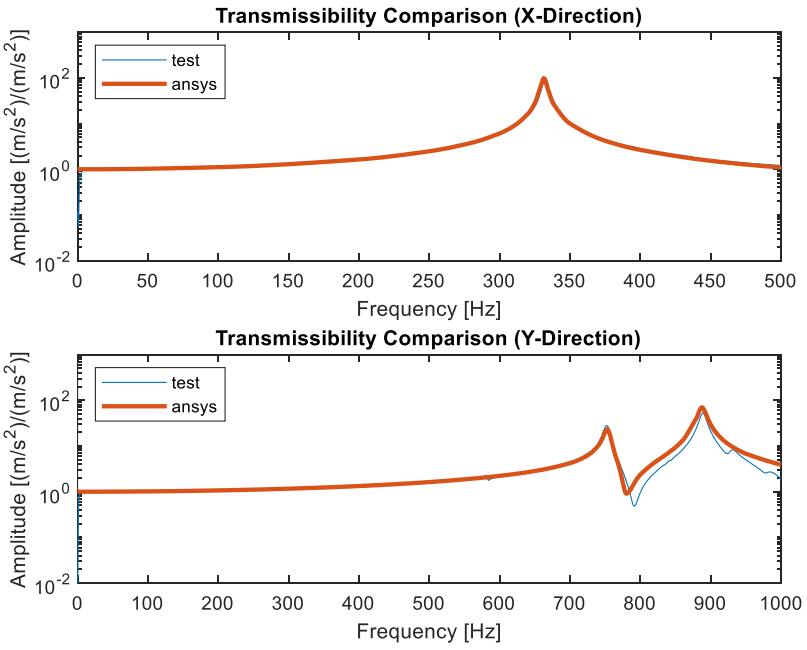

Figure 5.16 Comparison of Transmissibility Curves

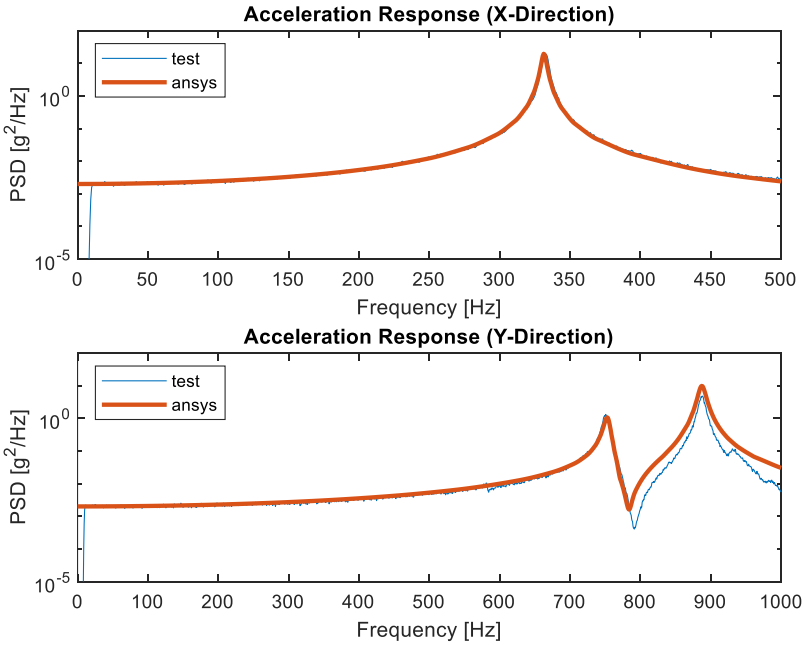

Figure 5.17 Comparison of Acceleration Response PSDs

6. FATIGUE LIFE ANALYSIS OF BRACKETS

Up to now, details about constructing the FE model and verification process are given in Chapter 4 and Chapter 5, respectively. All of these are prerequisites for theoretical and experimental fatigue life analysis of the brackets which will be mentioned on this chapter.

For fatigue life analysis of the brackets, a MATLAB code is developed in addition to analyzing by a commercial software, nCode DesignLife. This code is verified with the simpler geometry, a notched cantilever beam by comparing the results with nCode DesignLife. Details of verification will be given in Chapter 6.2. After obtaining the fatigue life results by the help of the developed numerical code and commercial software, an experiment is conducted by using the accelerated life testing principle.

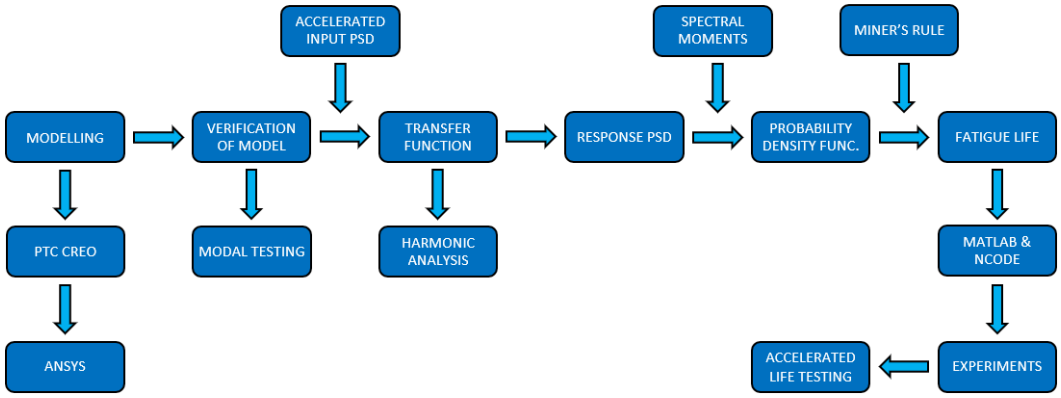

Figure 6.1 Flowchart of Fatigue Life Calculation Process

The flowchart above summarizes the process of reaching the fatigue life of the structure both theoretically and experimentally. After constructing and verifying the FE model, using the vibration load that the system is exposed, transfer function is needed to be calculated to reach the system response in terms of stresses. There are many stress combinations methods for obtaining transfer function of the structure as absolute maximum principal, critical plane, signed von-mises etc. These methods require principal or local stress values of the critical node. nCode DesignLife automatically combines stresses based on selected method when it is connected to Modal and Harmonic Response solutions. For calculating via MATLAB code, local stress values are reachable in ANSYS Mechanical interface while principal stresses can be obtained using APDL Product Launcher.

Harmonic Response Analysis is solved for x, y and z directions separately by applying unit g acceleration. After that, using the input and obtained transfer functions, stress response of the structure can be acquired. Then, using the spectral moments and one of the cycles counting methods like Dirlik, Lalanne, Narrow-Band, Steinberg etc., fatigue life of the structure is obtained.

Critical node of the whole structure is determined as node 530142 as mentioned previously on Chapter 4.2.1. All of the process mentioned on the flowchart is applied to this node and details will be mentioned on following chapters.

6.1. Data Acquisition and Signal Processing

For representing the real behavior of the operational conditions, it is preferred to use field vibration data instead of vibration profiles given in military standards. Field data is collected by using accelerometers while mission conditions are being generated. For this reason, acquired data reflects the vibration load that brackets will encounter during their operational usage. Data is collected in time domain with sampling rate of 8192 Hz and shown below in Figure 6.2. Due to confidentiality, axes values cannot be given.

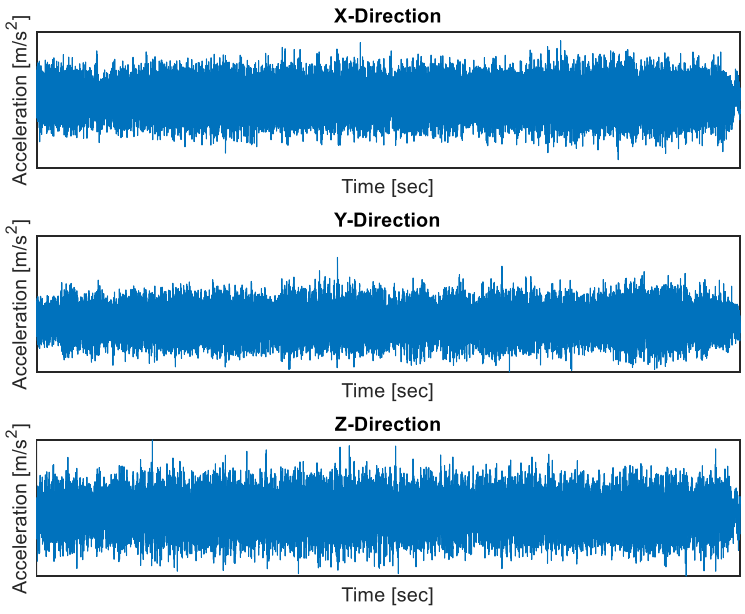

Figure 6.2 Field Data Collected in Time Domain

Since all calculations are performed in frequency domain, this data is transformed into frequency domain too. To do this, MATLAB is used for signal processing by setting the frequency resolution to 0.25 Hz and having an overlap of 67%. In addition, hanning window is used to eliminate unwanted noisy parts of the data. Since sampling frequency of data is 8192 Hz as mentioned above, PSD is obtained up to 4096 Hz. However, due to limits of electrodynamic shaker that will be used during fatigue life tests, data up to 2000 Hz is considered. In addition, higher frequencies have lower amplitudes by definition. Then, taking data up to 2000 Hz is not an incorrect approximation.

Since multiaxial fatigue life analysis will take place in further sections, CPSDs are calculated in addition to direct PSDs. Therefore, 3x3 load matrix with PSDs on diagonal and CPSDs on off-diagonal terms are obtained.

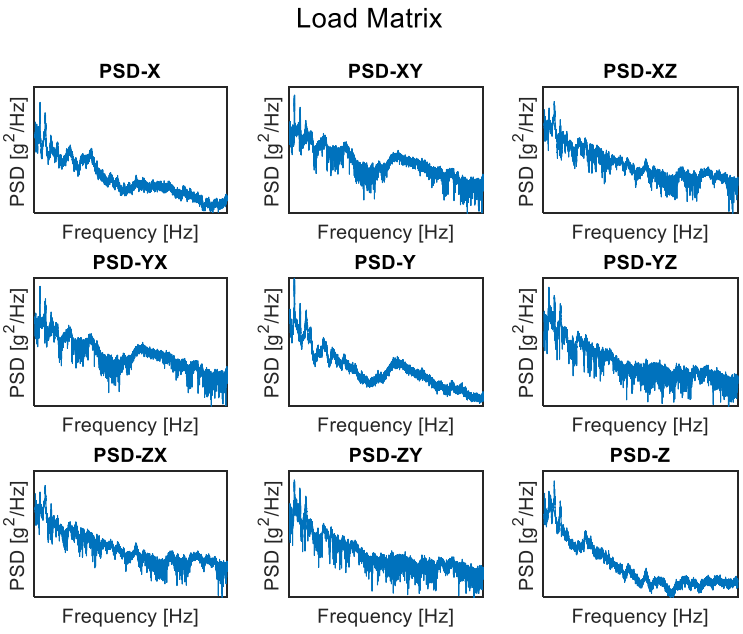

Figure 6.3 Multiaxial Load Matrix

Simultaneous multiaxial analysis is the best way of representing the real-life conditions, since it is the case in real vibration environments. However, it is not possible to have multiaxial fatigue life testing, since shaker that can apply multiaxial load simultaneously is not available. Thus, multiaxial input load will be converted to equivalent uniaxial load that will give same damage to critical node in weakest direction of the structure which is x direction. This situation will be covered in detail in further sections.

Field data that is collected from platform represents the load that structure will encounter for 2500 hours due to its requirements. Therefore, if the structure does not fail within 2500 hours while experiencing the loading given in Figure 6.3, it is treated as it satisfies the requirements. However, it is not possible to have an experiment that long. Hence, data should be accelerated according to military standards using Equation (3.53). If there is no PSDs to be combined, this equation is simplified as follows.

$$T_{test}{G_{test}}^{m/2} = T_{org}{G_{org}}^{m/2} \tag{6.1}$$

In Equation (6.1), T_{test} corresponds to aimed test duration that data will be accelerated and G_{test} represents the accelerated loading while T_{org} corresponds to original duration which is 2500 hours and G_{org} represents the original loading which is given in Figure 6.3. Here, m is the empirical scale factor and it is recommended to take $m = 7.5$ for random environments [53].

T_{acc} is selected to be 4 hours as generally requested in military standards and so, accelerated loading to 4 hours is found. Original and accelerated data can be seen in Figure 6.4.

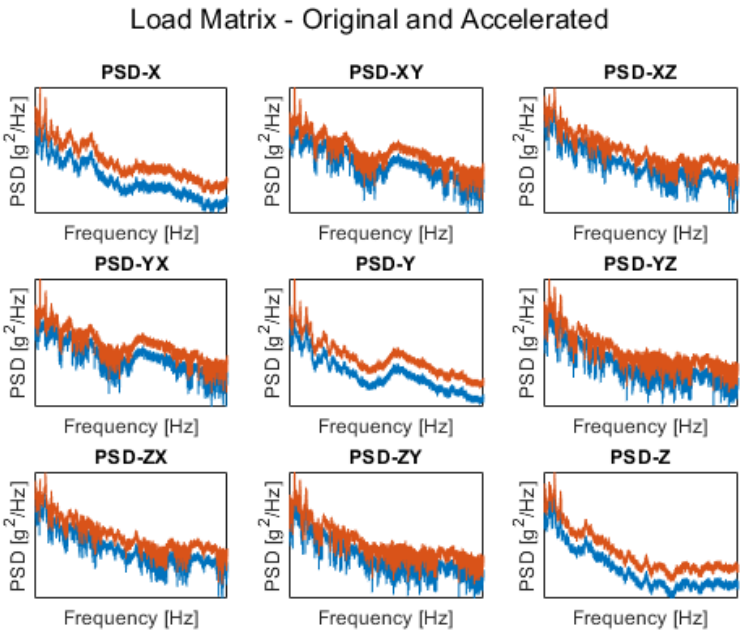

Figure 6.4 Original and Accelerated Loadings

gRMS values of original and accelerated data are shown below in Table 6.1. Since load matrix is symmetric, only six components are given.

Table 6.1 gRMS Levels of Original and Accelerated Input Loadings

Loading	gRMS (Original)	gRMS (Accelerated)
PSD-X	1.71	4.03
PSD-Y	2.82	6.65
PSD-Z	2.38	5.60
CPSD-XY	1.46	3.46
CPSD-XZ	1.47	3.46
CPSD-YZ	1.75	4.14

6.2. Verification of Numerical Code

A simpler geometry whose critical location is known without doubt is selected for verification of code written on MATLAB. For this purpose, a simple notched cantilever beam is selected as shown in Figure 6.5. It is designed using SpaceClaim and imported into ANSYS Mechanical.

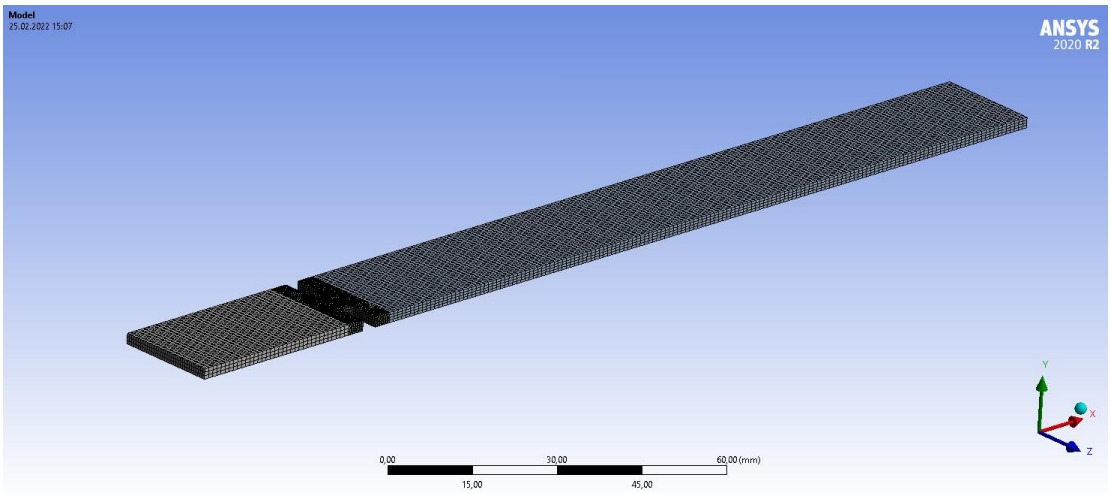

Figure 6.5 Notched Cantilever Beam

A finer mesh with smaller element size is used on the critical location of the geometry which is the notched portion. After modal analysis is performed, harmonic response analysis is taken place in three directions, separately. As expected, critical node appears around the notch as shown in Figure 6.6.

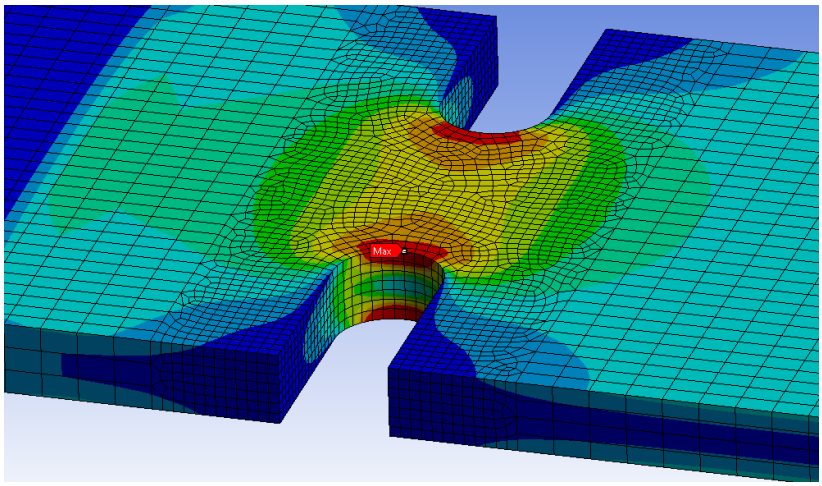

Figure 6.6 Critical Node of the Cantilever Beam

For this verification analysis, scaled version of the multiaxial loading given in Figure 6.3 is applied in 0-500 Hz frequency range. Damping ratio of 0.05 is used in analysis.

The local stress results of the critical node ($\sigma_x, \sigma_y, \sigma_z, \sigma_{xy}, \sigma_{xz}, \sigma_{yx}, \sigma_{yz}, \sigma_{zx}, \sigma_{zy}$) are taken from ANSYS Harmonic Response Analysis solutions for all x, y and z directions, separately and they are imported to MATLAB. Critical plane search method with multiple PSDs is used for both analyses. Results taken from nCode DesignLife and numerical code are compared. Obtained stress history plots from both analyses are given in Figure 6.7. In addition, tabulated results for spectral moments and statistical signal parameters are given in Table 6.2 and Table 6.3, respectively.

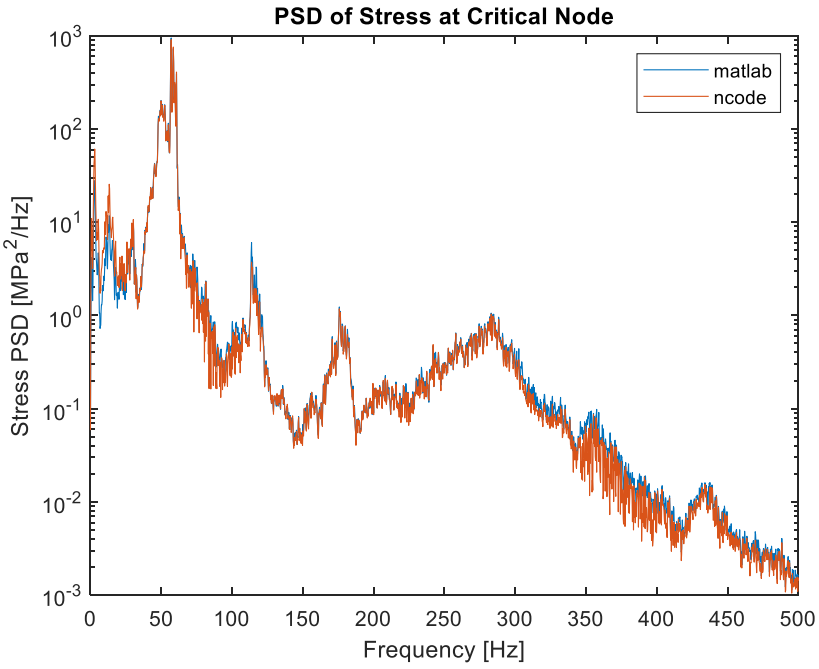

Figure 6.7 Comparison of Stress PSDs for Cantilever Beam

Table 6.2 Comparison of Spectral Moments for Cantilever Beam

	nCode DesignLife	Numerical Code
m_0	3.43e+03	3.44e+03
m_1	1.89e+05	1.97e+05
m_2	1.28e+07	1.41e+07
m_4	2.37e+11	3.36e+11

Table 6.3 Comparison of Statistical Parameters for Cantilever Beam

	nCode DesignLife	Numerical Code
RMS	58.58 MPa	58.64 MPa
E[0]	61.19	63.95
E[P]	135.81	154.58
γ	0.45	0.41

In addition to spectral moments and statistical parameters, stress range histograms and damage histograms are compared. They are shown in Figure 6.8 and Figure 6.9, respectively.

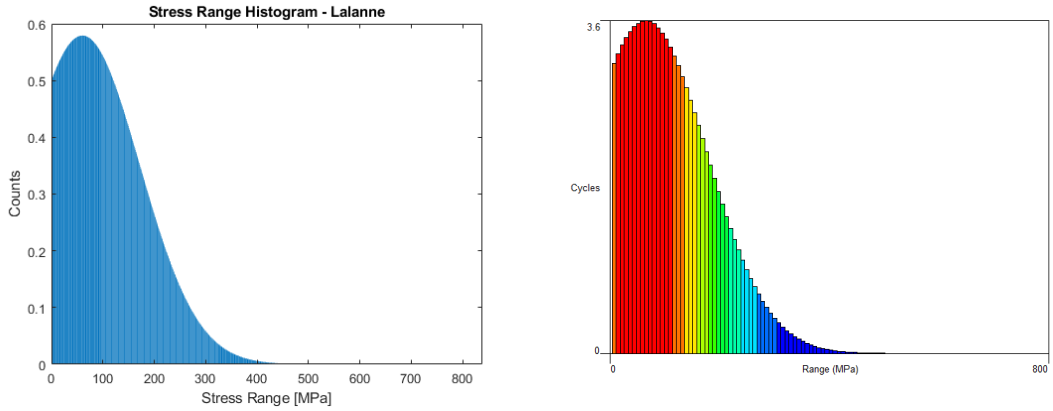

Figure 6.8 Comparison of Stress Range Histograms for Cantilever Beam

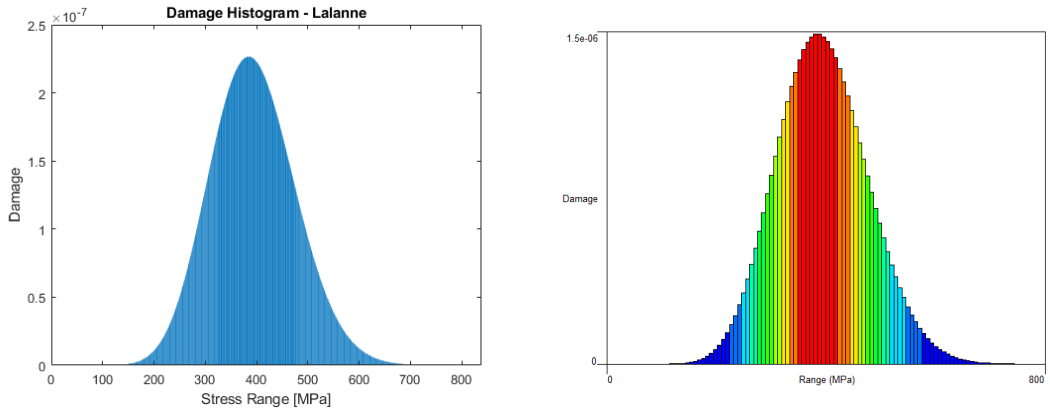

Figure 6.9 Comparison of Damage Histograms for Cantilever Beam

After obtaining all these parameters, fatigue life calculations are realized using spectral moments and statistical parameters. At this point, Dirlik and Lalanne's fatigue life estimations are used for comparison. Fatigue life estimations of notched cantilever beam using both commercial software and numerical code can be seen below in Table 6.4.

Table 6.4 Comparison of Fatigue Life for Cantilever Beam

	Dirlik		**Lalanne**	
	nCode DesignLife	**Numerical Code**	**nCode DesignLife**	**Numerical Code**
Critical Plane Angle	0°	0°	0°	0°
Expected Damage	4.11e-05	4.40e-05	4.22e-05	4.50e-05
Fatigue Life [sec]	2.44e+04	2.27e+04	2.37e+04	2.22e+04

When all comparison tables are examined, slight difference between parameters is noticed. Although stress response PSDs are very close to each other, fatigue life results are a bit different. This is because of the difference on spectral moments since all calculations are done based on them. nCode has a noise floor option for calculating spectral moments from stress PSD. Due to this option, some portion of stress PSD that has lower amplitude of stresses than this limit is neglected in calculations. Therefore, spectral moments which are directly related to area under the stress PSD plot, are estimated slightly different.

When spectral moments taken from nCode are imported into numerical code, all results including statistical signal parameters, damage and fatigue life become same. Therefore, by looking at all of these parameters, numerical code generated on MATLAB looks quite reliable to be used for further fatigue life calculations of brackets.

6.3. Fatigue Life Calculations of Brackets Using Numerical Code

After all pre-processing operations are finished on ANSYS as it is discussed in previous chapters, the aim is to get stresses and so, the transfer function of the critical node for all x, y and z directions. This is achieved by connecting three harmonic response analysis to the solution of modal analysis and applying unit g base excitation to system for all three directions, separately. As a result, local stress tensor for critical node is exported to numerical code.

For reaching the transfer function, one of the stress combination methods should be used. Generally, for non-proportional multiaxial loadings, it is suitable to use critical plane search method for combining stresses while for proportional multiaxial loadings, both critical plane and equivalent von mises theories can be used. Therefore, proportionality of the stress state at critical node is checked while selecting the method.

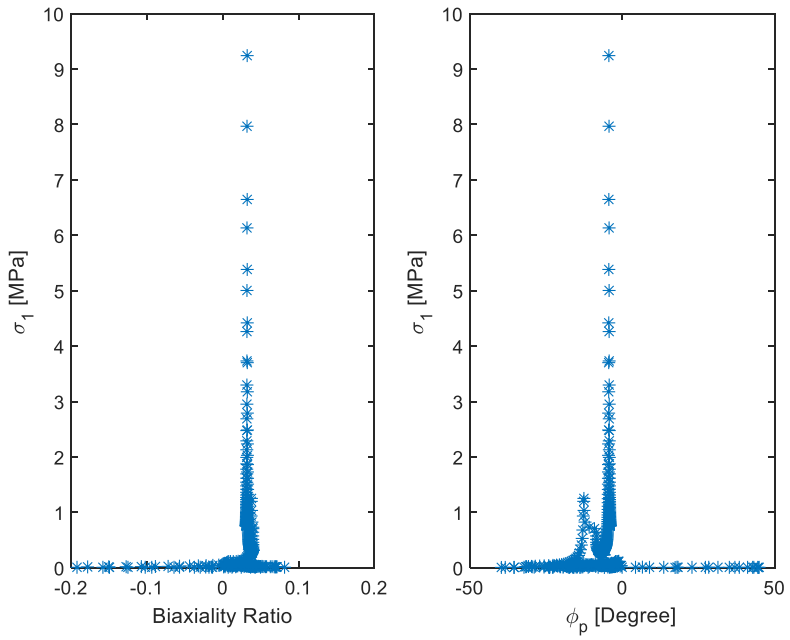

Figure 6.10 Biaxiality Ratio and Principal Stress Angle

When plots are examined, it can be summarized that the stress state at critical node is near-proportional. Then, using any of the critical plane or equivalent von mises methods may give reliable results. Both approaches are used in fatigue life calculations and results will be compared in next chapters. In this stage, calculations are performed using critical plane approach which is reliable in any case for multiaxial fatigue analysis. The transfer function obtained by using critical plane approach is given in Figure 6.11.

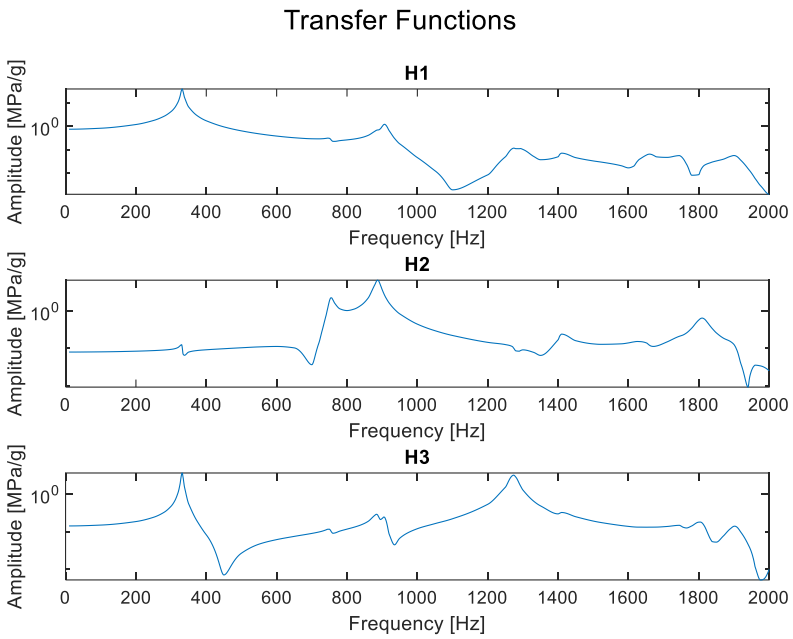

Figure 6.11 Transfer Functions Obtained by Critical Plane Approach

After acquiring the transfer function separately for all directions, next step is to reach stress response PSD of the critical node by combining inputs and transfer functions for multiaxial analysis by using equations mentioned on previous chapters. Loading that is given in Figure 6.3 is used as an input. Obtained stress PSD is shown below in Figure 6.12. Then, spectral moments can be found easily using the stress PSD curve and they are given in Table 6.5. After obtaining spectral moments, statistical parameters like RMS of stress, number of upward zero crossings per second E[0], number of peaks per second E[P] and irregularity factor γ which will later be used in PSD cycle counting methods can be found using the relations given in Chapter 3 and they are shown in Table 6.6.

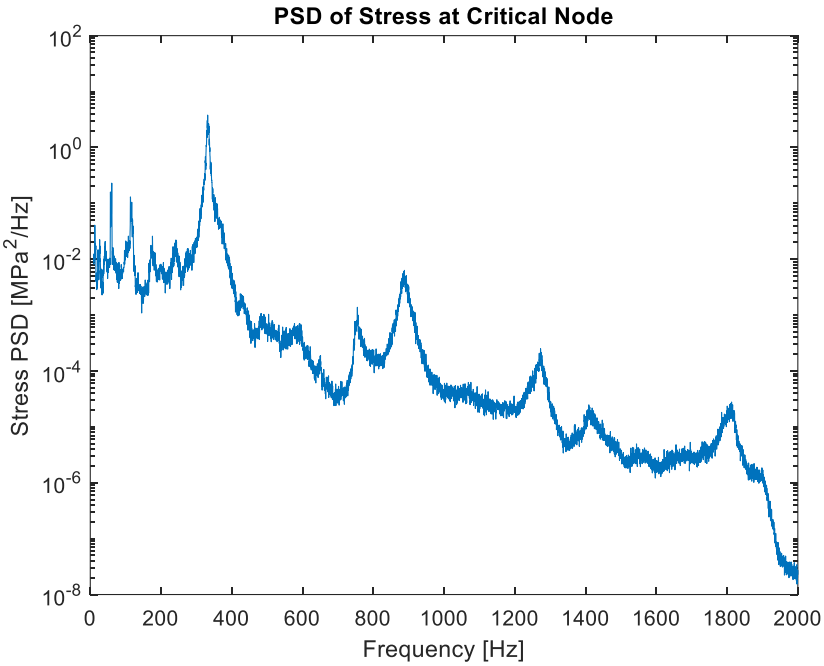

Figure 6.12 Stress PSD of Critical Node - MATLAB

Table 6.5 Spectral Moments of Critical Node - MATLAB

m_0	32.73
m_1	1.04e+04
m_2	3.54e+06
m_4	5.33e+11

Table 6.6 Statistical Parameter of Critical Node - MATLAB

RMS	5.72 MPa
E[0]	328.77
E[P]	387.99
γ	0.847

After obtaining all these parameters, proper cycle counting method for frequency domain can be chosen. Dirlik and Lalanne are two of the most robust empirical methods used in literature. Results obtained by both methods come out to be very similar. Therefore, Lalanne's method which is the most recent one is chosen to be given in this chapter. Stress range histogram that is obtained by using Lalanne's solution is given in Figure 6.13.

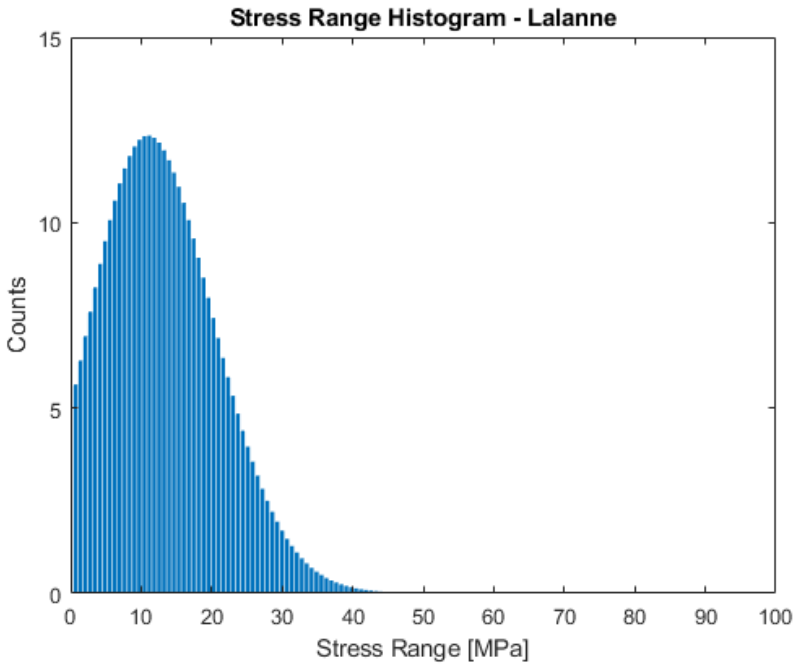

Figure 6.13 Stress Range Histogram Obtained Using Lalanne's Method

The next step after obtaining the probability density function is to find expected damage. This can be done by using Miner's cumulative damage theorem mentioned in Chapter 3. In addition to stress range histogram, S-N curve of Aluminum 6061-T6 which is the selected material for brackets is used for calculating the cumulative damage. The S-N curve is taken from ANSYS material database.

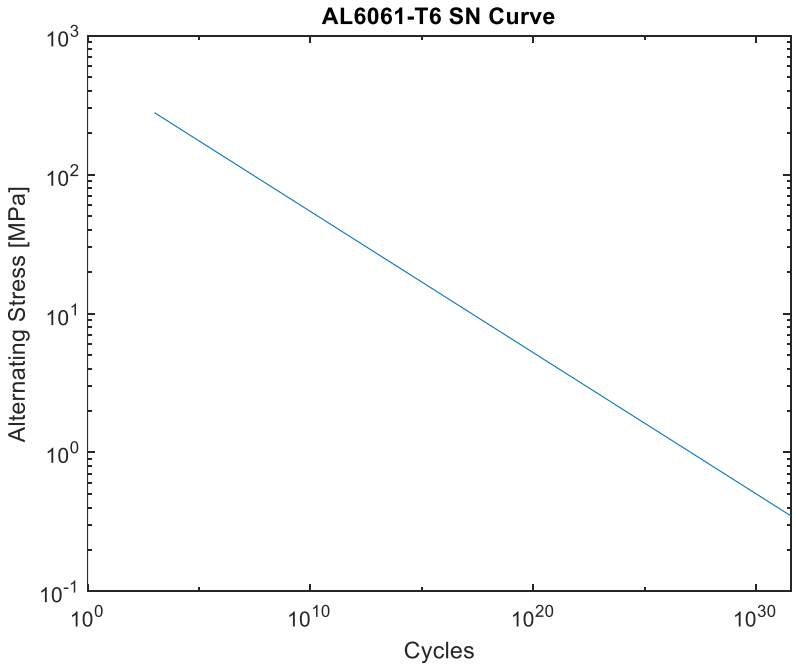

Figure 6.14 AL6061-T6 S-N Curve

Damage histogram is obtained by dividing the individual values of stress ranges coming from the stress histogram to corresponding stress ranges from S-N curve. Since S-N curve is given as alternating stresses in y-axis, it is converted into stress ranges by multiplying them with two. Damage histogram belongs to Lalanne method is given in Figure 6.15.

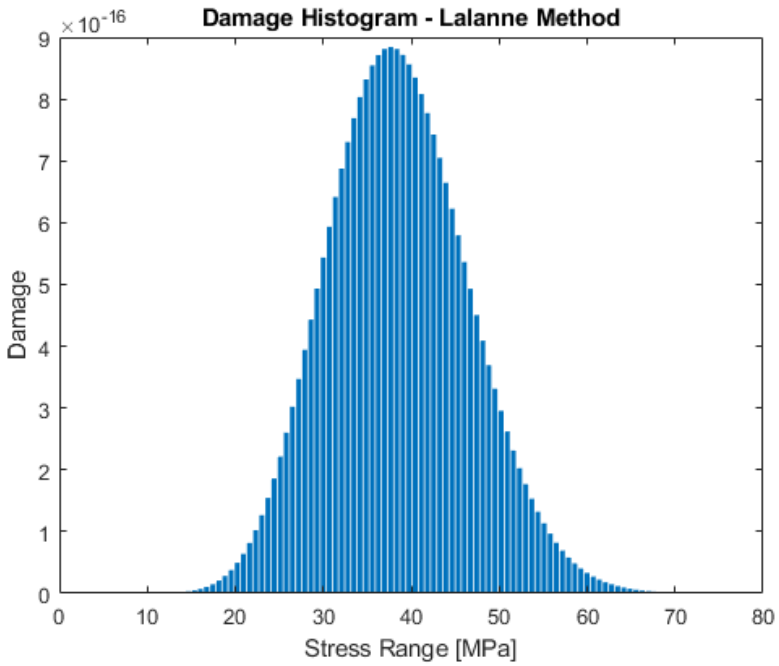

Figure 6.15 Damage Histogram Obtained Using Lalanne's Method

Then, summing all these individual damages of stress ranges shown in Figure 6.15 by using Miner's damage theorem, accumulated damage for critical node of the structure is found.

Life of the structure under multiaxial loading as indicated in Figure 6.3, can be easily found at the critical plane of the critical node, since critical plane search method is applied for stress combination. This method is applied by searching planes starting from 0° to 170° by 10° of increments. This means that all calculations after obtaining stress PSD are performed 18 times for each plane. The plane having greatest damage is named as critical plane.

Results given above like spectral moments, statistical parameters, damage histogram etc. belong to critical plane which is 90° in this case.

Fatigue life of the structure and corresponding damage values for different cycle counting methods are shown in Table 6.7.

Table 6.7 Fatigue Life Results for Different Cycle Counting Methods

Cycle Counting Method	Damage *(90° Plane)*	Life [sec] *(90° Plane)*
Narrow-Band	3.01e-14	3.32e+13
Wirsching	1.81e-14	5.52e+13
$\alpha_{0.75}$	2.89e-14	3.46e+13
Dirlik	2.46e-14	4.06e+13
Tovo-Benasciutti	2.16e-14	4.63e+13
Lalanne	2.55e-14	3.92e+13

As it can be seen clearly from table above, life results are high above the required operational life of the brackets which previously mentioned as 2500 hours. Therefore, it can be concluded that brackets ensure operational needs. Moreover, in Table 6.6, irregularity factor comes out nearly as 0.85 which is very close to 1. This means that signal is closer to narrowband. Therefore, narrowband solution also gives close results to another robust cycle counting methods.

6.4. Fatigue Life Calculations of Brackets Using Commercial Software

Detailed procedure and all steps for calculating life of brackets are explained in Chapter 6.3. Same procedure is applied in nCode DesignLife too. The difference is that nCode automatically creates all transfer functions with the help of the connection to modal and harmonic response analysis. For the multiaxial fatigue analysis, three harmonic response analyses solutions are connected to nCode Vibration PSD analysis.

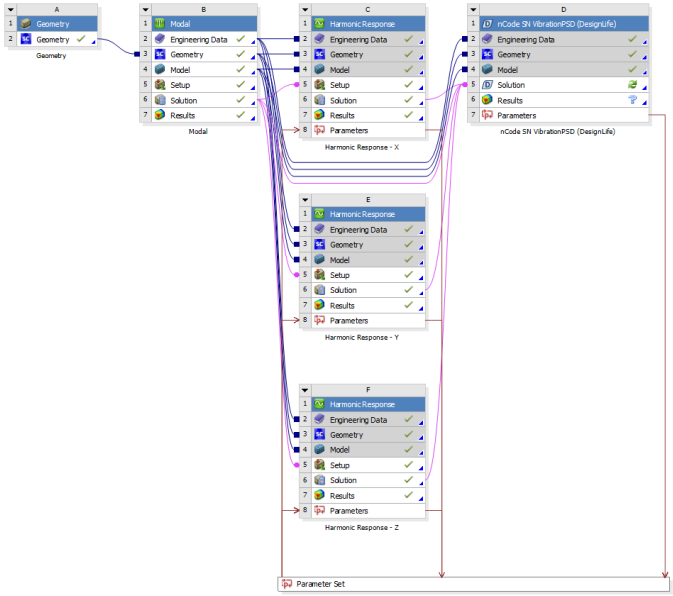

Figure 6.16 Relation Between Harmonic Response Analyses and nCode DesignLife

Before importing input to nCode, data is exported to Excel from MATLAB and transformed into appropriate nCode format. This can be done by using excel input and multi-column output glyphs as shown in Figure 6.17.

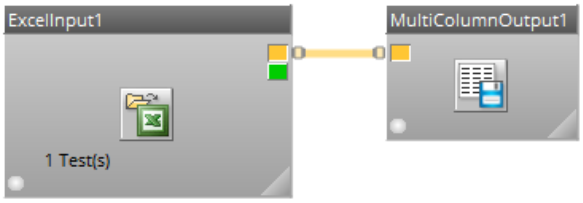

Figure 6.17 Transforming Data into nCode Format

Then, using multi-column input glyph, the created multi-column file that contains nine input components for all directions is added to analysis. General view of nCode analysis screen is shown in Figure 6.18.

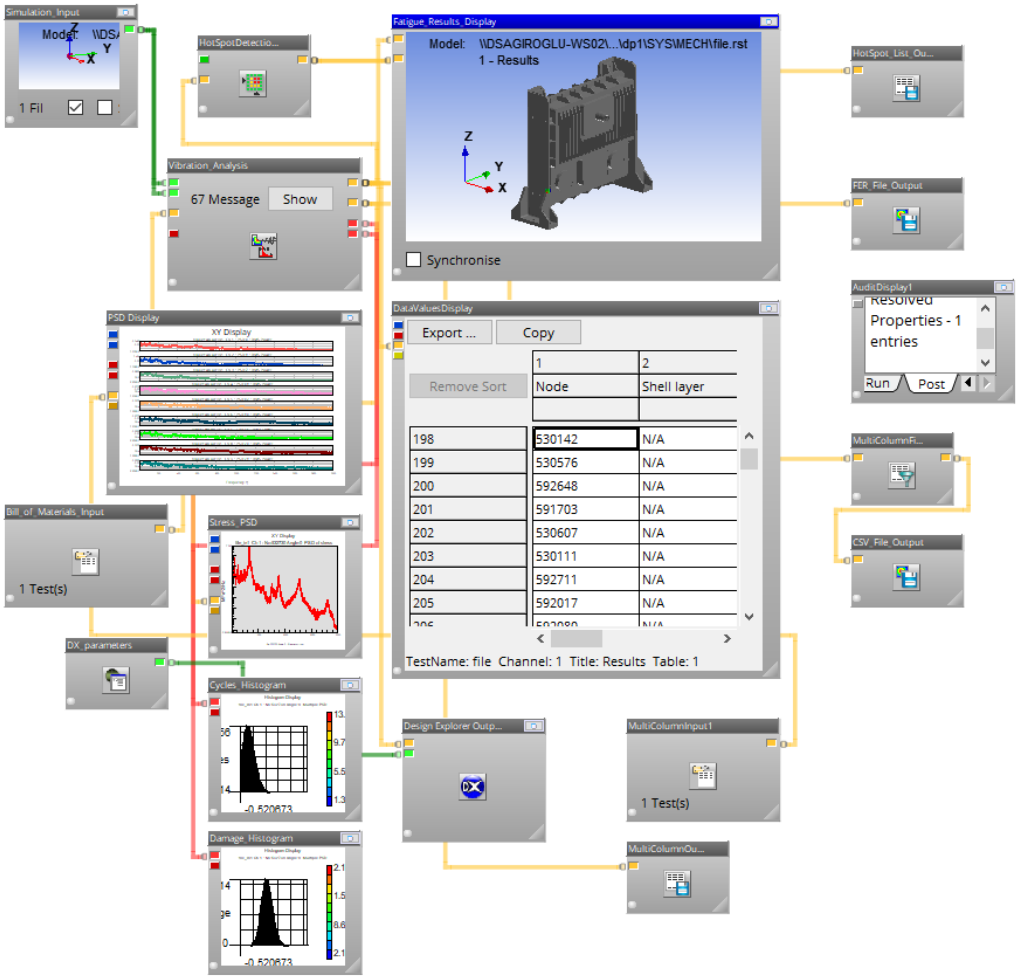

Figure 6.18 nCode Analysis Screen

Loading input is defined as 3x3 matrix as in numerical code. Therefore, data is exported from MATLAB and imported into nCode DesignLife as shown in Figure 6.19.

FRF Load Case Assignments — View Properties

	1	2	3
1	1 - PSD_X (braket_wo_acc)	4 - PSD_XY (braket_wo_acc)	5 - PSD_XZ (braket_wo_acc)
2	6 - PSD_YX (braket_wo_acc)	2 - PSD_Y (braket_wo_acc)	7 - PSD_YZ (braket_wo_acc)
3	8 - PSD_ZX (braket_wo_acc)	9 - PSD_ZY (braket_wo_acc)	3 - PSD_Z (braket_wo_acc)

Figure 6.19 nCode DesignLife Input Matrix

After importing multiaxial input, the next step is selecting appropriate stress combination method and cycle counting technique. nCode offers four PSD cycle counting methods, Narrow-Band, Dirlik and Lalanne and Steinberg. Critical plane approach is selected for stress combination as in numerical code. Normally, nCode solves each node of the components included in assembly one by one and this may cause very long analysis durations. Then, to have time-efficient analysis, only the sub-part of brackets that are subjected to the most damage, i.e. part including the critical node, is selected to be analyzed.

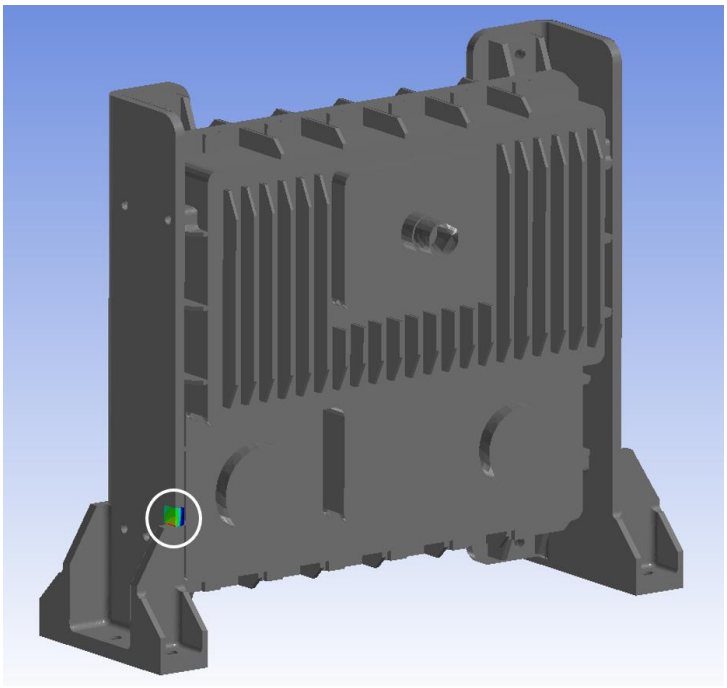

Figure 6.20 Analyzed Critical Node Location

PSD of stress response, spectral moments and statistical signal parameters obtained from nCode DesignLife is given in Figure 6.21, Table 6.8 and Table 6.9, respectively.

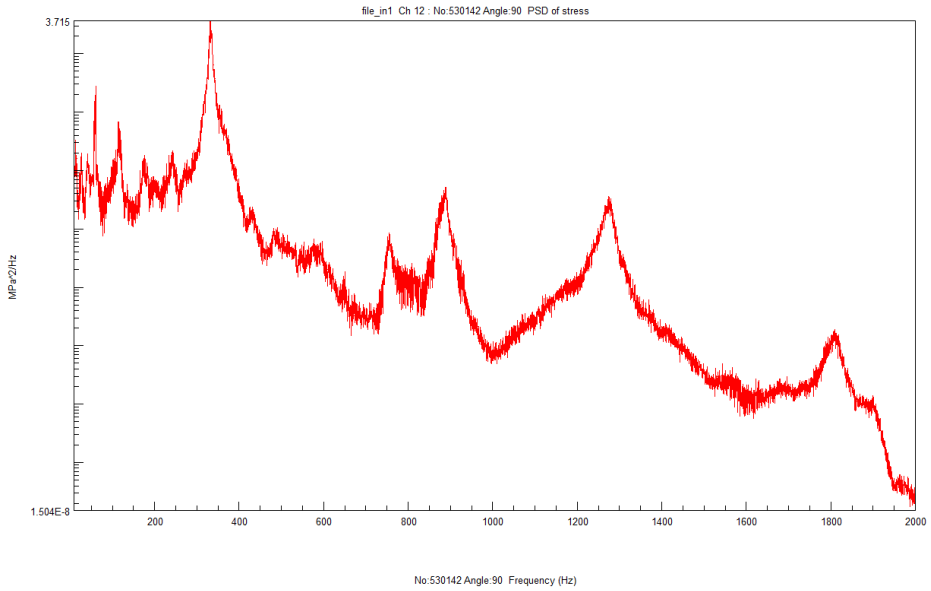

Figure 6.21 Stress PSD of Critical Node - nCode

Table 6.8 Spectral Moments of Critical Node - nCode

m_0	31.07
m_1	1.01e+04
m_2	3.45e+06
m_4	6.20e+11

Table 6.9 Statistical Parameters of Critical Node - nCode

RMS	5.57 MPa
E[0]	333.2
E[P]	424.1
γ	0.79

According to these parameters, probability density function and damage histogram obtained from nCode are given below in Figure 6.22 and Figure 6.23, respectively. Critical plane comes out to be 90° and all results given belong to that plane.

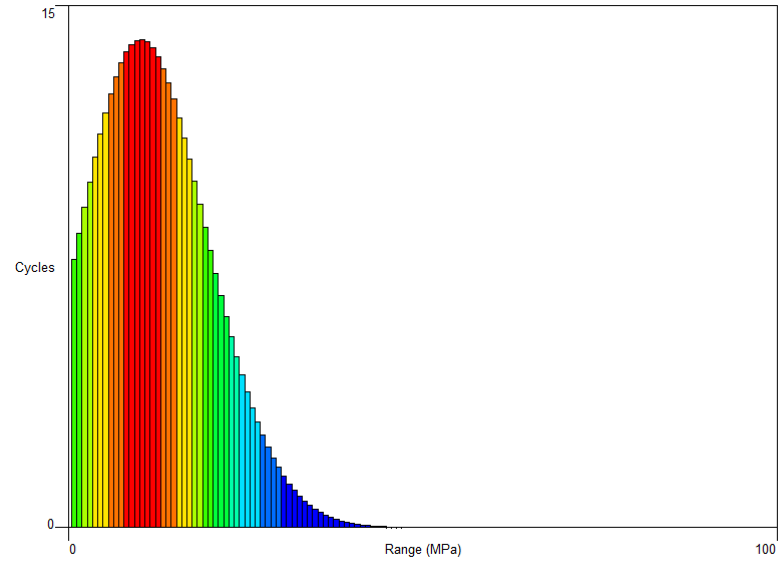

Figure 6.22 Stress Range Histogram Obtained Using Lalanne's Method – nCode

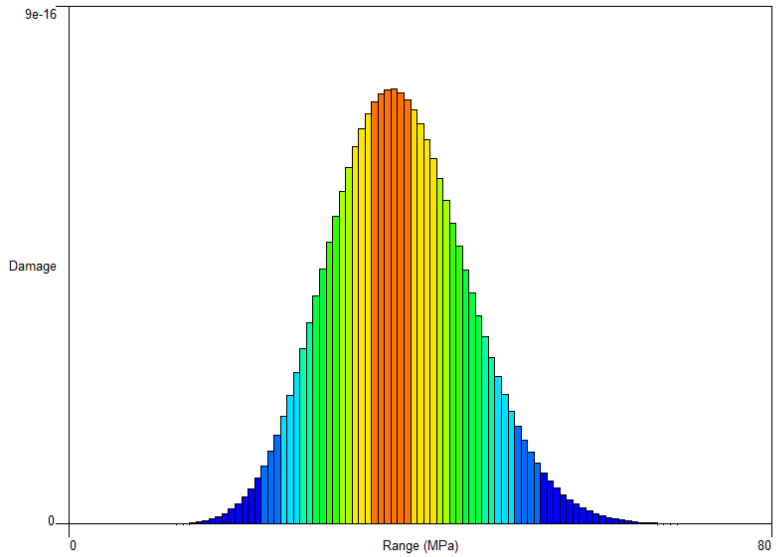

Figure 6.23 Damage Histogram Obtained Using Lalanne's Method – nCode

Expected damage and fatigue life results of the brackets for 90° plane acquired from nCode by using Narrow-Band, Dirlik and Lalanne approaches are given in Table 6.10.

Table 6.10 Fatigue Life Results for Different Cycle Counting Methods - nCode

Cycle Counting Method	**Damage** ***(90° Plane)***	**Life [sec]** ***(90° Plane)***
Narrow-Band	2.55e-14	3.93e+13
Dirlik	1.95e-14	5.14e+13
Lalanne	2.00e-14	4.99e+13

6.5. Comparison of Fatigue Life Results

Verification of MATLAB code is performed on Chapter 6.2 with simple notched cantilever beam geometry, but still comparison of fatigue life results of brackets is performed on this chapter. Since nCode has limited number of cycles counting methods as Narrow-Band, Dirlik and Lalanne, only damage and life results obtained by using these methods are compared in Table 6.11.

Table 6.11 Comparison of Fatigue Life Results for Brackets

Cycle Counting Method	**Numerical Code**		**nCode DesignLife**	
	Damage ***(90° Plane)***	**Life [sec]** ***(90° Plane)***	**Damage** ***(90° Plane)***	**Life [sec]** ***(90° Plane)***
Narrow-Band	3.01e-14	3.32e+13	2.55e-14	3.93e+13
Dirlik	2.46e-14	4.06e+13	1.95e-14	5.14e+13
Lalanne	2.55e-14	3.92e+13	2.00e-14	4.99e+13

The difference between results stem from the difference in spectral moments as mentioned in Chapter 6.2 and possible reasons are discussed. Numerical code is reliable enough, because of that when spectral moments of nCode are entered into numerical code, fatigue life results become same. Therefore, just numerical code results will be used in life calculations in following chapters.

6.6. Accelerated Life Testing of Brackets

In previous chapter, fatigue life analysis of brackets is performed using verified FE model. Input loading used for analyses represents the vibration load that brackets are exposed during their service life which is 2500 hours. However, as mentioned before, life of the brackets is far beyond that requirement and so, corresponding input cannot be used for experimental purposes.

In this chapter, different analyses will be performed using numerical code and suitable loading that allows to observe any crack at critical location is found.

6.6.1. Fatigue Life Analysis with Accelerated Data

Since fatigue life of the brackets are around 1.4e+10 hours under the input given in Figure 6.3, it should be accelerated for experimental purposes. Therefore, as mentioned previously in Chapter 6.1, data is accelerated to 4 hours as requested in military standards.

Fatigue life analysis is repeated using accelerated data before experiments to check whether results are suitable for experimental durations. Results obtained for different cycle counting methods under accelerated input is given in Table 6.12.

Table 6.12 Fatigue Life Results Under Accelerated Loading

Cycle Counting Method	**Life [hours]**
Narrow-Band	1.98e+06
Wirsching	3.29e+06
$\alpha_{0.75}$	2.06e+06
Dirlik	2.42e+06
Tovo-Benasciutti	2.76e+06
Lalanne	2.34e+06

When results are examined, it can be said that durations are still too high to be tested. Therefore, accelerating the data to 4 hours is not enough for having reasonable experimental durations. It is not possible to excite system that long until observing any crack at critical location. Therefore, fatigue life testing is not realized using accelerated input loading. This problem is overcome with rearranging the input as it will be mentioned in next chapter.

6.6.2. Fatigue Life Analysis with Rearranged Data

Since it is not logical to have experiments with accelerated data as emphasized in foregoing chapter, field data is scaled first to see if fatigue life results drop to reasonable levels. This is done by multiplying the field data with a constant number and then, it is accelerated to 4 hours. Scaled and accelerated input gRMS levels are given in Table 6.13.

Table 6.13 Scaled & Accelerated Input gRMS Levels

Loading	gRMS (Scaled)	gRMS (Accelerated)
PSD-X	6.84	16.13
PSD-Y	11.27	26.59
PSD-Z	9.50	22.42
CPSD-XY	5.86	13.82
CPSD-XZ	5.86	13.83
CPSD-YZ	7.02	16.55

Under this multiaxial loading, fatigue life results with different cycle counting methods are given below in Table 6.14.

Table 6.14 Fatigue Life Results Under Scaled & Accelerated Loading

Cycle Counting Method	Life [hours]
Narrow-Band	2.36
Wirsching	3.92
$\alpha_{0.75}$	2.45
Dirlik	2.88
Tovo-Benasciutti	3.28
Lalanne	2.78

The RMS of the stress at critical node is found as approximately 54 MPa which means that 3σ value is 162 MPa. Therefore, stresses can be evaluated as under the yield strength of aluminum 6061-T6. This guarantees that brackets will not fail due to yielding and input is eligible to use in fatigue life analysis.

Obtained fatigue life results for scaled and accelerated input loading looks logical for exciting the system with this input in experiments. However, these results are acquired by using the damping values calculated from modal tests. As stated in Chapter 5.1.1, system has non-linear behavior as damping ratio increases and natural frequency decreases with increasing input gRMS. Therefore, during rearrangement process, damping of the system should be considered very carefully. Increase in damping means higher fatigue life results than expected and unfortunately, it is not possible to measure damping under the input that fatigue tests will be performed with. Accelerometers are not capable of measure data under these types of loadings that has very high peaks, which is known as overloading.

This above-mentioned situation is handled by realizing the harmonic analyses parametrically for different damping ratios for all x, y and z directions. Fatigue life results are obtained for each damping ratios under scaled loading are given in Table 6.15. Since results for experimental damping ratios are given in previous table, it is not included in table below.

Table 6.15 Fatigue Life Results of Scaled Input for Different Damping Ratios

Damping Ratio, ζ	**Cycle Counting Method**	**Life [hours]**	**RMS of Stress [MPa]**
0.02	Narrow-Band	49.37	39.57
	Wirsching	82.10	
	$\alpha_{0.75}$	52.89	
	Dirlik	64.93	
	Tovo-Benasciutti	75.74	
	Lalanne	60.90	
0.03	Narrow-Band	264.51	33.32
	Wirsching	439.92	
	$\alpha_{0.75}$	290.74	
	Dirlik	371.19	
	Tovo-Benasciutti	434.79	
	Lalanne	339.61	

As summarized by examining Table 6.15, increasing damping ratio has major effect on fatigue life results of brackets. If damping of the structure is greater than one found from modal tests, duration of fatigue test becomes irrational. Therefore, input should be arranged by considering the possible highest damping ratio.

This can be overcome with increasing the input scaling factor but it causes significant raise in gRMS of the input signals which electrodynamic shaker cannot afford to apply. Then, another way to solve this problem is recognized.

To be able to reduce fatigue test durations without increasing gRMS levels significantly, rearrangement of input signal is realized by adding sine tones to neighborhood of the first and most dominant natural frequency of the structure. Therefore, input signals are regulated with respect to this strategy and finally input matrix is found as shown in Figure 6.24.

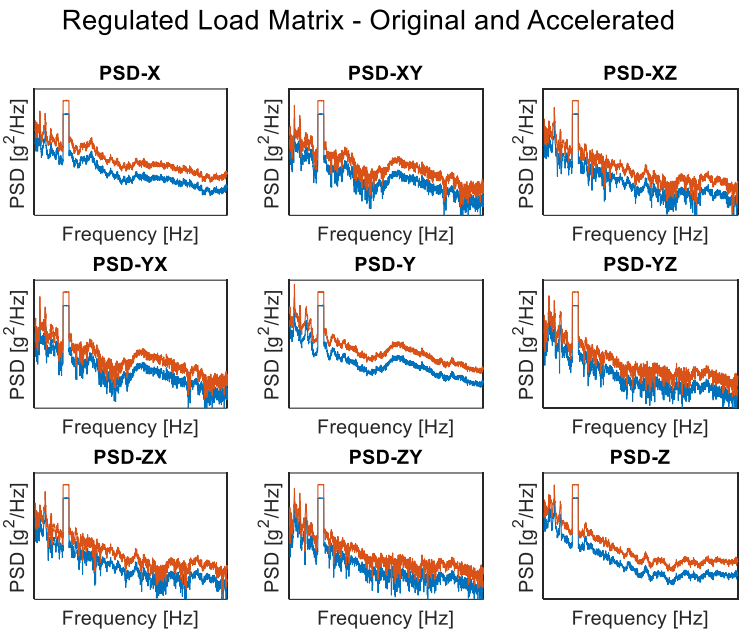

Figure 6.24 Regulated Load Matrix

Comparison of gRMS levels of direct field data, scaled data and sine-added input signals are given in Table 6.16. All given levels belong to accelerated PSDs and CPSDs to 4 hours. As it is seen clearly, it is more efficient to use this kind of arrangement instead of scaling whole frequency range, since it increases energy levels more plausibly.

Table 6.16 Comparison of gRMS Levels

Loading	gRMS (Field Data)	gRMS (Scaled)	gRMS (Sine-Added)
PSD-X	4.03	16.13	6.64
PSD-Y	6.65	26.59	8.24
PSD-Z	5.60	22.42	7.74
CPSD-XY	3.46	13.82	6.18
CPSD-XZ	3.46	13.83	6.33
CPSD-YZ	4.14	16.55	6.69

Fatigue life analysis for brackets is repeated using sine-added input matrix with different damping ratios and results are given below.

Table 6.17 Fatigue Life Results of Sine-Added Input for Different Damping Ratios

Damping Ratio, ζ	**Cycle Counting Method**	**Life [mins]**	**RMS of Stress [MPa]**
0.01	Narrow-Band	1.21	91.76
	Wirsching	1.58	
	$\alpha_{0.75}$	1.21	
	Dirlik	1.22	
	Tovo-Benasciutti	1.23	
	Lalanne	1.21	
0.02	Narrow-Band	39.76	62.41
	Wirsching	54.49	
	$\alpha_{0.75}$	39.79	
	Dirlik	40.14	
	Tovo-Benasciutti	40.37	
	Lalanne	39.89	
0.03	Narrow-Band	419.01	49.12
	Wirsching	591.58	
	$\alpha_{0.75}$	419.57	
	Dirlik	424.58	
	Tovo-Benasciutti	427.90	
	Lalanne	420.87	

When Table 6.17 is examined, it can be noticed that the 3σ value of resultant RMS of stress response in 0.01 damping ratio case is nearly 276 MPa which is the yield strength of the aluminum 6061-T6. Hence, it is not proper to use that input if system has 0.01 damping ratio since it may fail due to yielding before fatigue failure occurs. However, due to structure's non-linear behavior under increasing input levels, it is foreseen that it will have higher damping ratio than 0.01. According to obtained results, if the system experiences 0.02 damping ratio, fatigue failure will occur around 39-40 minutes or if the system experiences 0.03 damping ratio, crack initiation starts after nearly 7 hours. These results seem logical that the regulated input in Figure 6.24 can be applied in fatigue life testing.

6.6.2.1. Finding Equivalent Uniaxial Input for Fatigue Life Experiment

Although all analyses up to now are performed using multiaxial analysis strategies, it is not possible to excite the system with multiaxial inputs in real case, since shakers that are capable of giving simultaneous three-axial excitations are not commonly available. For this reason, a method is proposed to convert multiaxial input to an equivalent uniaxial signal that gives exact same damage to system.

As mentioned in previous chapters, all required information like spectral moments and statistical parameters, for reaching the fatigue life of any structure, is acquired from stress response PSD of critical node. Hence, if stress PSDs of multiaxial and uniaxial loading cases are same, damage and so, fatigue life results will be same.

Normally, for reaching stress response PSD, input and transfer function of the system is combined by using different techniques mentioned in Chapter 3. Stress PSD of critical node under multiaxial excitation is found as shown in Figure 6.12 and it is used for finding the corresponding uniaxial input loading.

$$G_{inp_{(eq)}}(f) = \frac{G_{rsp_{(ma)}}(f)}{H_c(f)^2} \tag{6.2}$$

Equation (6.2) shows the backward work that is performed to get equivalent input loading from previously obtained stress PSD of multiaxial loading case. In this equation, $G_{inp_{(eq)}}(f)$ represents equivalent uniaxial input loading to be found, $G_{rsp_{(ma)}}(f)$ represents previously obtained PSD of stress from multiaxial analysis and $H_c(f)$ represents the transfer function in corresponding critical direction. By dividing the stress PSD to transfer function of x direction which is the most critical direction among all three axes for brackets, equivalent uniaxial loading that gives same damage to system in that direction is found. Obtained equivalent uniaxial input is given in Figure 6.25.

After finding uniaxial loading that will be applied in fatigue testing, it is arranged with respect to shaker's capabilities. Since electromagnetic shaker has maximum limit of dividing frequency interval of excitation load to 1600 lines, frequency resolution is set to 1.25 Hz for input that will be applied in 10-2000 Hz range. Moreover, gRMS of converted loading is checked and it is found as 18.37 which is within shaker's input ranges.

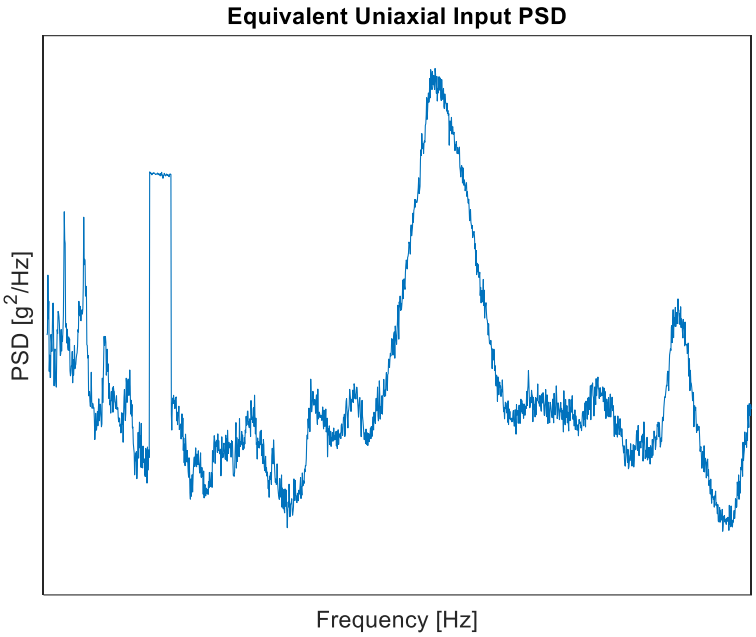

Figure 6.25 Equivalent Uniaxial Loading

6.6.3. Experimental Fatigue Life Testing

By using the equivalent uniaxial input obtained, fatigue life testing is performed. The expected duration to observe crack initiation is different for changing damping ratios as discussed in Chapter 6.6.2.

The crack is observed in the expected critical location in left bracket around 32-33 minutes after experiment is started. Since capturing the initiation of crack is quite difficult, propagated crack has been observed. Hence, real life might be a little lower than this duration.

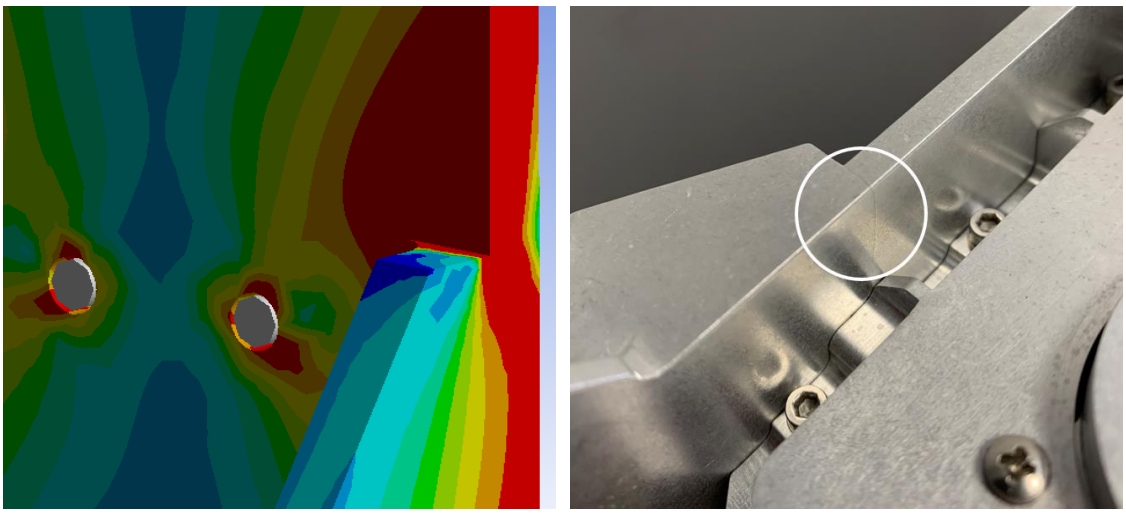

Figure 6.26 Crack Observed During Fatigue Test

Structure that has damping ratio of 0.02 is expected to have approximately 40 minutes of fatigue life as it can be seen from Table 6.17. When obtained result from fatigue test is evaluated together with the results in Table 6.17, it can be concluded that first natural frequency of the structure probably has damping ratio of about 0.02, or might be a bit lower than that, when excited under loading used in experiment. Damping ratio is evaluated as about 0.01 from the modal tests performed, but due to non-linear behavior of structure it increases with increasing loading amplitudes. Hence, it is an expected result to face with a raise in damping.

When different cycle counting techniques are compared by experimental result, it can be concluded that all methods except Wirsching method gives quite good results. Normally, if signal was wideband, Narrow-Band approach might give meaningless results. However, irregularity factor of response signal is around 0.98 for sine-added loading which is very close to 1 and this means signal is close to be narrowband. Hence, Narrow-Band approach gives reasonable results too.

To conclude, result obtained from fatigue life experiment is rather satisfactory to verify numerical analysis results. Although, there might be many uncertainties, damping ratio has one of the most forceful parameters that directly and significantly affect fatigue life. Therefore, difference in experimental and numerical results are evaluated as emerging due to increase in damping ratio.

7. CASE STUDIES

7.1. Effect of Different Stress Combination Methods on Fatigue Life

So far, many analyses are performed to understand the random vibration induced multiaxial fatigue. In all analyses, critical plane approach is used for stress combination. In this chapter, effect of using different stress combination methods as absolute maximum principal, equivalent von-mises and critical plane on fatigue life of structure is investigated.

The suitable stress combination method should be chosen by checking two parameters mentioned in Chapter 3. One of the most important parameters is biaxiality ratio which is used for understanding if stress state is proportional or not. For non-proportional multiaxial loadings, critical plane is the most proper method while for proportional multi axial loading case equivalent stress-strain theories can be used. In Figure 6.10, biaxiality ratio and principal stress angle is given with respect to the maximum principal. Examining these plots, it can be concluded that the stress state is near-proportional since biaxiality ratio and principal stress angle do not change much with increasing σ_1. Hence, equivalent stress-strain theories can be used in addition to critical plane approach.

Transfer functions acquired using different stress combination theories for all x, y and z directions are shown in Figure 7.1, Figure 7.2 and Figure 7.3, respectively.

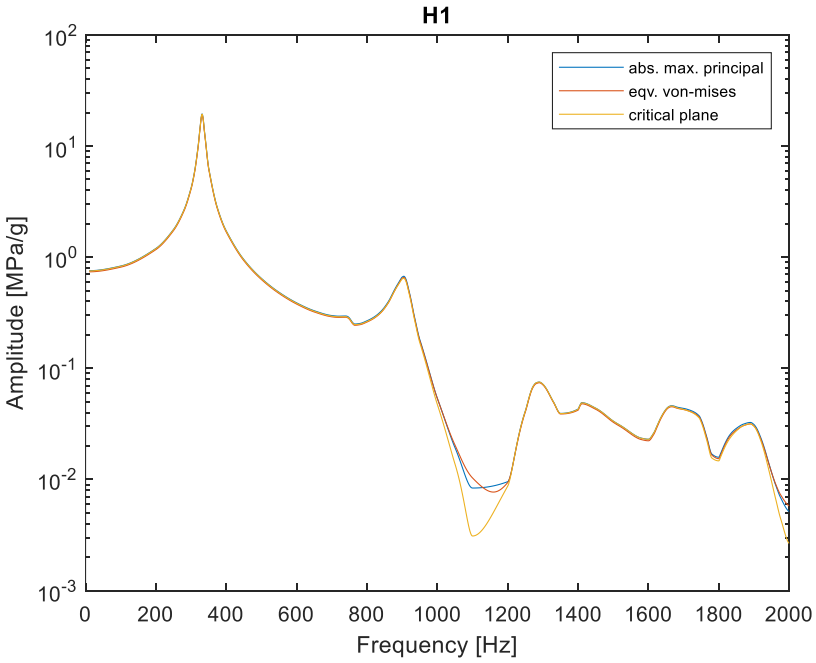

Figure 7.1 Transfer Functions for X-Direction

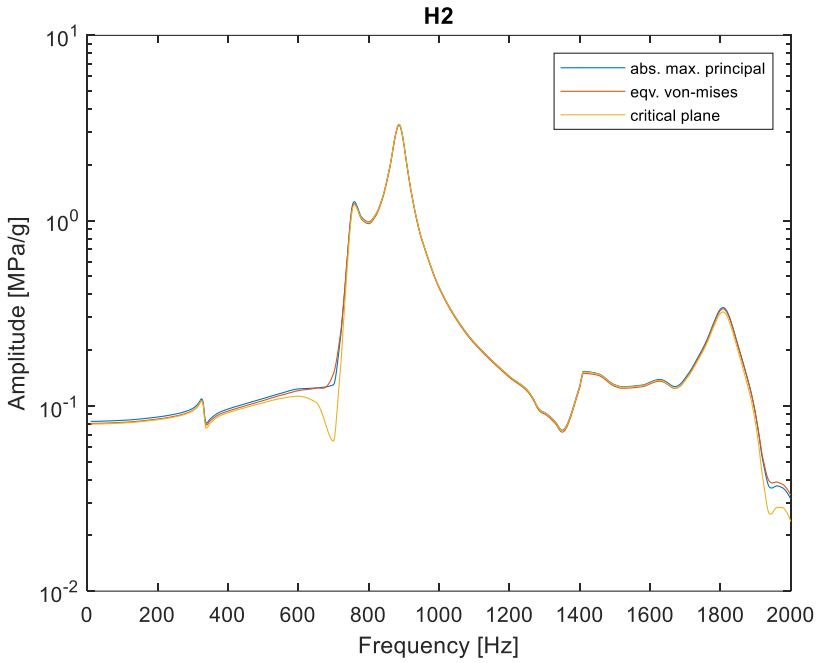

Figure 7.2 Transfer Functions for Y-Direction

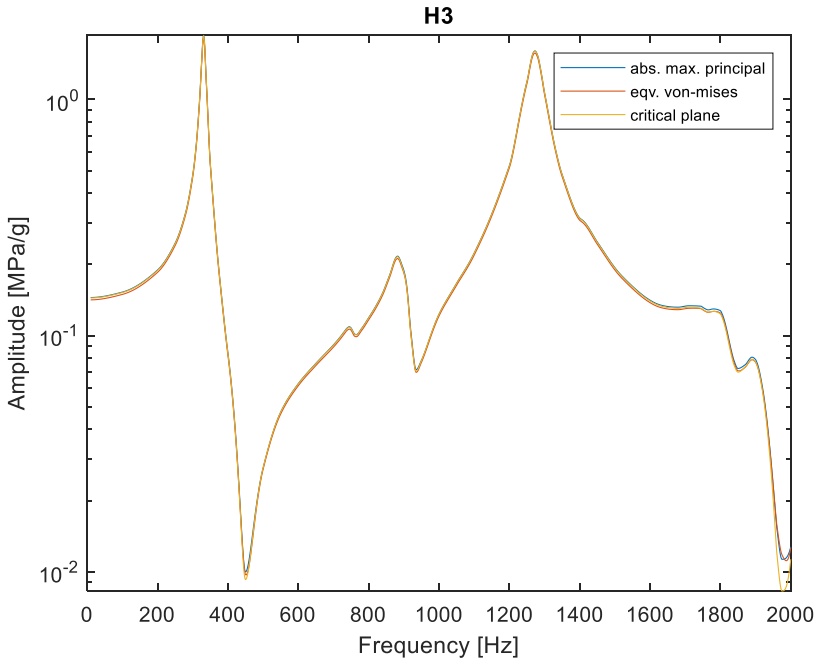

Figure 7.3 Transfer Functions for Z-Direction

As seen from plots, there are only very small differences between transfer functions obtained from all three methods. This means that stress response PSDs and so, fatigue life results are similar. Fatigue life results for absolute maximum principal, equivalent von-mises and critical plane approaches are given in Table 7.1.

Table 7.1 Comparison of Life Results with Different Stress Combination Methods

Stress Combination Method	Cycle Counting Method	Life [mins]
Absolute Maximum Principal	Narrow-Band	37.50
	Wirsching	51.41
	$\alpha_{0.75}$	37.54
	Dirlik	37.86
	Tovo-Benasciutti	38.08
	Lalanne	37.63
Equivalent von-Mises	Narrow-Band	47.51
	Wirsching	65.16
	$\alpha_{0.75}$	47.55
	Dirlik	47.97
	Tovo-Benasciutti	48.24
	Lalanne	47.68
Critical Plane	Narrow-Band	39.76
	Wirsching	54.49
	$\alpha_{0.75}$	39.79
	Dirlik	40.14
	Tovo-Benasciutti	40.37
	Lalanne	39.89

As expected, fatigue life results for different stress combination methods come out to be very similar. Since biaxiality ratio and principal stress angle do not vary much and stress state is examined previously as near proportional, using stress combination theories other than critical plane approach gives similar results too. This can be seen clearly when stresses are examined individually without any combination. Stresses that arise under x-axis excitation are relatively high compared to ones under y and z-axis excitations. Hence, these stresses dominate the stress state in every case.

Fatigue life results of absolute maximum principal and critical plane approaches are very close to each other. This is because of that alignment of principal stresses does not change over frequency range, i.e. σ_1 remains as highest principal stress while σ_3 remains as lowest one. Therefore, there is no effect of medium principal on transfer function.

Generally, absolute maximum principal and critical plane are the most requested and widely used methods. As indicated in this study, they give more conservative results and it is better to use them according to biaxiality of stress state.

7.2. Difference Between Multiaxial and Uniaxial Approaches

So far in this study, all analyses are performed based on multiaxial fatigue life estimation theories. However, taking the maximum of all data points for all frequencies is most commonly used method and it is known as enveloping. Generally, an envelope is created to cover maximum data points of x, y and z axis PSDs and it is used in uniaxial fatigue life analysis.

Another approach to vibration induced fatigue is having sequential loading and summing the damages that is acquired separately for all axes. In this chapter, difference between all these approaches is considered.

For checking the first approach, field data is enveloped by taking the maximum values of x, y and z direction loadings at each frequency point over the spectrum as mentioned in paragraph above. An enveloped loading is found as in Figure 7.4.

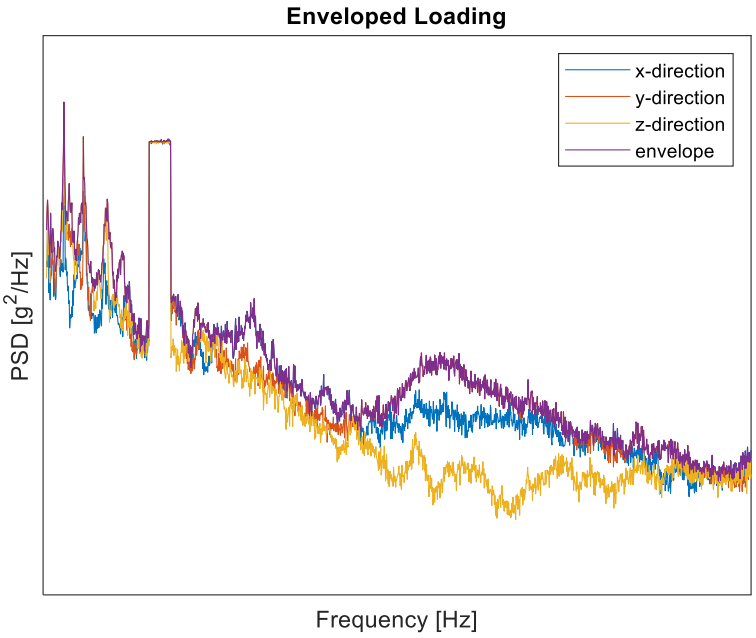

Figure 7.4 Enveloped Input Loading

This enveloped loading is used in uniaxial fatigue life analysis by applying in critical direction of structure which is x direction. Again, critical plane stress combination method is used to be consistent with multiaxial analyses performed before. Damage and fatigue life results obtained is given in Table 7.2.

Table 7.2 Fatigue Life Results Obtained from Enveloped Input Loading

Cycle Counting Method	Damage	Life [mins]
Narrow-Band	1.68e-04	99.01
Wirsching	1.24e-04	134.59
$\alpha_{0.75}$	1.68e-04	99.16
Dirlik	1.66e-04	100.27
Tovo-Benasciutti	1.65e-04	100.96
Lalanne	1.68e-04	99.32

For checking the second approach which is having sequential loading, vibration inputs coming from all x, y and z axes applied separately to system. Damage of critical node taken from all directions is collected together and cumulative damage is found. Table 7.3 shows damage values of individual axes while Table 7.4 shows the total damage and fatigue life values when structure is exposed to sequential loading case.

Table 7.3 Damage Results Obtained from Sequential Loading

Direction of Excitation	Cycle Counting Method	Damage
X	Narrow-Band	1.57e-04
	Wirsching	1.19e-04
	$\alpha_{0.75}$	1.56e-04
	Dirlik	1.55e-04
	Tovo-Benasciutti	1.55e-04
	Lalanne	1.56e-04
Y	Narrow-Band	3.60e-23
	Wirsching	2.16e-23
	$\alpha_{0.75}$	2.89e-23
	Dirlik	1.78e-23
	Tovo-Benasciutti	1.60e-23
	Lalanne	2.23e-23
Z	Narrow-Band	1.61e-14
	Wirsching	1.00e-14
	$\alpha_{0.75}$	1.61e-14
	Dirlik	1.56e-14
	Tovo-Benasciutti	1.52e-14
	Lalanne	1.58e-14

Table 7.4 Total Damage and Life Results Obtained from Sequential Loading

Cycle Counting Method	Total Damage	Life [mins]
Narrow-Band	1.57e-04	106.36
Wirsching	1.19e-04	140.22
$\alpha_{0.75}$	1.56e-04	106.45
Dirlik	1.55e-04	107.19
Tovo-Benasciutti	1.55e-04	107.66
Lalanne	1.56e-04	106.61

As Table 7.3 is examined, it can be clearly seen that y and z directions have negligible effect on life of the structure. Therefore, nearly all damage stems from the x-axis excitation. Since the structure is weaker in x direction relative to other two directions, results are reasonable.

Comparison of all results obtained by performing multiaxial analysis, uniaxial analysis with enveloped loading and sequential analysis are shown below in Table 7.5.

Table 7.5 Comparison of Life Results Obtained from Different Loading Cases

Cycle Counting Method	Loading Case Life Results [mins]		
	Multiaxial Loading	**Enveloped Uniaxial Loading**	**Sequential Loading**
Narrow-Band	39.76	99.01	106.36
Wirsching	54.49	134.59	140.22
$\alpha_{0.75}$	39.79	99.16	106.45
Dirlik	40.14	100.27	107.19
Tovo-Benasciutti	40.37	100.96	107.66
Lalanne	39.89	99.32	106.61

As all results are compared, it can be concluded that multiaxial loading condition gives the lowest results as expected. Sequential loading has nearly same case as applying the load only in x direction. For this reason, it gives relatively higher results than enveloped uniaxial loading case which is an expected result again.

The reason for having far more lower fatigue life results in multiaxial loading case is cross correlation effects of all individual axes to each other. It can be summarized that cross effects cannot be neglected when analysis case is evaluated. Other two cases may cause unexpected consequences as they predict higher fatigue life. Hence, having multiaxial analyses gives more realistic results.

7.3. Effect of Tightening Torque of Screws on Fatigue Life

Effect of damping on fatigue life was investigated previously on Chapter 6.6.2 and it was concluded that it has major effect on results. One of the most important parameters in assemblies that effects damping of the system is torching. Therefore, in this chapter, effect of torching of screws used in assembly is examined experimentally.

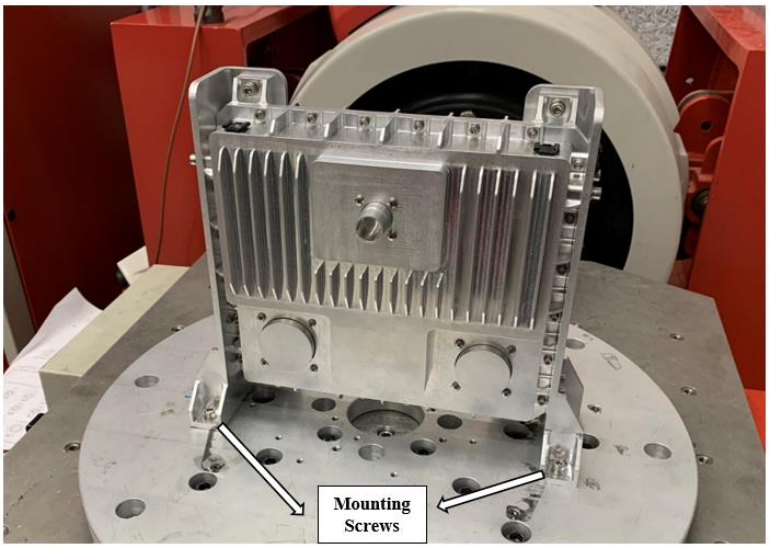

Figure 7.5 Mounting Screws in Assembly

Six mounting screws that are used for assembling the structure to a platform (see Figure 7.5) are torched to minimum value. Then, torque is increased gradually up to its maximum limit. Torque values are decided with respect to the preload applied to screws. Minimum torque is evaluated by adjusting the preload as 50% of the yield strength of screw material which is grade A2-70 stainless steel, while maximum torque is evaluated by adjusting the preload as 80% of the yield strength. Material properties of grade A2-70 stainless steel is given below.

Table 7.6 Material Properties of A2-70 Stainless Steel

Young's Modulus	200 GPa
Ultimate Tensile Strength	700 MPa
Yield Strength	450 MPa

At each step, data is collected with the help of the accelerometers. Using transmissibility curves obtained from these tests, damping ratios are calculated using half-power bandwidth method for every torque applied. White noise with an amplitude of 0.002 g^2/Hz is applied to system as input excitation. Transmissibility curves for different torques are presented in Figure 7.6.

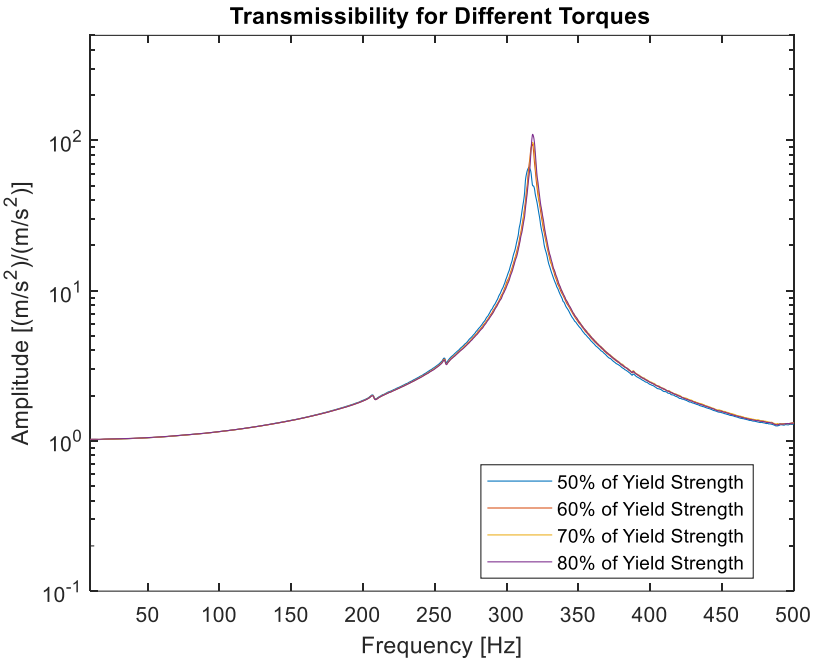

Figure 7.6 Transmissibility Curves for Different Torques

As expected, damping ratio is decreasing with increasing torque as transmissibility plots are getting sharper. This is because of the fact that structure becomes more rigid since pressure cone areas of mounting screws are increasing. Therefore, it affects the fatigue life as damping changes. Using obtained damping ratios, fatigue life analyses are repeated for accelerated multiaxial loading case given in Figure 6.4. Damping ratios and fatigue life results for different torques of mounting screws are tabulated in Table 7.7.

Table 7.7 Damping Ratios and Life Results for Different Torques

Percent of Yield Strength	Corresponding Torque [Nm]	Increase in Torque	Damping Ratio, ζ	Life [mins]
50%	2.7	-	0.0108	2.07e+08
60%	3.3	22.2%	0.0066	2.11e+07
70%	3.8	15.2%	0.0064	1.82e+07
80%	4.5	18.5%	0.0055	8.88e+06

As Table 7.7 is examined, it can be clearly seen that fatigue life changes significantly with changing torque. Even only 3% decrease in damping, as torque increases from 3.3 Nm to 3.8 Nm, causes nearly 15% decrease in fatigue life. This is an unsurprising result as effect of damping is investigated in detail in previous chapters. Therefore, torching effect should be considered carefully while having an accelerated fatigue life test of an assembly since uncontrolled torching may cause unexpected consequences

8. DISCUSSIONS AND CONCLUSION

Generally, structures used in engineering environments encounter dynamic loads in addition to the static ones. These dynamic loads mainly come as randomly fluctuating vibrations and excite the structures in all their frequencies. These fluctuating loads can cause structures to fail even by creating stresses under the yield strength of material. Therefore, in this thesis, random vibration induced fatigue theory and its implementations are investigated in detail. During this study, the structure is evaluated under simultaneous multiaxial loading which demonstrate real-life conditions better compared to uniaxial loading case. Only disadvantage of multiaxial analysis is that time-domain data is mandatory, since CPSDs are required along with direct PSDs. Hence, if field data is not available, PSD profiles described in military standards cannot be used directly.

To be able to have simpler process and time-efficient solutions, a numerical code is developed in MATLAB which is capable of calculate fatigue life of any structure using different stress combinations methods and different cycle counting techniques. Moreover, it can be used to evaluate any uniaxial loading case too. The code is verified with the help of the commercial software results, nCode DesignLife. A notched cantilever beam which is much simpler model is used as code verification model for being sure about structural effects. There were small differences on fatigue life results of numerical code and commercial software. Although, resultant stress PSDs of both solvers are quite similar, spectral moments come out to be slightly different. Numerical code is checked again by importing spectral moments found from nCode to numerical code and results became exactly same. Therefore, it is understood that nCode uses different methodology by calculating the spectral moments. It applies a noise floor to stress PSD which excludes some portion of stress information from stress PSD which causes to have lower spectral moments. Although fatigue life results have some differences, results obtained from numerical code is adequately satisfying. Hence, numerical code is evaluated to be used safely for fatigue life analysis of any kind of structure.

The analysis model used in fatigue calculations is verified by performing modal experiments in which natural frequencies and damping values are acquired. The FE model is updated regarding these modal test results and iterations are performed until the best model is found. This verification analysis is performed to cover first three modes of the brackets which have greatest effect on fatigue life.

One of the most important steps in fatigue life analysis is determining the stress response accurately. Small changes in stress history may cause significant changes in fatigue life. For this reason, critical location should be determined very carefully. Unfortunately, in complex models that contain surface to surface contacts and/or screw connections, it is inevitable to encounter with singularity phenomenon. This may be very deceptive if stresses at singularity points are treated as correct. This situation is overcome by performing mesh convergence analysis and critical node of the structure is decided.

In the first analysis, original field data is used to calculate fatigue life under real exposure conditions. However, it is found that brackets are not experiencing any fatigue failure with this loading conditions. Fatigue life of brackets is calculated approximately as 9.7e+09 hours under 2500 hours loading excitation. Moreover, analysis is repeated using accelerated data to 4 hours and life is found to be approximately 2.5e+06 hours. Hence, for experimental purposes, input loading is manipulated by adding a sine tones to vicinity of the first natural frequency to observe the crack in reasonable durations in fatigue tests. Scaling whole input by multiplying with constant number is not preferred, not to have irrational gRMS levels that shaker cannot be applied. Using rearranged loading, fatigue analyses are performed again and fatigue life is determined in reasonable levels for experimental purposes.

Fatigue is highly sensitive to many parameters like stress response as mentioned before. This response is directly related to system damping. The structure is detected as non-linear, damping ratio has increasing characteristics with increasing loading amplitude. Unfortunately, it was not possible to calculate damping under the loading which fatigue life tests are performed, since there are no available accelerometers to measure data at such high amplitude loadings. Therefore, to be able to have reasonable results, damping ratio of the system is selected as altered parameter and analyses are repeated with different damping ratios. Fatigue life of brackets is determined by taking the highest possible damping ratio as reference. Hence, fatigue life is found to be around 7 hours for 0.03 damping ratio and 40 mins for 0.02 damping ratio.

Moreover, multiaxial input is transformed into uniaxial input as giving the same damage to critical node of the structure. Since there are no available shakers that can apply simultaneous multiaxial loading, this method is preferred. This method completely relies on the mathematics behind fatigue theory in which all parameters for reaching life is attained from resultant stress PSD. Hence, previously obtained stress PSD from numerical multiaxial analysis is divided to directional transfer function of the most critical axis and so, equivalent uniaxial input is found.

The fatigue life experiment is conducted with the equivalent uniaxial input and crack is observed at expected critical location of left bracket within 32-33 minutes. From previous analyses, it is expected to have fatigue life of around 40 minutes with 0.02 damping ratio. Hence, it is concluded that the structure most probably has around 0.02 or slightly less damping. When results of different cycle counting methods are examined, all, except for Wirsching, gives reasonable results. Normally, Narrow-Band method might give irrelevant results if the signal was in wideband characteristics. Since irregularity factor of signal is found to be around 0.98 for sine-added input which is very close to narrowband, Narrow-Band approach gives reasonable results too, compared to other robust approaches. Hence, any of these cycle counting methods, except Wirsching, which are underlined in this study, gives consistent and reliable results.

In addition to investigations of fatigue behavior of mounting brackets, different case studies are performed to understand effects of different parameters on fatigue life better. Firstly, effect of different stress combination methods is examined. Since effect of loading in x axis is relatively high compared to other directions, it dominates the stress state. This is the reason of negligible differences on obtained transfer functions. Secondly, different approaches on fatigue life procedures are investigated. Unsurprisingly, multiaxial approach gives lower life results due to cross correlations arisen in equations. Final case study is conducted to cover effects of torching on damping ratio of the system. Damping ratio tends to decrease with increasing torques of mounting screws, since pressure cone areas of bolted joints increase.

As mentioned repeatedly in previous parts, fatigue life strictly depends on many different parameters. Deciding stress location correctly, choosing proper stress combination method and dealing with damping carefully are the parameters argued in the scope of this thesis. In addition to these parameters, there are some more factors affecting the fatigue life as mean stress. Although, all its disadvantages, time domain approach is more suitable for dealing with mean stresses arise in the structure. Rainflow cycle counting algorithm that is used in time domain analysis gives mean stress information in addition to stress ranges. However, cycle counting algorithms used for frequency domain analysis does not contain any mean stress information. Since frequency domain approaches are used in this thesis, mean stress effects are not considered.

To sum up, fatigue life results that are obtained from both numerical code analysis and experimental tests are quite satisfactory, considering all possible structural uncertainties that may arise in the analyzed system.

REFERENCES

[1] N.E. Frost, K.J. Marsh, L.P. Pook, Metal Fatigue, Courier Corporation, **1999**.

[2] Wikipedia, Fatigue (material), https://en.wikipedia.org/wiki/Fatigue_(material), (Last Accessed: **February 27, 2022**).

[3] W. Schütz, A History of Fatigue, Engineering Fracture Mechanics, 54 (**1996**) 263-300.

[4] W.J.M. Rankine, On the Causes of the Unexpected Breakage of the Journals of Railway Axles: and on the Means of Preventing Such Accidents by Observing the Law Continuity in Their Construction, Minutes of the Proceedings of the Institution of Civil Engineers, Thomas Telford-ICE Virtual Library, **1843**, pp. 105-107.

[5] F. Braithwaite, On the Fatigue and Consequent Fracture of Metals, Minutes of the Proceedings of the Institution of Civil Engineers, Thomas Telford-ICE Virtual Library, **1854**, pp. 463-467.

[6] O. Basquin, The Exponential Law of Endurance Tests, Proc Am Soc Test Mater, **1910**, pp. 625-630.

[7] A. Palmgren, Die Lebensdauer von Kugellargern, Zeitshrift des Vereines Duetsher Ingenieure, 68 (**1924**) 339.

[8] M.A. Miner, Cumulative Damage in Fatigue, **1945**.

[9] Westmoreland Mechanical Testing & Research, The History of Fatigue Testing, https://www.wmtr.co.uk/History_Of_Fatigue_Testing.html, (Last Accessed: **February 27, 2022**).

[10] G. Irwin, I. Fracture, Handbuch der Physik, Flüge, S, Springer-Verlag, New York, **1958**.

[11] P.C. Paris, The Growth of Cracks due to Variations in Load, Lehigh University, **1962**.

[12] M. Matsuishi, T. Endo, Fatigue of Metals Subjected to Varying Stress, Japan Society of Mechanical Engineers, Fukuoka, Japan, 68 (**1968**) 37-40.

[13] E. Wolf, Fatigue Crack Closure Under Cyclic Tension, Engineering Fracture Mechanics, 2 (**1970**) 37-45.

[14] M.W. Brown, K. Miller, A Theory for Fatigue Failure Under Multiaxial Stress-Strain Conditions, Proceedings of the Institution of Mechanical engineers, 187 (**1973**) 745-755.

[15] A. Fatemi, D.F. Socie, A Critical Plane Approach to Multiaxial Fatigue Damage Including Out-of-Phase Loading, Fatigue & Fracture of Engineering Materials & Structures, 11 (**1988**) 149-165.
[16] C. Wang, M. Brown, A Path Independent Parameter for Fatigue Under Proportional and Non-proportional Loading, Fatigue & Fracture of Engineering Materials & Structures, 16 (**1993**) 1285-1297.
[17] L. Susmel, A Simple and Efficient Numerical Algorithm to Determine the Orientation of the Critical Plane in Multiaxial Fatigue Problems, International Journal of Fatigue, 32 (**2010**) 1875-1883.
[18] R. Smith, The Versailles Railway Accident of 1842 and the First Research into Metal Fatigue (Retroactive Coverage), Fatigue 90, (**1990**) 2033-2041.
[19] Element, 5 Disasters Caused by Material Fatigue and What We Learned From Them, https://www.element.com/nucleus/2016/5-disasters-caused-by-material-fatigue-and-what-we-learned-from-them, (Last Accessed: **March 05, 2022**).
[20] A.S. Ribeiro, A.L. Silva, M. Abilio, Evolution of Fatigue History, 21st Brazilian Congress of Mechanical, **2011**, pp. 5-7.
[21] A. Taneja, Historical Failures and the Evolution of Fracture Mechanics, https://www.linkedin.com/pulse/historical-failures-evolution-fracture-mechanics-ajay-taneja, (Last Accessed: **March 05, 2022**).
[22] A. Brot, Development of Fatigue Life Regulations Based On Lessons Learned from Several Aircraft Accidents, 46th Israel Annual Conference on Aerospace Sciences, **2006**.
[23] Deutsche Welle, Eschede: Germany's Worst Train Disaster Remembered 20 Years On, https://www.dw.com/en/eschede-germanys-worst-train-disaster-remembered-20-years-on/a-44056391, (Last Accessed: **March 05, 2022**).
[24] S.O. Rice, Mathematical Analysis of Random Noise. Selected Papers on Noise and Stochastic Processes, Dover, New York, (**1954**) 133-294.
[25] J. Bendat, Probability Functions for Random Responses, NASA Report on Contract NAS-5-4590, **1964**.
[26] P.H. Wirsching, M.C. Light, Fatigue Under Wide Band Random Stresses, Journal of the Structural Division, 106 (**1980**) 1593-1607.
[27] G. Chaudhury, W. Dover, Fatigue Analysis of Offshore Platforms Subject to Sea Wave Loadings, International Journal of Fatigue, 7 (**1985**) 13-19.
[28] J. Tunna, Fatigue Life Prediction for Gaussian Random Loads at the Design Stage, Fatigue & Fracture of Engineering Materials & Structures, 9 (**1986**) 169-184.

[29] D.S. Steinberg, Vibration Analysis for Electronic Equipment, **2000**.

[30] T. Dirlik, Application of Computers in Fatigue Analysis, **1985**.

[31] N.W. Bishop, F. Sherratt, Finite Element Based Fatigue Calculations, NAFEMS, **2000**.

[32] N. Bishop, A. Woodward, MSC Software, Fatigue Analysis of a Missile Shaker Table Mounting Bracket, **2000**.

[33] A. Halfpenny, A Frequency Domain Approach for Fatigue Life Estimation from Finite Element Analysis, Key Engineering Materials, Trans Tech Publ, **1999**, pp. 401-410.

[34] R. Tovo, Cycle Distribution and Fatigue Damage Under Broadband Random Loading, International Journal of Fatigue, 24 (**2002**) 1137-1147.

[35] D. Benasciutti, R. Tovo, Spectral Methods for Lifetime Prediction Under Wideband Stationary Random Processes, International Journal of Fatigue, 27 (**2005**) 867-877.

[36] C. Lalanne, Mechanical Vibration and Shock Analysis, Mechanical Shock, John Wiley & Sons, **2013**.

[37] K. Karpanan, Critical Plane Search Method for Biaxial and Multiaxial Fatigue Analysis, Pressure Vessels and Piping Conference, American Society of Mechanical Engineers, **2016**, pp. V005T005A011.

[38] G. He, H. Chen, X. He, Fatigue Behavior and Influence Factor Analysis of the Structure Subject to Multiaxial Random Loading, Journal of Vibroengineering, 17 (**2015**) 3620-3634.

[39] M. Mršnik, J. Slavič, M. Boltežar, Frequency Domain Methods for a Vibration Fatigue Life Estimation–Application to Real Data, International Journal of Fatigue, 47 (**2013**) 8-17.

[40] M. Aykan, Vibration Fatigue Analysis of Equipments Used in Aerospace, **2005**.

[41] B. Koçer, Vibration Fatigue Analysis of Structures Under Broadband Excitation, **2010**.

[42] Y. Eldoğan, Vibration Fatigue Analysis of Structures Installed on Air Platforms, **2012**.

[43] Ö.M. Akbaba, Experimental and Theoretical Fatigue Analysis of Avionic Unit Mounting Brackets Integrated on an Unmanned Aerial Vehicle Under Random Vibration Environment, **2021**.

[44] Total Materia, Fatigue Life of Metals: Part Three, https://www.totalmateria.com/page.aspx?ID=CheckArticle&LN=TR&site=kts&NM=282, (Last Accessed: **March 12, 2022**).

[45] J.E. Shigley, Shigley's Mechanical Engineering Design, Tata McGraw-Hill Education, **2011**.

[46] M.A. Meyers, K.K. Chawla, Mechanical Behavior of Materials, Cambridge University Press, **2008**.

[47] Y.-L. Lee, T. Tjhung, Rainflow Cycle Counting Techniques, Metal Fatigue Analysis Handbook: Practical Problem-solving Techniques for Computer-aided Engineering, (**2011**) 89.

[48] HBM U.K. Limited, DesignLife Theory Guide, **2013**.

[49] Siemens, What is the Fourier Transform?, https://community.sw.siemens.com/s/article/what-is-the-fourier-transform, (Last Accessed: **March 26, 2022**).

[50] D. Benasciutti, Fatigue Analysis of Random Loadings, PhD University of Ferrara, Department of Engineering, **2004**.

[51] J. Jang, J.-W. Park, Simplified Vibration PSD Synthesis Method for MIL-STD-810, Applied Sciences, 10 (**2020**) 458.

[52] G.R. Henderson, A.G. Piersol, Fatigue Damage Related Descriptor for Random Vibration Test Environments, Sound and Vibration, 29 (**1995**) 20-25.

[53] M.K. Thompson, MIL-STD-810G Environmental Engineering Considerations and Laboratory Tests, US Department of Defense: Washington, DC, USA, **2008**.

[54] T. Irvine, Effective Modal Mass & Modal Participation Factors Revision H, **2013**.